

Role of volcanic and anthropogenic aerosols on the tropical ocean-atmosphere-land coupled system and the South Asian Monsoon

Submitted in partial fulfillment of the requirements
of the degree of

Doctor of Philosophy

by

**Manmeet Singh
(Roll No. 174407001)**

Supervisors:

**Dr. Chandra Venkataraman
Dr. R. Krishnan & Dr. Ayantika Dey Choudhury**



IDP in Climate Studies
INDIAN INSTITUTE OF TECHNOLOGY BOMBAY
May, 2022

Dedicated to the mother nature.

Thesis Approval

This thesis entitled **Role of volcanic and anthropogenic aerosols on the tropical ocean-atmosphere-land coupled system and the South Asian Monsoon** by **Manmeet Singh**, Roll No. **174407001** of IDP in Climate Studies, Indian Institute of Technology Bombay is approved for the degree of **Doctor of Philosophy**.

External Examiner:



Internal Examiner:



Supervisors:



Date:

Chairperson:



Place:



Document Details

Title	Thesis approval form Manmeet Singh 174407001
File Name	thesis_approval_form_manmeet.pdf
Document ID	a101f5e2b9124d19835982d397287bdf
Fingerprint	caccc9e16442b4fa01d7f90865e254d1
Status	Completed

Document History

Document Created	Document Created by Manmeet Singh (manmeet.singh@utexas.edu) Fingerprint: caccc9e16442b4fa01d7f90865e254d1	May 08 2022 02:56PM UTC
Document Sent	Document Sent to Dr. Dilip Ganguly (dilipganguly@cas.iitd.ac.in)	May 08 2022 02:56PM UTC
Document Sent	Document Sent to Dr. Sridhar Balasubramanian (sridharb@iitb.ac.in)	May 08 2022 02:56PM UTC
Document Sent	Document Sent to Dr. Chandra Venkataraman (chandra@iitb.ac.in)	May 08 2022 02:56PM UTC
Document Sent	Document Sent to Dr. R. Krishnan (krish@tropmet.res.in)	May 08 2022 02:56PM UTC
Document Sent	Document Sent to Dr. Ayantika Dey Choudhury (ayantika@tropmet.res.in)	May 08 2022 02:56PM UTC
Document Sent	Document Sent to Dr. Sharad Bhartiya (bhartiya@che.iitb.ac.in)	May 08 2022 02:56PM UTC
Document Viewed	Document Viewed by Dr. Sridhar Balasubramanian (sridharb@iitb.ac.in) IP: 103.21.127.60	May 08 2022 04:47PM UTC
Document Viewed	Document Viewed by Dr. Dilip Ganguly (dilipganguly@cas.iitd.ac.in) IP: 103.27.9.249	May 09 2022 04:53AM UTC
Document Viewed	Document Viewed by Dr. Sridhar Balasubramanian (sridharb@iitb.ac.in) IP: 103.21.127.60	May 12 2022 03:26AM UTC
Document Viewed	Document Viewed by Dr. Sharad Bhartiya (bhartiya@che.iitb.ac.in) IP: 103.21.127.104	May 12 2022 04:18AM UTC

Document Signed	Document Signed by Dr. Sharad Bhartiya (bhartiya@che.iitb.ac.in) IP: 103.21.127.104	May 12 2022 04:18AM UTC
Document Viewed	Document Viewed by Dr. Sridhar Balasubramanian (sridharb@iitb.ac.in) IP: 103.21.127.60	May 12 2022 04:39AM UTC
Document Signed	Document Signed by Dr. Sridhar Balasubramanian (sridharb@iitb.ac.in) IP: 103.21.127.60	May 12 2022 04:39AM UTC
Document Viewed	Document Viewed by Dr. Ayantika Dey Choudhury (ayantika@tropmet.res.in) IP: 103.251.184.2	May 12 2022 05:17AM UTC
Document Signed	Document Signed by Dr. Ayantika Dey Choudhury (ayantika@tropmet.res.in) IP: 103.251.184.2	May 12 2022 05:19AM UTC
Document Viewed	Document Viewed by Dr. Dilip Ganguly (dilipganguly@cas.iitd.ac.in) IP: 103.27.9.249	May 12 2022 08:54AM UTC
Document Viewed	Document Viewed by Dr. Dilip Ganguly (dilipganguly@cas.iitd.ac.in) IP: 103.27.9.249	May 12 2022 09:04AM UTC
Document Signed	Document Signed by Dr. Dilip Ganguly (dilipganguly@cas.iitd.ac.in) IP: 103.27.9.249	May 12 2022 09:05AM UTC
Document Viewed	Document Viewed by Dr. R. Krishnan (krish@tropmet.res.in) IP: 59.88.169.38	May 13 2022 02:34AM UTC
Document Signed	Document Signed by Dr. R. Krishnan (krish@tropmet.res.in) IP: 59.88.169.38	May 13 2022 02:35AM UTC
Document Viewed	Document Viewed by Dr. Chandra Venkataraman (chandra@iitb.ac.in) IP: 103.21.127.60	May 14 2022 05:49AM UTC
Document Signed	Document Signed by Dr. Chandra Venkataraman (chandra@iitb.ac.in) IP: 103.21.127.60	May 14 2022 05:51AM UTC
Document Completed	This document has been completed. Fingerprint: 8d0dfd881d91a7e599f935f6a5644c5f	May 14 2022 05:51AM UTC

Declaration

I declare that this written submission represents my ideas in my own words and where others' ideas or words have been included, I have adequately cited and referenced the original sources. I also declare that I have adhered to all principles of academic honesty and integrity and have not misrepresented or fabricated or falsified any idea/data/fact/source in my submission. I understand that any violation of the above will be cause for disciplinary action by the Institute and can also evoke penal action from the sources which have thus not been properly cited or from whom proper permission has not been taken when needed.

Date: May 14 2022

Manmeet Singh

Manmeet Singh
Roll No. 174407001



Document Details

Title	Manmeet Singh's signatures
File Name	declaration.pdf
Document ID	ca6be1e50bfc43eda50c37d9f939c194
Fingerprint	9f0d6e30826ac12792541981dd2927e1
Status	Completed

Document History

Document Created	Document Created by Manmeet Singh (manmeet.singh@utexas.edu) Fingerprint: 9f0d6e30826ac12792541981dd2927e1	May 14 2022 07:12AM UTC
Document Signed	Document Signed by Manmeet Singh (manmeet.singh@utexas.edu) IP: 106.215.92.250	May 14 2022 07:12AM UTC
Document Completed	This document has been completed. Fingerprint: 2ed77c8809f1808bd7910732509895a7	May 14 2022 07:12AM UTC

Abstract

Weather and climate on Earth are known to be influenced by atmospheric aerosols through interactions with solar radiation, clouds and precipitation in addition to the planet's circulation systems. Extensive scientific research has been conducted on the impact of aerosols on the South Asian monsoon. While acknowledging these scientific advancements, it is also recognized that quantifying the impacts of aerosols on the South Asian monsoon is a challenging problem due to the interactive nature of the tropical atmosphere-ocean-land coupled system. This dynamical system exhibits a wide range of spatio-temporal variations. A recent IPCC assessment report found that aerosols and clouds are the most significant source of inaccuracy in current climate models. In the context of the South Asian Monsoon, the role of natural aerosols such as volcanic ash and desert dust in addition to the anthropogenic aerosols are vital for an enhanced understanding of the physical processes in the coupled-climate system. The changes caused by volcanic aerosols on the South Asian monsoon are poorly understood. Moreover, there is a need to understand better the variability caused by dust and anthropogenic aerosols on the coupled ocean-atmosphere-land climate system.

Identifying the influence of volcanic radiative forcing on the El Niño Southern Oscillation (ENSO) and Indian monsoon (IM) coupling is the first objective. The Indian monsoon relies on the ENSO-Indian monsoon coupling for predictability, and there have been concerns that this synchronisation may be waning as a result of global warming. These results, which were obtained by combining a wide range of paleoclimate proxy data with large-ensemble climate model simulations and results from the CMIP5-PMIP3 experiments, reveal that the ENSO-IM phase locking relationship is complicated, nonlinear, and epochal. State-of-the-art non-linear methodologies are used to arrive at these results and it is shown that large volcanic eruptions induce coherence between ENSO and IM systems. The results have implications for the seasonal monsoon forecasts over India and assessing the changes in rainfall via the stratospheric geoengineering proposals.

The second objective aims to understand the role of dust and anthropogenic aerosols on the Indian monsoon via changes in the land-atmosphere coupled interactions. Previous studies have documented the various mechanisms responsible for the aerosol led changes to Indian monsoon precipitation. Different non-linear land-atmosphere coupling metrics show that the aerosols lead to a modulations of land-atmosphere coupled feedbacks. The test case of Indian monsoon 2002 is used to conduct large-ensemble targeted climate simulations with and without mixed natural-anthropogenic aerosols. It is found that the aerosols were responsible for up to

20% precipitation suppression over core monsoon zone. The year 2002 was also an El Niño and El Niños are known to be associated with monsoon droughts; however, none of the existing statistical or dynamical models at that time simulated the reduced precipitation in that year. Hence, a suppressed precipitation output by adding aerosols to the climate system is valuable. The results shed light on the importance of aerosol-land-atmosphere interactions within the framework of the South Asian monsoon. Analysis of atmosphere-only simulations of IITM-ESM suggest similar results thus establishing the causality on aerosols. Supplementary results from coupled climate models in AerChemMIP-CMIP6 and their corresponding atmosphere-only versions shed similar interpretations and a causal discovery algorithm on observational datasets shows one of the feedback as an indirect connection between aerosols and precipitation via land-surface. Understanding the combined aerosol-land-atmosphere interactions would be helpful in assessing the efficacy of dynamical models to simulate the weather and climate.

The work carried out in this doctoral dissertation aims to improve the understanding of natural and anthropogenic aerosols' role in modulating South Asian monsoon. Aerosols have been known to cause uncertainty in the weather and climate models, and enhanced knowledge would be useful towards improving the dynamical models. Future work would involve assessing whether the aerosols would improve model simulations in operational systems. Additionally, the aerosols in IITM-ESM, which has been used for the sensitivity studies in this work, are prescribed as optical radiative properties. A fully interactive aerosol model coupled with the other components is expected to represent processes such as collision and coalescence better and hence dynamically compute the indirect effects in addition to the direct radiative effects of aerosols. A reduction in aerosol related uncertainties within dynamical models are expected to lead to cascading benefits towards better precipitation forecasts.

Contents

Abstract	i
List of Tables	vii
List of Figures	ix
List of Abbreviations	xv
1 Introduction	1
1.1 Atmospheric aerosols	2
1.2 Aerosols over South Asia	4
1.3 Aerosols and the tropical ocean-atmosphere-land system: Open Issues	5
1.4 Thesis outline	6
2 Literature survey	11
2.1 Volcanic aerosols in the climate system	11
2.1.1 Volcanism forced climate response	12
2.1.2 Volcanism induced decadal to centennial variability	14
2.1.3 Hydrological response to volcanic eruptions	15
2.1.4 Impact of location & season of volcanism on climate response	16
2.1.5 Volcanic eruptions and climate change	16
2.1.6 Volcanic forcing and climate modelling: Open challenges	20
2.1.7 Volcanism forced changes in atmospheric carbon	20
2.1.8 Volcanic eruptions and ENSO	21
2.1.9 Volcanism forced ENSO-Indian Monsoon coupling and hydroclimate response	22
2.2 Natural and anthropogenic aerosols in the South Asian climate system	25
2.2.1 Natural dust and anthropogenic aerosols: Response of Indian monsoon .	26
2.2.2 Land-atmosphere interactions and Indian monsoon	26
2.2.3 Mixed state of dust and anthropogenic aerosols over the Indian region .	27
2.3 Research objectives	28

3 Volcanism induced phase coherence of ENSO and Indian monsoon	31
3.1 Synchronization	31
3.1.1 Self-Sustained Oscillator	31
3.1.2 Coupling of oscillating objects	32
3.1.3 Phase	33
3.1.4 Synchronization of Periodic Oscillators by External Force	34
3.1.5 Two Interacting Oscillators	35
3.2 Coupling of ENSO-Monsoon system	36
3.2.1 El Niño and Southern Oscillation (ENSO)	36
3.2.2 Why is ENSO oscillatory?	37
3.2.3 Monsoon	37
3.2.4 ENSO-Monsoon relationship	37
3.2.5 Role of Indian Ocean Dipole on ENSO-Monsoon Coupling	39
3.2.6 Role of Atlantic on ENSO-Monsoon Coupling	39
3.2.7 Role of Solar Irradiance on ENSO-Monsoon Coupling	40
3.2.8 Role of Greenhouse gas warming on ENSO-Monsoon coupling	40
3.2.9 Role of Basic State in ENSO-Monsoon coupling	40
3.2.10 ENSO-Snow-Monsoon relationship	41
3.2.11 Role of PDO and interdecadal oscillations in ENSO-Monsoon coupling	41
3.2.12 Indian Summer Monsoon influence on ENSO	41
3.3 ENSO-monsoon phase coherence during the historical period (1871-2016) . . .	42
3.4 Phase coherence analysis using the IPSL PMIP3 last millennium simulation .	43
3.5 Statistical Significance of Phase coherence analysis	45
3.6 Dynamical mechanism of volcanism induced ENSO-Indian monsoon coupling .	50
3.7 Conclusions	52
4 Volcanic fingerprint on ENSO-monsoon coupling: Climate model simulations & paleoclimate proxy records analysis	53
4.1 IITM Earth System Model	54
4.2 Volcanic footprint on ENSO-monsoon coupling in IITM-ESM	57
4.2.1 Mechanism of ENSO-IM coupling from IPSL PMIP3 outputs	62
4.3 Paleoclimatic evidence of volcanism forced ENSO-monsoon coupling	68
4.3.1 Event Coincidence Analysis	73
4.3.2 Bayesian Analysis	73
4.3.3 Northern Hemispheric Land Cooling	75
4.4 Climate Network Analysis	82
4.5 Conclusions	82

5	Role of anthropogenic aerosols on the tropical ocean-atmosphere-land coupled system and South Asian monsoon and associated aerosol-land-atmosphere interactions	85
5.1	IITM Earth System Model experiments	86
5.2	Initial conditions for the atmospheric model of IITM-ESM	88
5.3	Initializing ocean model in IITM-ESM	88
5.4	Initial states of the land surface in IITM-ESM	88
5.5	Aerosols and Chemistry Model Intercomparison Project (AerChemMIP)/CMIP6 outputs	89
5.6	Instrumental/reanalysis datasets	89
5.7	Coupling metrics of land and atmosphere	90
5.7.1	Terrestrial Coupling index	90
5.7.2	Memory of soil moisture	91
5.7.3	The atmospheric component of land-atmosphere coupling	91
5.7.4	Information theory-based metrics	92
5.8	Causal discovery using PCMCI	92
5.9	The IITM-ESM’s response to the introduction of anthropogenic aerosols	93
5.10	Coupling metrics between the land and the atmosphere for Anthrop minus NoAnthrop IITM-ESM simulations	93
5.11	Indian monsoon response to aerosols in AerChemMIP-CNRMESM-CMIP6 outputs	97
5.11.1	Response in the atmosphere only AerChemMIP-UKESM-CMIP6 simulations	102
5.12	Discovery of causal relationships within the monsoon context of the aerosol-land-atmosphere system	102
5.13	Mechanisms for aerosol-induced land-atmosphere interactions	106
5.14	Conclusions	108
6	Summary and Conclusions	109
6.1	Future directions	111
Appendix A	Codes and tools	113
A.1	Volcanic imprint on ENSO-monsoon coupling	113
A.2	Initial conditions for IITM-ESM simulations	113
A.3	PCMCI based causal algorithm	114
A.4	Event Coincidence Analysis	114
A.5	Event Synchronization Analysis	114
A.6	Climate Network Analysis	114
A.7	Generation of Twin surrogates and Recurrence plots	114
References		115

List of Publications	137
Fellowship Awarded	141
Acknowledgments	143

List of Tables

4.1	Datasets used	68
4.2	Pearson correlation coefficients for different volcanically induced epochs in the last millennium, their data sources and number of paleoclimatic reconstructions confirming significant correlation	71

List of Figures

1.1	A diagrammatic view of the different atmospheric aerosol sources and their impact on radiation. Adapted from Fadnavis et al. (2020) with permission	3
2.1	Aerosol-land-atmosphere interactions within the framework of South Asian monsoon	27
2.2	Potential aerosol–land–atmosphere interactions, as well as surface, convection, and precipitation feedbacks, in the monsoonal systems. Niyogi et al. (2007) Reproduced with permission	28
3.1	Two clocks which are ideally manufactured in the same way but the only difference in rhythm is due to error bars of production machines. The illustration is shown to visualize the interaction between two oscillators (Pikovsky et al. (2003)), Reproduced with permission	32
3.2	Phase space plot (left) for different states of the time series shown (right) (Pikovsky et al. (2003)), Reproduced with permission	33
3.3	Dynamics of the phase at the synchronization transition. (Pikovsky et al. (2003)), Reproduced with permission	35
3.4	All India JJAS Rainfall and the relationship with El Niño/La Niña events, source: https://mol.tropmet.res.in/monsoon-interannual-timeseries/	38
3.5	ENSO and IM Phase Coherence Analysis for the instrumental era (1871-2016) [Top]. Statistical Significance of instrumental-era and last millennium phase Coherence[Bottom]	44
3.6	Coefficient of correlation between (a) all India rainfall and Niño3.4, (b) Surface air temperature on Indian landmass and Niño3.4 from historical simulations (Tejavath et al. (2019)), Reproduced with permission	45

3.7 ENSO, IM filtered time-series and their respective phase space plot during last millennium: Time-series of Niño3 and IM indices during 850–1850 based on the last millennium IPSL PMIP3 simulations in blue and the filtered time-series in orange (top panel). The trajectory in complex plane of the Niño3 index and its Hilbert transform (bottom left panel), and the IM index and its Hilbert transform (bottom right panel) show oscillations of Niño3 and IM around a single attractor. The trajectory in complex plane demonstrate ENSO and IM to undergo self-sustained oscillations on a single attractor, respectively	46
3.8 ENSO and IM phase coherence from IPSL PMIP3 model runs during the last millennium. The ENSO-IM phase difference is shown in the top figure, while the volcanic radiative forcing during the last millennium is shown in the bottom plot (850-1850 AD). The backdrop is coloured green to indicate statistically significant epochs.	47
3.9 Comparison of Volc and NoVolc distributions of ENSO and IM angular frequency using quantil-quantile plots. Volc phase speeds are bootstrapped up to year 4. The remaining corresponds to NoVolc	48
3.10 (Caption next page.)	49
3.10 (Previous page.) LVE-induced changes in ENSO and IM oscillation angular frequencies in the previous millennium. Volc and NoVolc are bootstrapped similar to Figure 3.9	50
3.11 Probability Distribution functions of Phase Locking Value for PI Control (1000 years) and Historical run from IPSL PMIP3 simulations. Monte Carlo analysis is done with N=10000 for both PI control and historical runs and 10 year samples are taken out from the complete dataset. For historical subsampling only those samples that satisfy the presence of a volcanic eruption are chosen. (a) PI Control (b) correspond to the historical (last millenium) wherein the 10 years are choosen with the condition that volcanic eruption should have occured in that period, (c) same as (b) but for Tropical eruptions, (d) same as (b) but for extra-tropical eruptions.	51
4.1 Diagram illustrating the flow chart for the IITM-ESM simulations carried out to find the influence of volcanic explosions on ENSO-Indian monsoon coupling	55
4.2 Plots of SST anomaly distributions from the 100-member REF ensembles without volcanic forcing (i.e., based on the pre-industrial control simulation) from January of year 0 through December of year 2 are displayed. Realizations start with 47 Neutral ICs, 24 warm and 29 cold ICs compose the 100 members of the group.	56

4.3	ENSO modulations forced by LVE under varied initializations: Progress from January 1883 till the end of December, 1885 (a) AOD at mid-latitudes across the world (b) Box-whisker graphs illustrating the distribution of Δ Niño3 changes calculated from the difference between the VRF1x and REF ensembles.	58
4.4	Box-whisker plots illustrating the distribution of Δ Niño3 fluctuations from January 1883 to December 1885 showing ENSO's reaction on the intensity of the LVE	59
4.5	Spatial maps of VRF1x - REF generated by ensemble mean of 100 members of Krakatoa VRF realisations in tropical Indo-Pacific and monsoon domain	60
4.6	(Caption next page.)	61
4.6	(Previous page.) Response of the tropical Indo-Pacific region to varied magnitudes of volcanic activity	62
4.7	Composite of Net Surface Radiation, Walker Circulation(5S-5N averaged), Surface Air Temperature and Hadley Circulation (60E-100E averaged) for large volcanic eruptions ($\text{mag} > 1.0 \text{ W/m}^2$) for years -1 and +1 relative to the volcanic eruption	63
4.8	Composite of Net Surface Radiation, Walker Circulation(5S-5N averaged), Surface Air Temperature and Hadley Circulation (60E-100E averaged) for large volcanic eruptions ($\text{mag} > 1.0 \text{ W/m}^2$) for years +1 and +2 relative to the volcanic eruption	64
4.9	Composite of Net Surface Radiation, Walker Circulation(5S-5N averaged), Surface Air Temperature and Hadley Circulation (60E-100E averaged) for large volcanic eruptions ($\text{mag} > 1.0 \text{ W/m}^2$) for years +2 and +3 relative to the volcanic eruption	65
4.10	Composite of Net Surface Radiation, Walker Circulation(5S-5N averaged), Surface Air Temperature and Hadley Circulation (60E-100E averaged) for large volcanic eruptions ($\text{mag} > 1.0 \text{ W/m}^2$) for years +3 and +4 relative to the volcanic eruption	66
4.11	Composite of Net Surface Radiation, Walker Circulation(5S-5N averaged), Surface Air Temperature and Hadley Circulation (60E-100E averaged) for large volcanic eruptions ($\text{mag} > 1.0 \text{ W/m}^2$) for years +4 and +5 relative to the volcanic eruption	67
4.12	Composite time series of Nino3 and IM after an eruption	68
4.13	Superposed epoch analysis on proxy paleoclimatic data-sets for ISMR, ENSO, PDO and volcanic radiative forcing	72
4.14	Figure illustrating event coincidence analysis for assessing statistical interrelationships between two events time series A and B. Reproduced from Donges et al. (2016) with permission	73

4.15	Event Coincidence Analysis (Precursor coincidence rate) for ENSO(top) and Indian Monsoon (bottom). The Event Coincidence Rates are such that volcano precedes ENSO and IM drought	74
4.16	Conditional probability analysis of ENSO and IM coincidence subject to (left) ENSO (0), (right) ENSO (0) and Volcano (-1).	75
4.17	Conditional probability analysis of ENSO and IM coincidence subject to (left) ENSO (0), (right) ENSO (0) and Volcano () for different years relative to the LVE	76
4.18	Similar to Figure 4.17, except that the conditioning is also done using the PDO index based on Mann et al. (2009)	77
4.19	Similar to Figure 4.18, except that the PDO index is based on MacDonald and Case (2006)	78
4.20	Similar to Figure 4.19, except that the PDO index is based on D'Arrigo and Wilson (2006)	79
4.21	Similar to Figure 4.20, except that the PDO index is based on Biondi et al. (2001)	80
4.22	Response of summer temperatures in the Northern Hemisphere to very strong volcanic eruptions in the last millennium. The volcanoes are selected as top 25 from Sigl et al. (2015). Surface air temperature data from the last millennium is from Cook et al. (2010)	81
4.23	Climate Network Analysis: Degree Centrality of the Climate Network (Tsonis) from the monthly surface air temperature (tas) from the CMIP5 IPSL-CM5B-LR historical simulation. The left panel (a, c, e) shows the degree centrality before the eruption (-3, -2, -1 years relative to the eruption) and the right panel shows the network after the eruption (0, 1, 2 years relative to the eruption). It can be seen that the Indian landmass/Indian Ocean areas are not a part of the system/not in the network from b after Krakatoa 1884 eruption. Tsonis et al. (2006)	83
5.1	Design of IITM-ESM experiments	87
5.2	Suppression of precipitation due to mixed natural-anthropogenic aerosols in IITM-ESM for July 2002. July was the month in monsoon drought of the year 2002 that was responsible for the failed monsoon and also corresponds to the maximum ever dust aerosol loading over the Northern Indian plains	94
5.3	Similar to Figure 5.2, but from the atmosphere only version of IITM-ESM with and without anthropogenic aerosols	95
5.4	(B-M)According to the MERRA-2 reanalysis, the anomaly in the dust aerosol optical depth when compared with the climatology (2000-2020). (N-Y) Except for black carbon (BC) aerosols, this is the same as (B-M). Figure shows analysis from the year 2001 because the instrumental datasets from AERONET that are used to evaluate reanalysis aerosols over India are only available from that year.	96

5.5	Aerosol optical depth due to anthropogenic emissions at 550 nm averaged for the South Asian domain (5-40N, 60-100E) for each year from 1850-2014 from MACv2-SP dataset	96
5.6	From the output of the IITM-ESM corresponding to July 2002, the absolute values land-atmosphere coupling metrics for the ensemble mean of Anthrop and NoAnthrop simulation. Mann-Whitney test is performed over the distributions of the coupling metrics from two simulations. The p-values and medians are annotated in the C	98
5.7	Taylor plot showing the comparison of historical simulations of different CMIP6 models and instrumental all India summer monsoon rainfall	99
5.8	Comparison of total aerosol optical depth for May-September 2014 from AerChem-MIP simulations and MERRA-2 reanalysis. It can be seen that CNRMESM represents the most realistic representation of aerosols amongst all AerChemMIP models. All the AerChemMIP models have interactive aerosols.	100
5.9	Aerosol induced changes in land-atmosphere interactions from AerChemMIP/CMIP6 outputs. The rows in the first two columns correspond to changes in precipitation, surface soil moisture, surface latent heat flux, surface air temperature and surface specific humidity. The rows in the last two columns represent terrestrial coupling index, atmospheric-leg of terrestrial coupling index, mutual information, nonlinear mutual information, and vegetative-atmosphere coupling. The first and third column show the response of all aerosol experiment relative to the preindustrial (clean). Second and fourth column represent the response of doubling dust relative to the preindustrial control.	103
5.10	Precipitation response due to aerosols in atmosphere only simulation of UKESM/AerChem-MIP/CMIP6. The control (piAer) consists of preindustrial aerosols and the sensitivity (Aer) experiment consists of aerosols corresponding to the year 2014. Sea-surface temperature is fixed in these experiments.	104
5.11	The causal discovery network was assessed using the PCMCI causal algorithm. The datasets used are daily time series of precipitation (P), evaporation (E), sea surface temperature over Arabian Sea (SST_AS), two meter air temperature (T2M), soil moisture at the surface (SM), normalized difference vegetation index (NDVI) and aerosol optical depth (AOD). The datasets used are ERA5 reanalysis, GLEAM reanalysis, IMD, NCEP/NCAR reanalysis, and MERRA-2 reanalysis. Robustness of the indirect relationship between precipitation and aerosols via land-surface is established by performing PCMCI over different epochs	105
5.12	Physical mechanisms leading to precipitation suppression due to anthropogenic aerosols in IITMESM for July 2002	107

List of Abbreviations

ENSO	El Niño Southern Oscillation
IM	Indian monsoon
IOD	Indian Ocean Dipole
PDO	Pacific Decadal Oscillation
NAO	North Atlantic Oscillation
LVE	Large Volcanic Eruptions
MI	Mutual Information
MMI	Multivariate Mutual Information
TCI	Terrestrial Coupling Index
IPCC	Intergovernmental Panel on Climate Change
CMIP	Coupled Model Intercomparison Project
PMIP	Paleoclimate Modelling Intercomparison Project
AerChemMIP	Aerosols and Chemistry Model Intercomparison Project
IITM-ESM	Indian Institute Of Tropical Meteorology Earth System Model
SAT	Surface Air Temperature
CESM	Community Earth System Model
ITCZ	Intertropical Convergence Zone
NCAR	National Center for Atmospheric Research
AMOC	Atlantic Meridional Overturning Circulation
AMO	Atlantic Multidecadal Oscillation
TC	Tropical Cyclone
SST	Sea Surface Temperature
AMV	Atlantic Multidecadal Variability
LRS	Length of Rainy Season
NAM	Northern Annular Mode

CGCM	Coupled General Circulation Model
EWSC	Eurasian Winter Snow Cover
VRF	Volcanic Radiative Forcing
AISM	All India Summer Monsoon Rainfall
ISMR	Indian Summer Monsoon Rainfall
SASMI	South Asian Summer Monsoon Index
IMD	India Meteorological Department
ESM	Earth System Model
HPC	High Performance Computing
GHG	Greenhouse Gas
CCCR	Centre for Climate Change Research
CFSv2	Climate Forecast System version 2
NCEP	National Centers for Environmental Prediction
GFS	Global Forecasting System
LSM	Land Surface Model
SAS	Simplified Arakawa Schubert
MOM	Modular Ocean Model
GFDL	Geophysical Fluid Dynamics Laboratory
AR	Assessment Report
TOA	Top of the Atmosphere
AOD	Aerosol Optical Depth
IPSL	Institute Pierre Simon Laplace
NDVI	Normalized Difference Vegetation Index
EVI	Enhanced Vegetation Index
MERRA-2	Modern-Era Retrospective analysis for Research and Applications version 2
ECMWF	European Centre for Medium-Range Weather Forecasts
ERAS	ECMWF Reanalysis 5th Generation
PCMCI	Peter and Clark Momentary Conditional Independence
CNRMESM	Centre National de Recherches Météorologiques Earth System Model
MIROC	Model for Interdisciplinary Research on Climate
NorESM	Norwegian Earth System Model

UKESM	United Kingdom Earth System Model
NASA GISS Studies	National Aeronautics and Space Administration Goddard Institute for Space
MPI-ESM	Max-Planck-Institut für Meteorologie Earth System Model
ESGF	Earth System Grid Federation

Chapter 1

Introduction

Atmospheric aerosols are significant drivers of the coupled climate system and are responsible for changes in the Earth's energy budget. Their effects are manifested by variations in precipitation, evaporation, temperature and other critical physical fields directly affecting life on Earth. Moreover, for accurate weather and climate predictions, aerosols' improved understanding, including their physical/chemical processes, distribution, sources and sinks are necessary. South Asian monsoon which drives more than 50 % of the region's agricultural activities, is directly and indirectly impacted by the aerosols. Aerosols also act as regional forcing on the hydrological cycle over the Indian subcontinent. They interact with clouds, altering the clouds' radiative characteristics.

Aerosols and clouds interact with each other. This interaction modifies the radiation and precipitation at the surface. These responses are manifested by various processes occurring while incoming solar radiation interacts with aerosols, leading to scattering and absorption. Desert dust transported by winds, industrialisation, biomass burning, agriculture, and other activities contribute to high aerosol concentrations. There has been a substantial increase in emissions, creating various forms of aerosols due to rapid population expansion, industrialisation, and urbanization throughout East, South, and Southeast Asia. An increasing anthropogenic aerosol (Satheesh et al. (2017)) and associated reduced amount of solar radiation reaching the Indian subcontinent, there is a change in net surface radiation and also the energy fluxes at the surface (Soni et al. (2012), Ramanathan et al. (2005)). Changing hydrological cycles over the region have been related to the region's high aerosol load. A decrease in southwest monsoon precipitation across South Asia has been linked to human aerosol forcing over the long run

(Krishnan et al. (2016)).

1.1 Atmospheric aerosols

Aerosols are microscopic solid/liquid/mixed particles originating from natural or man-made sources and are suspended in the air. In the troposphere, aerosols have a half-life of days to weeks, while in the stratosphere, they have a half-life of roughly a year. Various types of aerosol particles have different climate-altering effects. Aerosol particles absorb and scatter solar energy, altering the global and regional radiative budgets. In contrast to absorbing aerosols, non-absorbing aerosols like sulfate, nitrate, and others reflect shortwave sunlight to space, cooling the net climate system. The characteristics of the aerosol and the surrounding environment influence the warming or cooling effects of carbonaceous aerosols (black carbon, organic carbon) and mineral dust. For example, when absorbing aerosols are present in snow, they impact climate by reducing snow surface albedo. This results in a positive radiative forcing that alters snow and ice melting. Although the regional anthropogenic aerosol radiative forcing can be either negative or positive depending on local emissions and transport mechanisms, it is widely documented that the global radiative impact of anthropogenic aerosols cools the globe.

The first aerosol indirect effect is the cooling of the Earth's surface caused by an increase in cloud condensation nuclei (CCN) producing aerosols in cloudy regions, which result in more but smaller cloud droplets reflecting solar radiation to space (cloud-albedo effect). As a result of the increased cloud albedo and enhanced cooling caused by the so-called second indirect effect, smaller droplets reduce collision coalescence and therefore increase the time it takes to develop to raindrop size. In contrast, an increase in CCN-forming aerosols in a saturated and buoyant environment can energize the cloud through microphysical processes. The semi-direct effect is caused by absorbing aerosols altering the air temperature, which increases lower level static stability and inhibits convection, resulting in less cloud cover.

It's challenging to separate the causes and effects of aerosols on climate change. Aerosols in the atmosphere have a significant impact on temperature fluctuations, and it's important to note that transport processes modulate aerosol distribution (for example, dust transport from West Asia in the pre-monsoon season). One method by which atmospheric aerosols get into the atmosphere is by the direct emission of primary sources (such as dust, salt from the sea, and OC) or the production of secondary aerosols as a byproduct of chemical processes in the atmosphere (e.g., sulfate, nitrate, ammonium, and SOA). Sea salt, dust, and primary biological aerosols are all naturally generated in the atmosphere, unlike BC, which has anthropogenic origins such as incomplete combustion of biomass and fossil fuel.

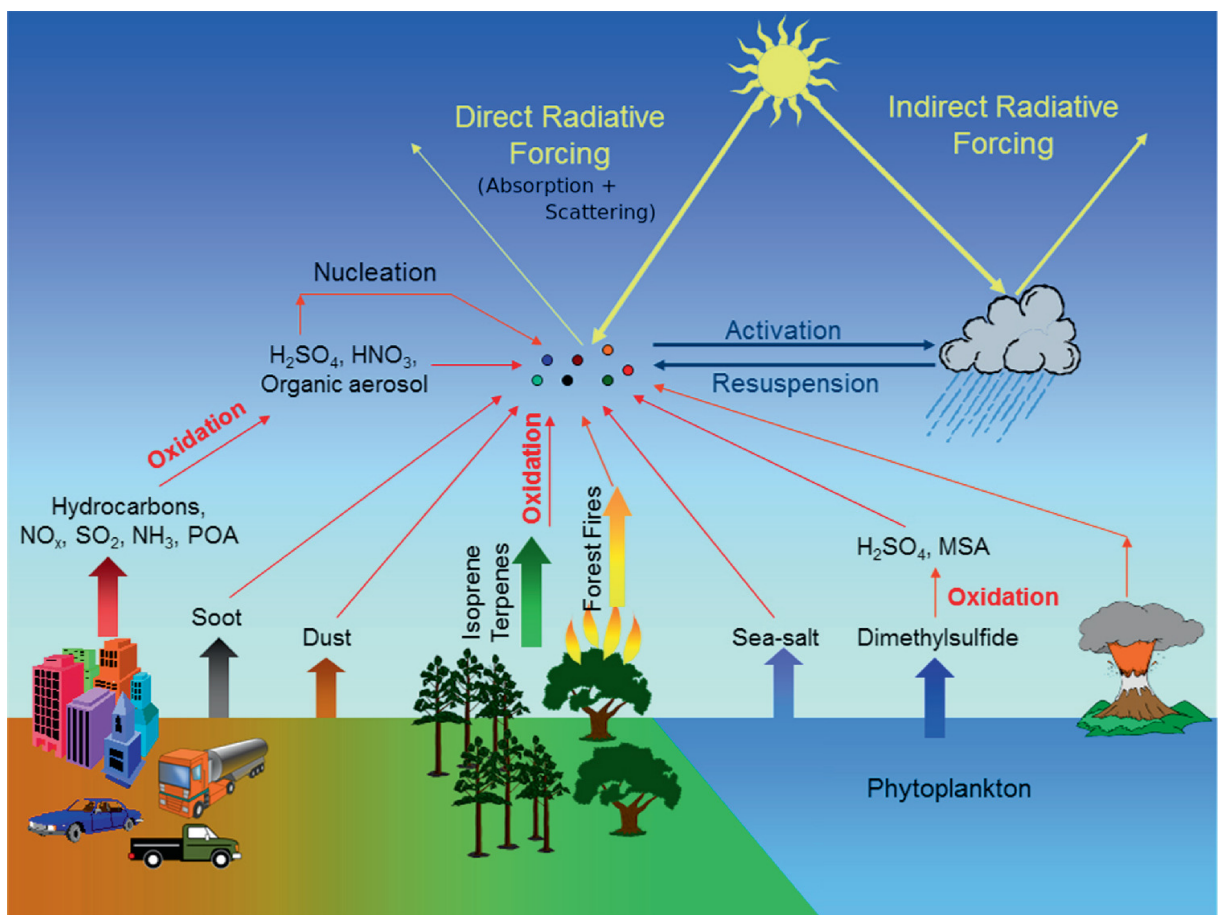


Figure 1.1: A diagrammatic view of the different atmospheric aerosol sources and their impact on radiation. Adapted from Fadnavis et al. (2020) with permission

1.2 Aerosols over South Asia

An observational network database based on long-term ground-based observations (>25 years for certain stations) has been used to predict long-term changes in aerosol loading over the Indian subcontinent (Babu et al. (2013), Dani et al. (2012), Kaskaoutis et al. (2012b)). Krishna Moorthy et al. (2013) shows a 2.3% yearly rise in the mean AOD compared to its value in 1985. However, in rural areas, however, estimates of AOD trends are weakly negative whereas industrial stations in peninsular India indicate strong positive trends (Babu et al. (2013)). An annual AOD increase of 2% has been seen in Pune between 1998 and 2007 (Dani et al. (2012)). An upward trend of 2.4% per year can also be seen in the most recent AERONET data over Pune from 2008 to 2017. Dry winter months (December–March) have a substantial (0.0005–0.04 per year) increase in aerosol loading. Still, pre-monsoon and summer monsoon seasons see moderate or negligible increases due to competing effects of dust transportation and wet scavenging (Babu et al. (2013)). More evidence points to a buildup of human-emitted fine particles relative to natural coarser aerosols over India, as seen by the rising trend in Angstrom wavelength exponent throughout the country (Satheesh et al. (2017), Dani et al. (2012)).

Satellite measurements have shown changes in AOD over the Indian subcontinent. Over the Indian mainland, the yearly mean trend of AOD from MODIS measurements is up by 40% from the year 2000 (Srivastava (2017)). According to MODIS regional patterns, the annual mean AOD has risen by more than 40% in large cities like Jaipur, Hyderabad, and Bengaluru between 2000 and 2009. In contrast, it has reduced by less than 10% in high-altitude areas like Dehradun and Shimla. (Ramachandran et al. (2012)). Satellite data shows that AOD trends have significant seasonal variation. During the winter (DJF), the subcontinent, particularly IGP, has a strong rising tendency (Srivastava (2017)). With a trend of 0.0053 to 0.0011 per year during DJF from 1998 to 2010, SeaWiFS (Sea Viewing Wide Field of View Sensor) AOD indicates an increasing trend over India (Hsu et al. (2012)). There has also been a rising trend in the range of 0.01–0.04 per year across metropolitan centers and heavily populated rural regions post-monsoon/winter from MISR (Multi-angle Imaging SpectroRadiometer) for March 2000–February 2010 (Dey and Di Girolamo (2011)). Satellite datasets (MODIS, MISR, and OMI) show a significant and widespread decline in AOD during the pre-monsoon (MAM) period across areas of northern India (Pandey et al. (2017)). Because of the heterogeneous distribution of aerosols in the atmosphere, there are changes in atmospheric circulation and regional rainfall due to the uneven heating and cooling patterns. In the long term, the decreasing Indian summer monsoon precipitation trend since the 1950s has been related to the increasing anthropogenic aerosol burden (Undorf et al. (2018), Krishnan et al. (2016), Sanap et al. (2015), Ganguly et al. (2012), Bollasina et al. (2011) Ramanathan et al. (2005)). South Asian monsoon is greatly influenced by changes in land-ocean temperature contrasts and the tropospheric temperature structure, caused by local and distant aerosols.

1.3 Aerosols and the tropical ocean-atmosphere-land system: Open Issues

The processes associated with aerosols are one of the least understood in the climate system, and previous research has attributed this lack of understanding to the uncertainties in model simulations (Stocker (2014)). Some of the open issues within aerosol research in the purview of climate science are as follows:

1. For the volcanic aerosols, it has been known that strong volcanism can lead to El Niños; however, their role on ENSO-Indian monsoon coupling remains unclear. The coupling between ENSO and Indian monsoon is significant for the seasonal monsoon predictions of the Indian monsoon. The coupling can be noted from the observational datasets; as for every ten droughts (excess monsoons), six to seven on an average are associated with El Niños (La Niñas). Hence, although there is a strong relationship between ENSO and the Indian monsoon, it is non-linear in nature. And it is difficult to assess beforehand whether an El Niño (La Niña) would lead to a monsoon drought (excess). Studies such as Maraun and Kurths (2005) have shown that the coupling between ENSO and Indian monsoon occurs in epochs and may not be a continuous relationship. It was conjectured by Maraun and Kurths (2005) that large volcanic eruptions may be triggering the coupling of ENSO and Indian monsoon. However, since there were only five such eruptions since the instrumental observations began, it is difficult to fingerprint the role of large volcanic eruptions on ENSO-Indian monsoon coupling only with the explosions that have occurred in the instrumental period.
2. Previous research has investigated the relationship between (aerosols and Indian monsoon) or (land-atmosphere coupling and Indian monsoon). All the components aerosol-land-atmosphere behave in a unified nonlinear coupled manner owing to the coupled nature of the system. There is a limited understanding of aerosol-induced changes in land-atmosphere interactions and further implications in essential fields such as precipitation or temperature in the context of the South Asian monsoon. And hence there is a need to study the impacts of aerosols from a combined framework of aerosols-land-atmosphere coupling. The monsoon years such as 2002, which encountered the highest dust loading over the Indian subcontinent was also associated with one of the worst droughts. Moreover, it was also the year of an El Niño and the one for which none of the existing statistical or dynamical models at that time were able to correctly simulate the precipitation suppression (Gadgil et al. (2005)). Observational studies have shown that the regions over which the year 2002 had maximum natural dust loading, i.e. the Northern Indian plains, the most probable mixed state of aerosols is a combination of natural and anthropogenic aerosols (Kedia et al. (2014), Srivastava and Ramachandran (2013), Kaskaoutis

et al. (2012a), Dey et al. (2008), Dey et al. (2004)). That the desert dust from the Middle East (Dey et al. (2004)) mixes with the anthropogenic aerosols over the land and the land-surface processes are crucial for the region (Niyogi (2019), Halder et al. (2018), Bollasina and Ming (2013), Ferranti et al. (1999), Shen et al. (1998), Meehl (1994)). An assessment of aerosol-induced changes in land-atmosphere interactions is yet to be fully explored for the South Asian monsoon region.

1.4 Thesis outline

Following the introduction of thesis in this chapter, the remaining thesis is organized as follows:

- ✓ **Chapter-2 Literature Survey:** This chapter illustrates the literature survey on aerosols in the climate system and their impacts on the South Asian monsoon. Discussion on the volcanic and anthropogenic aerosols leads up to the designed research objectives. The publications and conference proceedings emerging out of this chapter are as follows:
 - Fadnavis, S., Mahajan, A.S., Choudhury, A.D., Roy, C., Singh, M., Biswas, Manmeet Singh, Pandithurai, G., Prabhakaran, T., Lal, S., Venkatraman, C. and Ganguly, D., 2020. “Atmospheric aerosols and trace gases. In *Assessment of Climate Change over the Indian Region* (pp. 93-116). Springer, Singapore.
 - Krishnan, R., Gnanaseelan, C., Sanjay, J., Swapna, P., Dhara, C., Sabin, T.P., Jadhav, J., Sandeep, N., Choudhury, A.D., Singh, M. and Mujumdar, M., 2020. “Introduction to climate change over the Indian region. *Assessment of Climate Change over the Indian Region* (pp. 1-20). Springer, Singapore.
 - R Krishnan, Singh Manmeet, Vellore Ramesh, Mujumdar Milind, 2018. “Progress and Prospects in Weather and Climate Modelling”, Physics News
 - Swapna, P., Krishnan, R., Sandeep, N., Prajeesh, A.G., Ayantika, D.C., Manmeet, S. and Vellore, R., 2018. “Long-Term Climate Simulations Using the IITM Earth System Model (IITM-ESMv2) With Focus on the South Asian Monsoon. *Journal of Advances in Modeling Earth Systems*, 10(5), pp.1127-1149.
 - Krishnan, R., Swapna, P., Vellore, R., Narayanasetti, S., Prajeesh, A.G., Choudhury, A.D., Singh, M., Sabin, T.P. and Sanjay, J., 2019. “The IITM earth system model (ESM): development and future roadmap. *Current Trends in the Representation of Physical Processes in Weather and Climate Models* (pp. 183-195). Springer, Singapore.
- ✓ **Chapter-3 Volcanism induced phase coherence of ENSO and Indian monsoon:** This chapter starts with a discussion on the concept of synchronization in nonlinear sciences.

The terminologies such as self-sustained oscillator, coupling, phase, interacting oscillators are explained in detail. Then, considering ENSO and Indian monsoon as two oscillators, the coupling of ENSO and Indian monsoon is discussed, and an introduction to phase coherence analysis is provided. The phase coherence analysis for the instrumental period from 1871-2016 is conducted in addition to the phase coherence analysis on the last millennium simulation outputs from IPSL/PMIP3 model. A dynamical mechanism responsible for the phase coupling between ENSO and Indian monsoon forced by large volcanic eruptions is found out. The publications and conference proceedings emerging from this chapter are as follows:

- Singh, M., Krishnan, R., Goswami, B., Choudhury, A.D., Swapna, P., Vellore, R., Prajeesh, A.G., Sandeep, N., Venkataraman, C., Donner, R.V. and Marwan, N., 2020. “Fingerprint of volcanic forcing on the ENSO–Indian monsoon coupling. *Science advances*, 6(38), p.eaba8164.
- M. Singh, R. Krishnan, B. Goswami, A. D. Choudhury, S. Panickal, R. Vellore, P. A. Gopinathan, S. Narayanasetti, C. Venkataraman, R. V. Donner, N. Marwan, J. and Kurths, 2021. “Fingerprint of volcanic forcing on the ENSO–Indian monsoon coupling”, *EGU General Assembly Conference Abstracts*
- M. Singh, R. Krishnan, B. Goswami, A. D. Choudhury, S. Panickal, R. Vellore, P. A. Gopinathan, S. Narayanasetti, C. Venkataraman, R. V. Donner, N. Marwan, J. and Kurths, 2021. “Fingerprint of volcanic forcing on the ENSO–Indian monsoon coupling”, *WCRP workshop on attribution of multi-annual to decadal changes in the climate system*

✓ **Chapter-4 Volcanic fingerprint on ENSO-monsoon coupling: Climate model simulations & paleoclimate proxy records analysis:** This chapter begins with a discussion on the IITM Earth System model. It further details the experiments conducted to fingerprint the role of volcanoes on ENSO-monsoon coupling. Paleoclimate proxy datasets are also used to assess the role of volcanoes on ENSO-IM coincidence. The publications and conference proceedings emerging from this chapter are as follows:

- Singh, M., Krishnan, R., Goswami, B., Choudhury, A.D., Swapna, P., Vellore, R., Prajeesh, A.G., Sandeep, N., Venkataraman, C., Donner, R.V. and Marwan, N., 2020. “Fingerprint of volcanic forcing on the ENSO–Indian monsoon coupling. *Science advances*, 6(38), p.eaba8164.
- M. Singh, R. Krishnan, B. Goswami, A. D. Choudhury, S. Panickal, R. Vellore, P. A. Gopinathan, S. Narayanasetti, C. Venkataraman, R. V. Donner, N. Marwan, J. and Kurths, 2021. “Fingerprint of volcanic forcing on the ENSO–Indian monsoon coupling”, *EGU General Assembly Conference Abstracts*
- M. Singh, R. Krishnan, B. Goswami, A. D. Choudhury, S. Panickal, R. Vellore, P. A. Gopinathan, S. Narayanasetti, C. Venkataraman, R. V. Donner, N. Marwan, J.

and Kurths, 2021. “Fingerprint of volcanic forcing on the ENSO–Indian monsoon coupling”, *WCRP workshop on attribution of multi-annual to decadal changes in the climate system*

✓ **Chapter-5 Mixed natural-anthropogenic aerosols and land-atmosphere interactions:**

Role on South Asian Monsoon: This chapter delves into the role of aerosol-induced land-atmosphere interactions in modulating the South Asian monsoon. Targeted sensitivity experiments using IITM-ESM are performed to assess the role of mixed natural-anthropogenic aerosols in the variability of monsoon system. Analysis using advanced statistical techniques such as causal algorithms are used, and AerChemMIP/CMIP6 outputs are also analysed. The results show that when present in their most probable mixed natural-athropogenic state, aerosols can lead to suppression of monsoon rainfall via changes in the land-atmosphere interactions. The publications and conference proceedings emerging from this chapter are as follows:

- Singh, M., Persad, G. G., Zong-Liang Yang, R. Krishnan, Ayantika, D. C., Wen-Ying Wu, Sabiha Tabassum, Venkataraman, C., Swapna, P., Prajesh, A.G., Sandeep, N., Ramesh, V., Mujumdar, M., Dev Niyogi, 2021. “Interactions between anthropogenic aerosols and land-atmosphere coupling in modulating Indian summer monsoon precipitation ”, (under preparation)
- Manmeet Singh, G. G. Persad, Z. L. Yang, R. Krishnan, A. D. Choudhury, W. Y. Wu, S. Tabassum, C. Venkataraman, S. Panickal, P. A.G., S. Narayanasetti, R. Vellore, M. Mujumdar, and D. Niyogi, 2021. “Modulations of Indian summer monsoon rainfall by aerosols induced land-atmosphere coupling ”, *In 102th American Meteorological Society Annual Meeting. AMS.*
- DC Ayantika, R Krishnan, M Singh, P Swapna, N Sandeep, AG Prajesh, R Vellore, 2021. “Understanding the combined effects of global warming and anthropogenic aerosol forcing on the South Asian monsoon”, *Climate Dynamics*, 56(5), pp.1643-1662.
- Dey Choudhury, A., Raghavan, K., Singh, M., Panickal, S., Narayansetti, S., Gopinathan, P.A. and Vellore, R., 2020, May. “Combined effects of anthropogenic aerosols and global warming on the South Asian Monsoon. *EGU General Assembly Conference Abstracts* (p. 923).
- Raghavan, K., Dey Choudhury, A., Singh, M., Panickal, S., Vellore, R. and Prajesh, A.G., 2018, December. “The Indian Monsoon Response to Climate Change in the IITM Earth System Model. *AGU Fall Meeting Abstracts* (Vol. 2018, pp. A51Q-2467).

✓ **Chapter-6 Conclusions and future directions:** An overview is provided of the hypothesis and the discussions of outcomes, which includes significant findings from the research.

Future research work scopes are offered sequentially after the conclusion and are outlined in further detail.

This page was intentionally left blank.

Chapter 2

Literature survey

Atmospheric aerosols form an important element of the coupled climate system and can lead to changes via direct or indirect effects. These changes can transpire into variations in the circulations, clouds and land surface feedbacks. In this thesis, the response of the climate system to aerosols is studied. The first part deals with understanding the changes caused by volcanic aerosols over the Indian monsoon followed by understanding the role of natural and anthropogenic aerosols over the Indian region.

2.1 Volcanic aerosols in the climate system

Volcanic aerosols are responsible for the natural mode of climate variability by ejecting massive amounts of gases and aerosols into the stratosphere. Volcanic eruptions are currently being employed as a validation test for cutting-edge Earth System Models. During major eruptions, volcanic aerosols reach the stratosphere and remain there for up to a year. There are several ways volcanic aerosols affect the climate system, but radiative forcing is the most significant. Volcanic aerosols block the sun's incoming radiation responsible for driving the Earth's energy. The influence of volcanic aerosols in climate and climate change has been studied extensively, despite being regarded as localized phenomena. However, there have been arguments to the contrary (Cole-Dai (2010)). If sustained for a long time, volcanic eruptions have been asserted as climate drivers (Robock (2000)).

2.1.1 Volcanism forced climate response

As temperatures have risen steadily since the 1850s, the volcanic signal in temperature has been masked. As a result, volcano and human-caused climate change are seen as compensating effects for one another. Volcanic eruptions can also act as a prediction source (Gaddis (2013)) by modulating stratospheric ozone (Solomon (1999)) and having ties to tropical precipitation (Xie et al. (2017)). Some studies have shown that volcanic aerosols can influence climate by causing El Niños (Khodri et al. (2017), Ohba et al. (2013), Mann et al. (2005), Hirono (1988)). Volcanic eruptions influence the atmosphere and ocean's chemistry on many different scales. They raise the temperature in the stratosphere while lowering it on the earth's surface. Observations have shown warming in the Northern Hemisphere during winter and cooling in the Middle Eastern area after volcanic eruptions (Fischer et al. (2007), Stenchikov et al. (2006), Shindell et al. (2004), Robock and Mao (1992)).

Because of these temperature changes, the circulation and polar vortex strengthen, which results in a positive phase of North Atlantic Oscillation (NAO) and Arctic Oscillation (AO). Unfortunately, Earth System Models are unable to replicate these dynamical relationships. One theory proposed to explain the missing dynamical relationship is that there is an extremely strong polar vortex and vertical resolution in the stratosphere in the models (Otterå (2008), Stenchikov et al. (2006), Shindell et al. (2004), Brasseur (2005)). To be sure, even with enhanced vertical resolution in the stratosphere from Marshall et al. (2009), HADGEM1 still couldn't simulate winter warming in the Northern hemisphere following volcanic eruptions. Numerous studies have examined the connection between volcanic eruptions and El Niños in the recent past (Emile-Geay et al. (2008), Adams et al. (2003)).

To explain the occurrence of El Niño after volcanic eruptions, Khodri et al. (2017) suggested the significance of tropical African cooling. They propose another way to measure the SST response by introducing relative SST as a metric to eliminate the conflicting findings on the direction of ENSO signal following volcanic eruptions. Also, they run targeted ensembles of volcanoes and no volcanoes to examine the role played by the state of the system in the tropical Pacific. They find that the volcanism pushes the system towards an ENSO-like state in the tropical Pacific regardless of the state of the system.

Wang et al. (2017) examined the impact of significant volcanic eruptions on the El Niño-Southern Oscillation (ENSO) from 1400 to 1999. Their hypothesis differs from Khodri et al. (2017). They find that a strong volcanic eruption induces cooling along the West Coast of South America and strengthens trade winds across the eastern equatorial Pacific, resulting in an intermediate La Niña-like condition. During the peak of the volcanic outburst, mid-latitudes and the Maritime continent will experience far more cooling than the tropical Pacific. With an increased latitudinal temperature differential (equator to mid-latitudes), ITCZ moves towards the equator, and large negative temperature anomalies over the Maritime continent lower the

tropical Pacific's longitudinal sea level pressure gradient. As a result of all these climatic shifts, the tropical Pacific transitions into an El-Niño-like event. Ménégoz et al. (2018a) conducted important research in which the authors attempted to assess the role that volcanic eruptions have in influencing the degree of predictability on decadal time scales.

Saturno et al. (2018) tried to understand better the impact of minor volcanic eruptions on tropospheric aerosols. When two Nyamuragira eruptions occurred in 2014, the HYSPLIT Lagrangian model shows that aerosols from both eruptions migrated over the South Atlantic and up to central Amazonia, where they settled at the Amazon Tall Tower Observatory. Evidence supports this long-range transmission of volcanic emissions from the ACRIDICON-CHUVA aircraft program. Numerous studies have looked at the impact of volcanic eruptions on ENSO in the recent past. According to Hopcroft et al. (2018), a scenario with growing tropospheric aerosols includes the role of a potentially powerful (Tambora 1815-like) eruption.

Ménégoz et al. (2017) have explored the relationship between Atlantic Multidecadal Variability and volcanic eruptions. In the third year after an eruption, the CNRM-CM5 model simulations show that volcanic eruptions have a delayed reaction throughout the North Atlantic. The likelihood of a negative NAO phase occurrence drops throughout the third year, and the cold Atlantic Multidecadal Variability exacerbates the deficit caused by a negative NAO phase. A volcanic eruption has an indirect effect since the changes are not caused directly by the atmosphere, but by the ocean sea-ice system's delayed reaction. The function of volcanic eruptions in altering these networks as a strategy for studying global teleconnections is an intriguing way to look at the topic from a non-linear perspective (Kittel et al. (2017))

Erlat and Türkeş (2019) used observational data for temperature over Turkey and conducted superposed epoch analysis to understand the response of volcanic eruptions within two years of the volcanic explosions. They find negative anomalies in maximum and minimum temperatures in the first two years following the volcanic eruption. Their results demonstrate that the winter cooling can be attributed to strong NAO during the first and second post-volcanic winters. Liu et al. (2020) discuss whether a recent volcanic eruption, i.e. Luzon's Taal volcano in the Philippines that erupted on January 12, 2020 could trigger El Niño and cause Eurasian warming. The Taal Volcano is still in active phase, and the Philippine Institute of Volcanology and Seismology has warned the Taal Volcano to note that further explosive eruptions could occur.

Zambri et al. (2019) studied the climate response of the Icelandic Laki eruption, which occurred in June 1783. It decreased precipitation and drought, grain loss, and surface cooling. Contrary to the observed cooling in 1784–86, the summer of 1783 was anomalously warm in Western Europe, with temperatures in July exceeding 3 K. However, Europe's winter of 1783–1784 was as cold as 3 K below normal. Although climate models typically replicate surface cooling and reduced rainfall associated with volcanic eruptions, model experiments have struggled to replicate Western Europe's intense warming following the Laki eruption. Owing

to the failure to replicate the anomalous heat, a question arises whether this event was a reaction to the eruption or simply an indication of internal temperature fluctuations. Using the National Center for Atmospheric Research's CESM Model, the authors analyse the impact of Laki eruption on the atmosphere of the Northern Hemisphere atmosphere within 12 months of the eruption. They note that the mild summer of 1783 originated from atmospheric blocking across Northern Europe. Understanding the causes of these events is important for historical reasons and considering and forecasting potential climate responses to future volcanic high-latitude eruptions.

Xing et al. (2020) evaluate global surface air temperature (SAT) responses to five major tropical volcanic eruptions from 1870 to 2005 using outputs from 97 historical and 58 AMIP runs that participated in the Coupled Model Intercomparison Project (CMIP5) phase 5. They observe that the AMIP models simulate the global cooling following volcanic eruptions, as noted in the observations. Whether volcanoes could trigger an El Niño, was found to be dependent on the ocean initial conditions. The models were unable to capture the Eurasian warming as seen in the observations post volcanic eruptions due to a weak response of the polar vortex. They also explored the responses of global surface air temperature (SAT) in CESM large ensemble simulation.

Using a "perfect-scale" method and atmospheric-ocean general circulation model, Gregory et al. (2020) test the precision with which CO₂ effective climate sensitivity (ECS) can be measured in the "historical" time-frame from climate change. They note that the intrinsic variability in global models makes the estimation of historical ECS both biased and unpredictable. The reaction of the climate system to volcanic forcing induces a much stronger spatial trend of sea surface temperature change than in AOGCMs.

2.1.2 Volcanism induced decadal to centennial variability

Volcanic eruptions may be thought of as short-term forcing since their aerosols remain in the stratosphere for 1-2 years after they occur. Studies (Brönnimann et al. (2015), Timmreck et al. (2012), Jones et al. (2005)) have discovered evidence for decadal to centennial-scale variability caused by volcanic eruptions. Sustained volcanic activity has also drawn interest, and a series of volcanic explosions have been claimed to affect the climate on decadal scales (Church et al. (2005)). For the hypothesis of the Little Ice Age being brought on by increased volcanic activity, experiments using coupled climate models have been explored (Zhong et al. (2011), Schneider et al. (2009)). The climate system's long-term volcanic signal has been attributed to the ocean's long-term memory (Gregory (2010), Shiogama et al. (2010), Gleckler et al. (2006), Delworth et al. (2005)).

Slawinska and Robock (2018) used the NCAR CESM climate model to examine decadal to centennial-scale variability during the last millennium. The scientists looked for times reminiscent of the Little Ice Age when Arctic sea ice anomalies were positive. They then studied the variability on a decadal to centennial time scale induced by various external forcings and internal model variability. Finally, they try to figure out what triggered the Little Ice Age and what function sea-ice ocean feedback played in it. According to the findings, Arctic Sea Ice and Atlantic Meridional Overturning Circulation both showed considerable positive changes after the eruption. For volcanic forcing, they discover that the model creates circumstances similar to those of the Little Ice Age but with a smaller magnitude.

2.1.3 Hydrological response to volcanic eruptions

ITCZ position has been observed to migrate south after volcanic eruptions in the last millennium, according to research done by Ridley et al. (2015) on the effect of volcanic eruptions. A change in hemispheric temperature gradient can cause the ITCZ to move (Schneider et al. (2014), Kang et al. (2008), Broccoli et al. (2006)). The location of the ITCZ impacts the monsoons, which influence the lives of billions of people in South and Southeast Asia. It's critical to understand how volcanic eruptions affect precipitation, which directly influences the hydrological cycle. Except for a few studies that report an increase in the precipitation response after an eruption because of a change in the land-sea thermal gradient (Joseph and Zeng (2011)), the majority of modelling studies and proxy records show a consistent decrease in rainfall after volcanic eruptions (Carley E. Iles and Schurer (2015), Trenberth and Dai (2007), Gillett et al. (2004), Broccoli et al. (2003), Robock and Liu (1994)). When it comes to precipitation following an eruption, the proxy data indicates a distinct pattern. Nakatsuka (2015) and Anchukaitis et al. (2010) illustrate this pattern. The volcanic plume is directly injected into the stratosphere. This results to a change in the gradient due to a rise in tropical tropopause temperature. The stratospheric water vapour displays a rising trend after volcanoes when compared to the tropospheric water vapour.

The study by Paik and Min (2018) used Superposed Epoch Analysis to look at extreme temperature and precipitation data from CMIP5 models for five recent volcanic eruptions. Beyond the inherent variability of the models, a fall in temperature was seen in the year after the eruption. The monsoon zones see the most outstanding amount of this cooling. In addition, all models show a comparable decline in precipitation above and beyond the models' internal variability, which is also seen in the monsoon areas.

2.1.4 Impact of location & season of volcanism on climate response

After the two high-latitude eruptions in 2008 and 2009, the location of volcanic eruptions has become critical in researching their influence on the climate system (Sarychev and Kasatochi eruptions). The climate is considered to be affected more by tropical eruptions than by those in high latitudes. Timmreck et al. (2012) discovered that integrating volcanic eruptions at high latitudes led to a model that replicated the winter warming caused by volcanoes. The Laki 1783 eruption affected the Asian monsoon system, according to Schmidt (2012). They also discovered that if a Laki-type explosion occurred now, it would cause major health-related problems across Europe. Volcanic eruptions have varying climate impacts depending on the season of year they occur. On the other hand, Kravitz and Robock (2011) discovered that the magnitude of an eruption takes precedence over its location. The distribution of volcanic aerosols in the troposphere and stratosphere is also determined by seasonal variations in atmospheric circulation patterns. The radiation budget of the Earth's system may be modulated by powerful volcanic eruptions, which can indirectly affect vegetation and the global carbon cycle.

Zuo et al. (2018) looked at the impact of volcanic eruptions in the northern, southern, and tropical hemispheres on tropical Pacific SSTs during the latest CESM millennium-scale ensemble run. Dogar (2018) showed the role of tropical volcanoes and found that they decrease the Hadley circulation and shift the ITCZ towards the equator. Reanalysis data, observations, and earlier studies are used to confirm the findings, which can have a significant influence on South Asian precipitation.

Based on ensemble simulations conducted using the Community Earth System Model, the impacts of the northern high-latitude volcanic (NHV) explosions on El Niño-Southern Oscillation are explored in Sun et al. (2019). The seasonal nature of the atmospheric circulation affects the dispersion of aerosols from the NHV. It causes the Northern Hemisphere to cool stronger/weaker after the eruptions of January and April (July and October). The reaction of ENSO is more seasonal, with the explosion in January causing El Niño in the eruption year, while El Niño occurs in year (1) after the eruption in October. After the April - July eruption, there was no significant El Niño.

2.1.5 Volcanic eruptions and climate change

Using paleoclimatic proxy records dating back to 17.7 ka, McConnell et al. (2017) found a link between the glaciation and a series of 192 years of volcanic eruptions that were halogen-rich and resulted in a dramatic drop in stratospheric ozone levels. As a result, volcanic forcing plays a critical role in triggering climate change on various scales. Yost et al. (2018) studied

the influence of the 74 ka Toba eruption and its closeness to a human population bottleneck during that time to understand better how volcanic eruptions affect human evolution. Various proposals to halt climate change have utilized volcanoes as analog and natural examples of geo-engineering. Volcanic eruptions have thus influenced geoengineering techniques and concepts. Previous model-based studies that favored geoengineering as a potential strategy for combating global warming may have exaggerated its efficiency by over 20%, according to Plazzotta et al. (2018). Further complicated reactions to biodiversity, agriculture, ecology, health, and climate change by geoengineering solar radiation management might impair the earth's system if these approaches are abruptly terminated (Trisos et al. (2018)).

Slawinska and Robock (2018) study the triggering of Little Ice Age and centennial-scale cooling accompanied by NH sea ice expansion in the context of volcanic eruptions using last millennium simulations of the NCAR CESM model. They define the Little Ice age as periods with enhanced Arctic sea ice and explain decadal to centennial-scale response in the global climate model. The poleward oceanic heat transfer is anti-correlated with the Arctic sea ice extent. Strong volcanic eruptions can enhance both the Atlantic meridional overturning circulation and Arctic sea ice on decadal time scales. Arctic sea ice extent oscillations dominate the coupled fluctuations of Arctic sea ice and AMOC after volcanic eruptions. In reality, the immediate radiative forcing resulting from volcanic eruptions and solar decrease can cool the North Atlantic and Pacific enough to force the Arctic into a cold climate that persists after the forcings disappear. Multidecadal decoupling of AMOC and the Arctic may be linked with the abrupt emergence of such AMOC drivers as mid-Atlantic freshening decrease, subpolar gyre reinforcement and profound convection intensification in the Labrador Sea. Post strong volcanic eruptions and a few decades of AMOC reinforcement, a long period of AMOC weakening occurs, leading to a new system of mean overturning circulation on a centennial-scale which is considerably weaker than the mean for the control run. While the favorable Arctic marine-ice anomalies resulting from radiative cooling are considerably lowered during strengthening AMOC periods, the Arctic sea-ice anomaly is ultimately mildly positive with a weaker AMOC for over a century.

Duan et al. (2019) study solar geoengineering as a possible solution to combat global warming using volcanic eruptions as a proof-of-concept. They use the NCAR CESM model to evaluate the climate feedbacks to two highly idealised stratospheric aerosol forcings of different durations: a short-term pulse reflecting volcanic eruptions and a long-term continuous geoengineering impact. Their findings indicate distinction in climate reaction to volcanic and geoengineering stratospheric aerosol forcings. They suggest that caution should be practised when extrapolating volcanic eruption findings to geoengineering deployments. Stocker et al. (2019) focus on smaller volcanic eruptions and their role on climate. They discuss that large eruptions release aerosols in the stratosphere, and less attention has been given to small eruptions. They show that the vertical trend of temperature has a significant contribution from the smaller volcanic eruptions.

Guillet et al. (2020) studied the impact of a series of volcanic eruptions that erupted from 1108 to 1110 but have not been studied in detail. They show that a dust cloud over Europe was associated with a series of volcanic blasts. These eruptions have been documented by the observers of those times, and changes in climate can be noted from these. Xu et al. (2019) discuss the stratospheric ozone and volcanic eruption. They argue that although the ozone layer has recovered due to worldwide legislation, volcanic eruptions may damage the ozone layer in the stratosphere. They use a transport model and a combined chemical-climate model to predict the ozone depletion impacts of super-volcanoes. Their results suggest that in the RCP8.5 100x Pinatubo scenario, the proportion of global mean total column ozone loss is around 6% relative to two years before the eruption and 6.4% in the tropics. Yang et al. (2019) study the symmetricity and asymmetric forcings by volcanic eruptions such as by Pinatubo (symmetric) and Santa Maria/Agung(asymmetric). They find that asymmetric forcings adjust the latitude of tropical rainfall characteristics, contributing to larger local precipitation / tropical cyclone shifts. They argue that the distribution of volcanic aerosols towards climatic impacts needs to be addressed when analysing the role of global and regional climate volcanoes. Hermanson et al. (2020) use models performing decadal climate predictions and study the role of volcanic aerosols in decadal predictability. They compare models and observations for the three volcanic eruptions during the well-observed time since 1850.

Recently Gupta et al. (2019) have shown that the oscillations of Earth's climate between different states (warm, cold and snowball) can occur if sufficiently large volcanic eruptions sustain for decades. They conclude that volcanic explosions of the order of -100 W/m² should occur continuously over several decades to transform the planet to a snowball state completely. Their transition time is much more than the previous studies, and they find out that the entire ocean depth should reach a freezing point for freezing to start at the surface. However, this is only true if starting from a warm state, if starting from a cold state, then the time scales are of the order of tropical thermocline only. Starting from a cold state would also require decades of eruptions like Toba to transform Earth completely into a snowball. Volcanic eruptions are not only significant from the context of monsoon hydroclimate. Rather their role in depleting ozone layer has been quantified in Xu et al. (2019), wherein a super eruption 100x of Pinatubo has been estimated to lead to a depletion of total column ozone up to 6.4 % in tropics.

Using a coupled climate model, Brönnimann et al. (2019) study the global climatic effects of the 1808 or 1809 eruption whose source is unknown and the 1820s and 1830s eruptions which have received less publicity. They note substantial summer temperature decreases across the Northern Hemisphere land areas following the eruptions. In addition, they show that simulated ocean – atmosphere cooling sustained several years after the volcanic outbreaks, in addition to two decades of drought struck Africa, weakened global monsoons, and southward shift in the tracks of low-pressure systems across the North Atlantic. They conclude that the Little Ice Age end was characterised by recovery from a series of volcanic eruptions, making it difficult to establish a single pre-industrial baseline.

Hu et al. (2020) studied the Late Ordovician Mass Extinction (LOME), which killed about 85% of marine organisms worldwide and was ranked the second most extreme Phanerozoic biotic crisis. Global cooling and habitat destruction resulting from waxing and diminishing glaciers is historically considered to have triggered LOME. However, glaciation processes and subsequent sea-level rise were possibly more complex than initially thought. Temporal shifts in global redox conditions that could synchronise with LOME pulse remain elusive. The authors record pyrite sulphur isotope data from two sedimentary successions from South China and use a characteristic signal from stratospheric photochemical reactions to restrict the existence of volcanic eruptions during Late Ordovician. The findings provide new evidence relating stratospheric volcanic eruptions to the LOME.

Camargo and Polvani (2019) study the fascinating question of whether volcanic eruptions can play a role in tropical cyclone (TC) activity. In general, volcanic aerosols released by volcanic eruptions into the stratosphere reflect incoming solar radiation, causing lower sea surface temperature (SST) leading to poorer and lower TCs. Moreover, the TC intensity is directly proportional to SST and inversely proportional to outflow temperature. In the North Atlantic, hurricane frequency increase 3–4 years after large volcanic eruptions has been reported in the observations. The authors investigate whether volcanic aerosols have decreased recent global TC activity. They have evaluated previous findings, reanalysis products, and numerical models. They note that due to very few major volcanic eruptions during the historical TC records, models are critical to address this issue.

Dogar and Sato (2019) aim to better understand and evaluate the Middle East, Africa, and South Asia's regional climate response and vulnerability to major explosive volcanic eruptions in the summer season. They use an atmospheric general circulation model with a very fine spatial resolution equivalent to regional climate model resolutions. Then, they simulated the impact of recent well-observed volcanic activities on the Middle East, African and South Asian monsoon areas. The use of a high-resolution simulation methodology makes this study exceptional. They mainly focus on the following issues, viz. (a) What are the consequences of volcanic eruptions and ENSO teleconnections on African and South Asian monsoon regions? (b) What is the actual radiative and indirect effect of volcanic eruptions on the Middle East, Africa, and South Asia? And (c) How well can a high-resolution atmospheric model, replicate direct radiative and circulatory changes over monsoon regions? This study focuses on the surface responses rather than stratospheric response of the volcanic eruptions. Following the volcanic blasts, they report substantial warming and drying over the boreal summer monsoon regions. Sun et al. (2019) study the role of high-latitude volcanic eruptions in modulating ENSO with a particular focus on the season of eruption. The anomalous North Pacific Cyclone (NPC) evolves in early summer after the January eruption and interacts with a weak Asian summer monsoon exciting anomalous westerlies over the Indo-Western Pacific. The anomalous NPC and intensified East Asian winter monsoon bring cool air to the Maritime Plateau following the October eruption, warming the subtropical central North Pacific. Their findings indicate the

importance of the time of eruption as a crucial aspect of data-model comparisons of the impacts of volcanic eruptions on climate.

2.1.6 Volcanic forcing and climate modelling: Open challenges

To drive climate models for volcanic forcing, reconstructions of volcanic forcing have been created (Sigl et al. (2015), Gao et al. (2008), Robock and Free (1996), Sato et al. (1993)). Validation of the climate models utilizing the climate system's reaction to volcanoes is performed using the prescribed volcanic forcing. However, there are many gap areas related to the effects of volcanism on climate. Can volcanic eruptions trigger El Niños? Was the Little Ice Age caused by a rise in the number of volcanic eruptions? To what extent should Winter warming be attributed to volcanic eruption or natural variability? The process by which winter warming happens is unknown. Only in observations can it be observed; thus why can't models replicate it? Estimating an eruption's power in relation to the South Asian Monsoon is necessary. There needs to be a better understanding of the relationship between volcanic eruptions and summer monsoon decrease (in models), and winter warming and cooling at the surface. It's essential to examine how an El Niño and its accompanying climate forces respond to eruptions.

The review on volcanism and climate by Cooper et al. (2018) discusses pertinent questions concerning the interplay between volcanic eruptions and the climate, considering the important social and economic constructs created just around the aviation industry in the recent times. The ash coming out of the strong volcanic eruptions has the potential to reach the stratosphere and stay there for a couple of years, leading to global radiative cooling. It has been hypothesized that the Toba volcanic eruption of 75 kya could have led to prolonged cooling of the planet and hence the migration of ITCZ and circulation for centuries. It has been recently shown (Izumo et al. (2018)) that the tropical volcanic eruptions lead to a negative subsurface Indian Ocean Dipole response in the eruption year triggered by the westerlies driven by land cooling from tropical Africa. However, the surface response is an anomalously cold northwest Indian Ocean leading to a northwest southeast sea surface temperature gradient in the Indian Ocean. Camargo and Polvani (2019) have shown that the tropical cyclone activity is expected to remain the same following tropical volcanic eruptions. This is contradictory that volcanoes modulate TC as they are driven by sea surface temperatures.

2.1.7 Volcanism forced changes in atmospheric carbon

While all of the research demonstrates the importance of land in driving carbon-di-oxide variations due to volcanic eruptions (Rothenberg et al. (2012), Tjiputra and Otterå (2011), Brovkin

et al. (2010), Kravitz et al. (2010), Angert et al. (2004), Lucht et al. (2002), Jones and Cox (2001)), they differ in their mechanisms leading to the variability. Reduction in heterotrophic respiration owing to surface cooling increases the carbon storage in tropical and subtropical soils, which is one of the processes. Other mechanisms have suggested that higher latitudes absorb more carbon than lower latitudes do. Volcano-induced changes in diffuse radiation and changes in net primary productivity (Gu et al. (2003)) are two significant processes that these analyses overlook (Duggen et al. (2010)). This is because the photolysis rates are changed due to the stratospheric volcanic aerosols scattering and reflecting the incoming solar radiation, as shown by Graf et al. (2007) and Textor et al. (2004). Trace gases are carried into the stratosphere by buoyancy due to stratospheric heating. Due to chemical processes taking place over aerosol surfaces, nitrogen oxides are reduced while chlorine activation increases Equivalent effective stratospheric chlorine (EESC) while reducing ozone (Tabazadeh et al. (2002), Tie and Brasseur (1995)). Scientists have been able to understand better how volcanic aerosols affect the climate system using cutting-edge climate models. The first of its sort in the modern age, the Mt. Pinatubo eruption has contributed dramatically to our understanding of the impact of volcanoes on the climate (Robock (2002)). Recently, several modeling groups have attempted to comprehend the function that volcanoes play in modulating the climate (Maher et al. (2015), Pausata et al. (2015), Swingedouw et al. (2015), Santer et al. (2014), Driscoll et al. (2012), Emile-Geay et al. (2008), Fischer et al. (2007), Yokohata et al. (2005)).

2.1.8 Volcanic eruptions and ENSO

The changing evolution of ENSO forced by strong volcanoes has been studied by Wang et al. (2018). They report a negative-positive-negative response of ENSO to strong volcanic eruptions. The first stage is a very short lived La Niña, which might be even sometimes missed by a lot of analysis due to its weakness and duration, followed by an El Niño in the next year following the eruption, which a La Niña again follows in the second year after the volcanic eruption. They base their results on the Bjerknes feedback. A La Niña like cooling in the initial state of the Tropical Pacific associated with a stronger cooling over the maritime continent leads to an east-west gradient in the sea level pressure, thus changing the wind anomalies leading to an El Niño. Now from the El Niño conditions, the cooling caused by the volcanic eruptions leads to a discharge in the thermocline state in the west Pacific, taking the system back to a La Niña like state.

Dee et al. (2020) show that the vulnerability of El Niño – Southern Oscillation (ENSO) to external forcing remains unclear. They note that the modeling studies indicate susceptible changes in ENSO to sulphate aerosol forcing associated with explosive volcanism with little support from observations. Hence they use superposed epoch analysis on proxy data to show a poor propensity of El Niño-like response in the year after an eruption, however statistically

insignificant. They use fossil corals from the central tropical Pacific to estimate this response. They suggest that climate models overestimate the reaction of volcanic eruptions to ENSO. The predictions of climate models to greenhouse gas emissions depend crucially on the accurate response of ENSO to external forcing. Although global climate models may rely on ensembles to increase signal-to-noise ratios, the paleoclimate proxy reconstructions are limited to one realisation, limiting proxy records' capability to detect ENSO changes from model-based targets. The volcanic response of major climate modes like ENSO is crucial to evaluating regional climate impacts under solar radiation management scenarios. Hence a comparison of proxy records to model simulations is essential for a rigorous assessment of the climate effects of sulphate aerosol-induced geoengineering scenarios.

Fang et al. (2020) study the relationship between volcanic eruptions and ENSO to understand better how they interact and drive global or regional extreme climate events. They compare 195 major volcanic eruptions (Volcanic Emissivity Index >4) with the types and magnitudes of 398 ENSO events present in the 0–2 years following the eruptions from 1525 to 2000 and analyse the relationship between major volcanic eruptions and ENSO events. They show that from 1525–2000, the ENSO events that occurred within 0–2 years of a large volcanic eruption were greater than those without a volcanic eruption; the ratio of El Niño to La Niña events changed from 2:3 to 1:1. After a massive volcanic eruption, weak El Niño events occurred more often than all other forms in all 0–2 years. Although powerful La Niña events occurred in the 0th year and +1 year after the volcanic eruptions, moderate La Niña events were more frequent in the +2 year. The results were based on paleoclimatic reconstructions.

2.1.9 Volcanism forced ENSO-Indian Monsoon coupling and hydroclimate response

Stratospheric Aerosols induced global radiative cooling from strong volcanic eruptions have been postulated to be the reasons behind crop failure, famine, social disruption, drought, summer-free year, fall of empires due to the climatic impacts of these eruptions (Newhall et al. (2018)). The role of aerosols, which broadly includes other natural aerosols such as dust, sea salt etc. and those of the anthropogenic origin, have been of interest (particularly concerning the Indian Monsoon) to the scientific community in recent times (Vinoj et al. (2014), Bourassa et al. (2013), Ganguly et al. (2012), Bollasina et al. (2011), Lau et al. (2008), Niyogi et al. (2007), Lau et al. (2006)). The uncertainty due to aerosols in present-day global climate models has been shown to be the largest source of error in simulations (Stocker (2014)). Recent attempts in the development of climate models, including the incorporation of aerosols, have shown promising results in improved monsoon teleconnections with other climate variables (Swapna et al. (2018)). Much research has gone into understanding the role of non-volcanic aerosols (e.g. Bollasina et al. (2011)), the understanding of the impacts of volcanic eruptions on the Indian

Monsoon and the ENSO-Indian Monsoon teleconnection remains limited.

Gao and Gao (2018) use multiproxy May to September rainfall reconstruction for the five major volcanic eruptions since the industrial revolution to show the hydroclimate response of Asian Monsoon system to the strong volcanic eruptions. Their results are consistent with the reanalysis datasets and past studies (Cui et al. (2014)). They attribute the rainfall deficit to negative anomalies in the southerly winds from the ocean to the Monsoon region. These anomalies are, in turn, a result of the reduced land-sea thermal contrast. We can see that in the years +1 and +2 relative to the volcanic eruption, there is a significant dryness over the Indian landmass. In contrast, in the year +3 there is a wet monsoon type of behavior over the South Asian domain. These precursors should be kept in mind considering the hypothesis on the enhanced coupling of ENSO and Indian Monsoon systems following a volcanic eruption. Whereas studies such as Wang et al. (2018) have shown an increase in the phase speed of ENSO system, the drought and wet monsoons in Gao and Gao (2018) exactly coincide with the El Niño in year +1 and La Niña in the +2 to +3 years.

The role of the Indian Monsoon in modulating the temperatures over the Tibetan Plateau in the context of the volcanic eruptions is discussed in Duan et al. (2018). Indian Monsoon precipitation is the major source of rainfall for the total precipitation occurring over the Tibetan Plateau. The drought years over India are also associated with reduced cooling of the Tibetan Plateau landmass in summer. The volcanically induced ENSO-Indian Monsoon coupling can thus also play a role in the variability of surface temperatures over Tibet in summer.

Zanchettin et al. (2019) have also emphasized the importance of initial conditions to the extent that they claim uncertainties arising out of initial conditions to overwhelm the variability caused by volcanic radiative forcing. They use the strongest volcanic eruption of the last 500 years, i.e. the 1815 eruption of Mount Tambora, to have a strong signal to noise ratio to prove this point. Ménégoz et al. (2018b) have shown the role of Atlantic Multidecadal Variability (AMV) in modulating the climate response to volcanic eruption. They find a weakened Hadley Circulation following the volcanic eruption irrespective of the phase of AMV in the initial years and inhibition of negative NAO phase further supported by the cold phase of AMV. Blake et al. (2018) show the response of Australian precipitation due to explosive tropical volcanic eruptions. They use the NASA GISS ModelE2-R last millennium simulations conducted as a part of the PMIP3 CMIP5 activity. An El Niño and positive IOD response in the year following the eruption along with enhanced precipitation over SE and NW Australia is reported by the study. The work citing the importance of volcanic eruptions concludes that although El Niño and positive IOD lead to a rainfall deficiency in Australia, the direct effects of volcanic aerosols overrides the precipitation response due to ENSO and IOD.

Alfaro-Sánchez et al. (2018) study the movement of the northern boundary of the tropics, which impacts the hydrology of various regions of NH due to volcanic and anthropogenic forcings. They base their work on the existing literature suggesting a widening of the tropical belt

due to human induced factors. The role of natural forcings in determining the width of tropical belt is poorly understood. They use paleo-climatic datasets from tree rings from diverse regions to reconstruct the positions of the northern boundary of tropical belt for the last 800 years. They report the belt's contraction (expansion) during El Niños (La Niñas). They also find a reduction in the width following strong volcanic eruptions. Their work is a caution on the global warming halting proposals by the geo-engineering community involving the injection of aerosols into the stratosphere. Hopcroft et al. (2018) report a reduced global cooling following strong volcanic eruptions in a warmer world in future. They attribute these changes to the increased tropospheric albedo due to aerosols and reductions in sea ice. An increase of Tropospheric height, which can lead to lesser ash entering the stratosphere, can add to the reduced cooling by volcanic eruptions. Volcanic eruptions have been reported to lead to mass extinctions of life in the past, e.g. end-Permian mass extinction (around 250 million years ago) was caused by the voluminous degassing from volcanic eruptions leading to the extermination of 70 % of all life on the land(Cui (2018)).

The hydro-climatic response of volcanic eruptions depends upon the location (latitude) of eruption and which has a direct impact on the monsoon regions around the globe (Zuo et al. (2019a)). Stratospheric volcanic aerosols are well mixed along a latitude circle due to circulations in the stratosphere but have variability across the latitudes. The impacts on Monsoon systems due to the latitudinal variability of volcanic response is not well understood. Using a variety of datasets, Zuo et al. (2019a) study the impacts of volcanic eruptions at different latitudes on net primary productivity, surface runoff and extreme rainfall. They conclude that volcanic explosion in one hemisphere reduced the monsoon related precipitation in that hemisphere. They corroborate the results based upon instrumental data, model simulations using CESM and attribute this contrasting result to the dynamics in the atmosphere. The physical mechanism of this is broadly related to the weakened land-sea thermal contrast, cross-equatorial flow and walker circulation. They find out the reduction in NH monsoon precipitation after northern eruptions and an increase after southern eruptions and vice versa by the thermal contrast. In the case of tropical eruptions, the reduction is enhanced by the El Niño like conditions that develop in the east-central Pacific. They point to the vital role of volcanic eruptions in the decadal predictability of the climate. Although tropical eruptions are considered the most important when understanding the response to volcanic eruptions is concerned, the study by Toohey et al. (2019) shows that extratropical strong eruptions in the NH can lead to 80 % higher radiative forcing over the NH as compared to that caused by the tropical eruptions.

Liang et al. (2019) explore the less-explored hydroclimatic anomalies induced by large volcanic eruptions using a network of tree-ring data in the central Himalayas. They have conducted superposed epoch analysis for the reconstructed proxy data since 1650. They find that the droughts over central Himalayas are linked to volcanic eruptions and that the Tambora eruption followed the most severe of them. The assassination of Julius Ceasar in 44 BC led to a control struggle, finally leading to the fall of the Roman empire. McConnell et al. (2020)

note that this was accompanied by a period of extreme weather, hunger and disease in the Mediterranean region. A volcanic eruption was pointed out to be the reason for the anomalous weather. The authors conducted modeling study indicating that radiative push from this is huge, high-latitude eruption contributed to pronounced hydroclimate changes. The temperature of the Mediterranean regions fell 7° C below average during 2-year duration of the eruption. The volcanic eruption led to the destruction of crops, famine, disease intensification and social unrest contributing to the political realignment of the Mediterranean society. Ning et al. (2020) analyse altitude-dependant variations in temperatures to volcanic eruptions in the last millennium. Since these high-altitude/high-mountain regions play a vital role in global irrigation supply feeding huge global populations, assessing the impact of volcanic eruptions on these high-altitude regions becomes important. Zuo et al. (2019b) study the role of volcanic eruptions on arid regions. The study over arid areas is important as they cover 41% of the terrestrial land surface of Earth and around 38% of the world's population dwells in these regions. The understanding of hydroclimatic impacts to volcanic eruptions over arid regions is limited. The authors analyse CESM last millennium ensemble simulation data and find enhanced precipitation over global arid areas due to circulation changes.

2.2 Natural and anthropogenic aerosols in the South Asian climate system

Anthropogenic aerosols, which constitute black carbon, sulphate and others, are emitted into the atmosphere by human activities. Past studies have pointed that the anthropogenic aerosols can lead to suppression or enhancement of precipitation over the Indian subcontinent at varying spatiotemporal scales (Aadhar and Mishra (2021), Undorf et al. (2018), Jin et al. (2016), Krishnan et al. (2016), Jin et al. (2015), Bollasina et al. (2014), Chakraborty et al. (2014), Jin et al. (2014), Vinoj et al. (2014), Ganguly et al. (2012), Bollasina et al. (2011), Krishnamurti et al. (2010), Wang et al. (2009), Meehl et al. (2008), Chung and Ramanathan (2006), Lau and Kim (2006), Chung and Seinfeld (2005), Ramanathan et al. (2005)). A combination of naturally transported dust from the Middle East and locally emitted anthropogenic aerosols is the most probable mixed state of aerosols over the region (Sanap et al. (2015), Kedia et al. (2014), Srivastava and Ramachandran (2013), Kaskaoutis et al. (2012a), Dey et al. (2008)). This mixed state of natural-anthropogenic aerosols is responsible for the radiative impacts of aerosols over the region. Past studies have explored the relationship between aerosols and Indian monsoon while also studying the interactions between land-atmosphere coupling and Indian monsoon (Ganeshi et al. (2020), Lodh (2020), Halder et al. (2018), Dirmeyer and Halder (2017), Dirmeyer and Halder (2016), Halder et al. (2016), Halder et al. (2015)). In addition, Niyogi et al. (2007) proposed that the role of coupled aerosol-land-atmosphere framework should be studied owing to

the importance of land surface processes for the South Asian domain.

2.2.1 Natural dust and anthropogenic aerosols: Response of Indian monsoon

Precipitation suppression and enhancement as the response of aerosols over the Indian region occur at different spatio temporal scales (Aadhar and Mishra (2021), Fadnavis et al. (2020), Undorf et al. (2018), Jin et al. (2016), Krishnan et al. (2016), Jin et al. (2015), Bollasina et al. (2014), Chakraborty et al. (2014), Jin et al. (2014), Vinoj et al. (2014), Ganguly et al. (2012), Bollasina et al. (2011), Krishnamurti et al. (2010), Wang et al. (2009), Meehl et al. (2008), Chung and Ramanathan (2006), Lau et al. (2006), Chung and Seinfeld (2005)). Ramanathan et al. (2005) attribute the increase in precipitation to distant aerosols, whereas the reduction in monsoon rainfall is attributed to local aerosols. Other studies which have used global or regional models, have found that faraway aerosols, such as those from Tibet or the Middle East, consistently improve the rainfall. In contrast, local aerosols suppress the precipitation by altering radiation, circulation.

2.2.2 Land-atmosphere interactions and Indian monsoon

Land-atmosphere interaction in the Indian subcontinent has received only a limited amount of attention (Budakoti et al. (2021), Hsu and Dirmeyer (2021), Lodh (2020), Dirmeyer et al. (2018), Halder et al. (2018), Dirmeyer and Halder (2017), Morwal et al. (2017), Dirmeyer and Halder (2016), Halder et al. (2016), Halder et al. (2015), Dirmeyer et al. (2013), Dirmeyer (2011), Delworth and Manabe (1989),). In this field, a series of publications by Halder and Dirmeyer constitute a substantial portion of the research done. Several hypotheses have been advanced to explain how land-atmosphere interactions influence the Indian summer monsoon's frequency and intensity. The soil moisture content and memory of the soil are the most essential factors in improving the predictability of the Earth system resulting from land surface activities. Other factors, such as the leaf area index, land use/land cover, and the Bowen ratio, also contribute to the skill of precipitation in coupled ocean-atmosphere-land general circulation models, as does the land surface temperature.

Anthropogenic aerosols and associated land-atmosphere interactions within South Asian monsoon

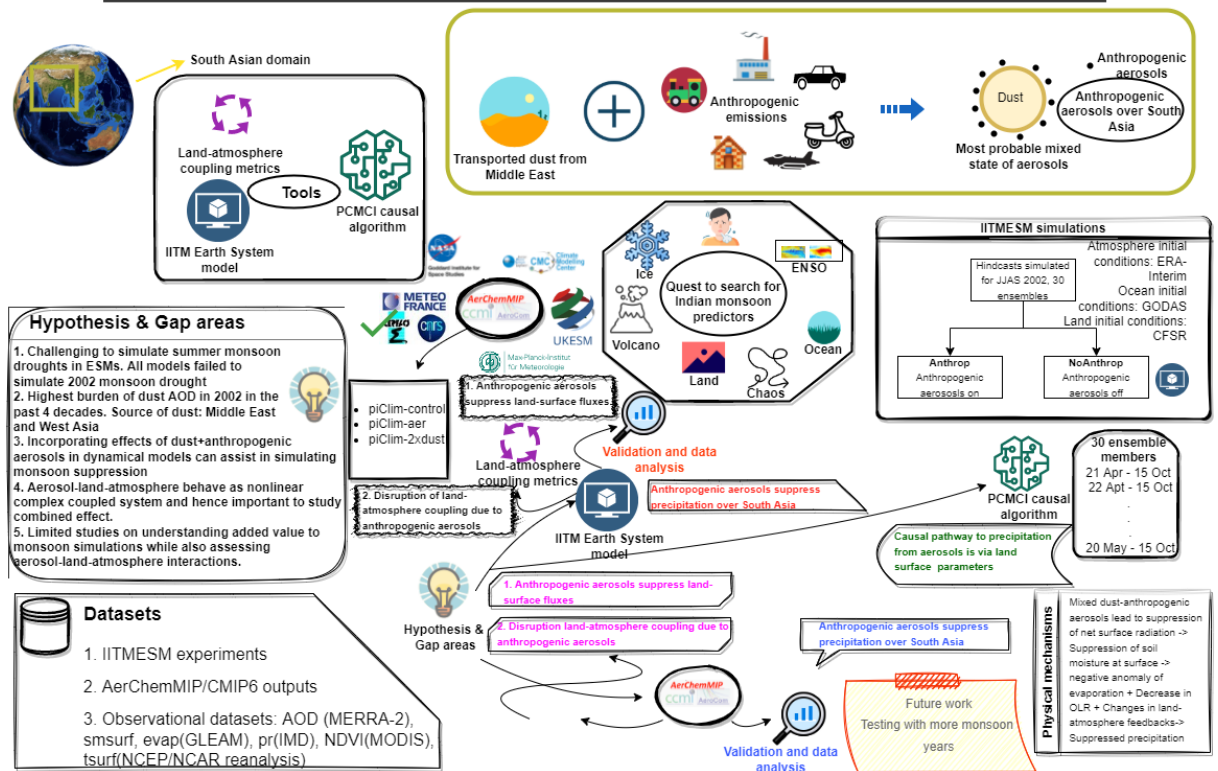


Figure 2.1: Aerosol-land-atmosphere interactions within the framework of South Asian monsoon

2.2.3 Mixed state of dust and anthropogenic aerosols over the Indian region

Natural and anthropogenic aerosols over the Indian subcontinent are the two main emissions categories. Dust from the Middle East and North Africa carried into the South Asian area is a primary source of natural aerosols. On the other hand, anthropogenic aerosols are composed primarily of black carbon and sulfate particles and have local origins. The observational patterns across the whole region demonstrate that anthropogenic emissions have increased in aerosol loading. This rise in aerosol loading has also resulted in changes in the radiation and circulation resulting in increased rainfall variability. After conducting an observational investigation, Kedia et al. (2014) discovered that the particles carried from the west of India (the Middle East and Sahara), which is known to include mineral dust, combine with BC to produce the most probable condition of aerosols when both particles are present. Pre-monsoon aerosol mixing states, according to Dey et al. (2008), include black carbon covering on dust, which is the most probable state of mixing. On the other hand, there are seasonal changes in the most probable mixed state aerosols (mineral dust that has been coated with black carbon) (Srivastava and Ramachandran (2013)). Experiments such as the Cloud Aerosol Interaction and Precipita-

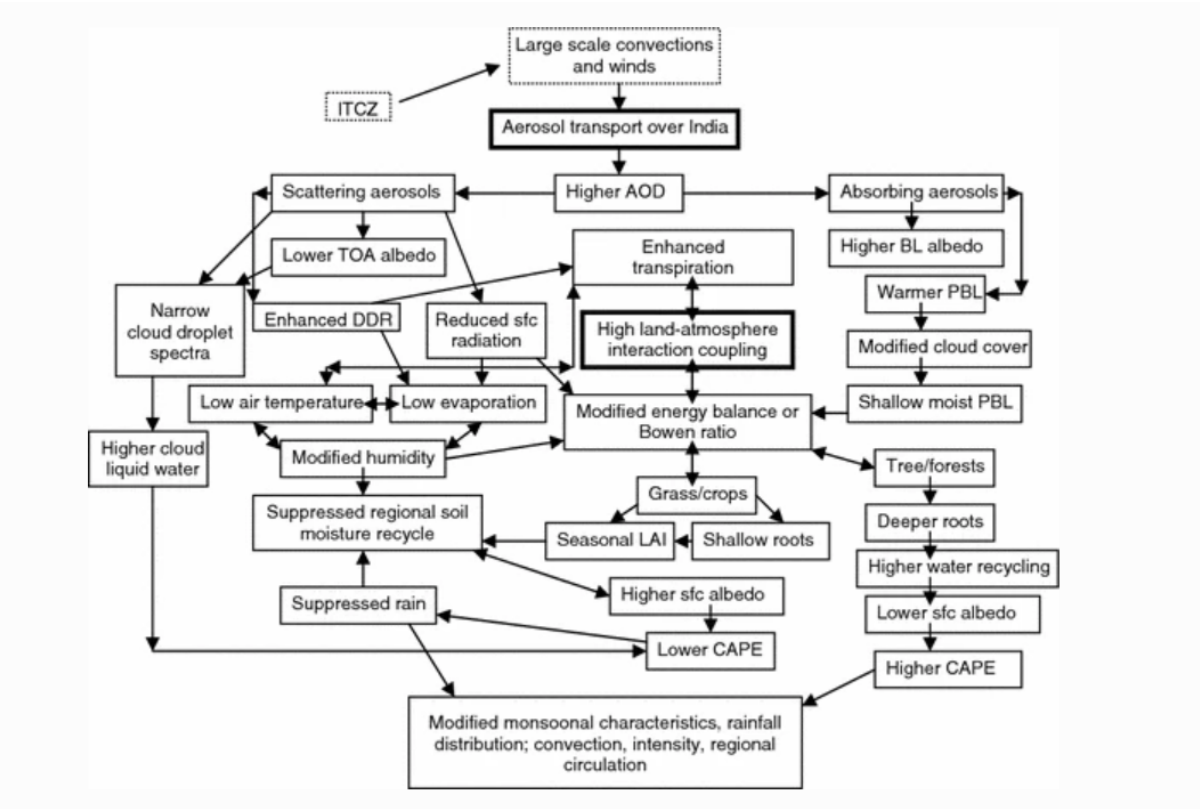


Figure 2.2: Potential aerosol–land–atmosphere interactions, as well as surface, convection, and precipitation feedbacks, in the monsoonal systems. Niyogi et al. (2007) Reproduced with permission

tion Enhancement Experiment (CAIPEEX) have revealed higher aerosol loading at 2–5 km from the surface, despite the presence of increased precipitation. Previous research on aerosols and the Indian monsoon (for example, Sanap et al. (2015)) suggest that a large quantity of aerosols over the Northern Indian region consists of transported natural desert dust that has been coated with black carbon. Because of the complexity and non-linearity of the aerosol response to the hydrological cycle across South Asia, it is embedded within other global teleconnections such as ENSO and IOD (Ayantika et al. (2021), Singh et al. (2020), Goswami et al. (2006), Krishnan and Sugi (2003), Ashok et al. (2001), Sikka (1980)). The response also varies depending on the kind of particles present (scattering versus absorption).

2.3 Research objectives

The objectives were designed for this doctoral thesis after the literature survey and the identification of gap areas in the understanding of climate response over South Asia to aerosol forcing. The thesis aims at developing a better understanding of the role of natural/volcanic and anthropogenic aerosols in modulating the tropical ocean-atmosphere-land coupled system and the

South Asian monsoon. The objectives of this doctoral thesis are twofold and as listed below:

1. To understand the role of volcanic eruptions on the coupled ocean-atmosphere-land system using observations and numerical modelling studies.
 - Understand the role of volcanic eruptions on the ENSO-Monsoon system with a special focus on South Asian Monsoon using observations, proxy data from paleoclimatic records and CMIP5/PMIP3 model simulations.
 - Conduct targeted model simulations using IITM-ESM to build upon the results from observational data.
 - Analysis of the data from simulations to understand the mechanism behind the volcanic link to South Asian Monsoon via ENSO.
2. To assess the potential predictability emerging out of incorporating the anthropogenic and volcanic aerosols in IITM-ESM
 - Conduct simulations with the newly developed aerosol module in IITM-ESM for its role in additional skill for the predictability.
 - Analysis from simulations to understand the role of volcanic and anthropogenic aerosols in potential predictability.

This page was intentionally left blank.

Chapter 3

Volcanism induced phase coherence of ENSO and Indian monsoon

3.1 Synchronization

Early in the 17th century, Christian Huygens, a Dutch scientist noted his ideas on optics and building clocks and telescopes, became the first to notice and explain synchronization. He was inspired by how pendulum clocks hung together when he was young. Because one clock always had its pendulum moving counterclockwise, he realized the oscillations had synced and were precisely timed.

3.1.1 Self-Sustained Oscillator

This form of active self-oscillation system has an internal energy source and is characteristic of this type. The oscillatory motion is created by converting the stored energy into an oscillating signal. Self-sustaining oscillations continue to oscillate at a particular frequency until the energy source inside the oscillator is depleted. It may be theoretically characterized as a dynamical system that is not explicitly time-dependent. The self-sustained oscillator is independent of how the system transitioned from a transient to a steady state oscillation and only depends on the system's characteristics. It is in a condition of equilibrium and will revert to its original state

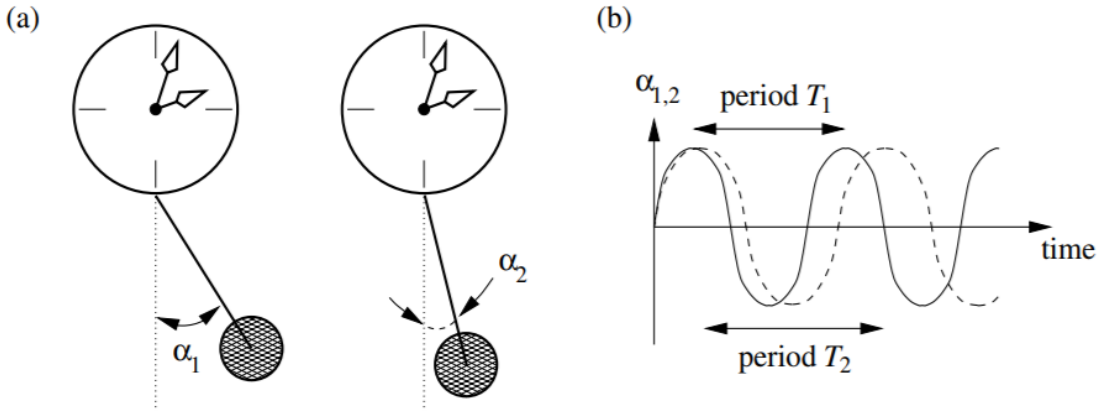


Figure 3.1: Two clocks which are ideally manufactured in the same way but the only difference in rhythm is due to error bars of production machines. The illustration is shown to visualize the interaction between two oscillators (Pikovsky et al. (2003)), Reproduced with permission

if there is a slight disruption.

3.1.2 Coupling of oscillating objects

Let's assume that we have two identical clocks, both made by the same manufacturer and sold to the same person. Even if the production machines' error bars are as close as possible to ideal, there will be moments of oscillation due to the slight variations. As a result, the time displayed by the two clocks would be slightly off, and the pendulums would be in somewhat different locations at that moment.

If the two clocks are now assumed to be linked and not isolated or independent, they will affect one another. Different sorts of interaction are possible; for example, say that a shared fixed beam supports the two clocks, as was the case with Huygens' observation. Any beam bending, vibration, or horizontal motion will be sent to the two clocks, causing them to interact or sense one another. Even if the shaft vibrates, it will show up in both watches to modify their rhythms. Two clocks oscillating precisely in synchrony can be determined by measuring their motion to see if they move simultaneously, which is a complex and time-consuming task. There may be a phase shift between the two oscillations due to the two clocks starting at different phase speeds. Depending on the difference in the systems' starting frequencies, it might be modest or significant. If the oscillators travel in opposite directions, they are in anti-phase. Huygens documented and discussed this in his writings. Phase locking refers to a connection that might develop between two oscillators' phases. A set of rules must be met to describe an oscillator system as synchronous.

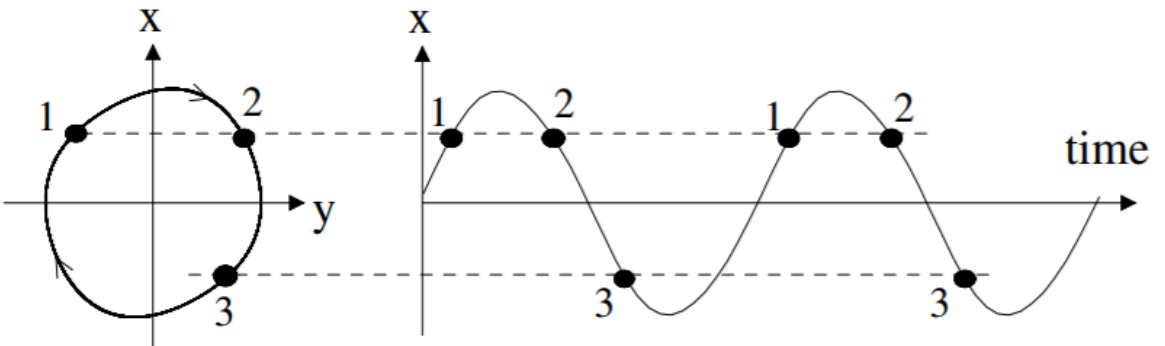


Figure 3.2: Phase space plot (left) for different states of the time series shown (right) (Pikovsky et al. (2003)), Reproduced with permission

For the oscillators in the system to drive their rhythms, they must be able to generate an internal energy source. Two oscillators' frequencies are adjusted as a result of weak contact. In other words, changing one oscillator causes the coupled oscillator to follow suit. If the coupling is too strong, it isn't synchronization; rather, the two oscillators function as if they were one. Synchronization is not the same as resonance. Hence, the phase space plot, commonly known as the limit cycle, suffices to explain self-sustaining oscillations. Systems internal characteristics determine the kind of cycle and the form of oscillation. The phase space plot or limit cycle looks like a circle if the oscillation is like a sine or cosine wave. Strong non-linear systems exhibit oscillations in various shapes. Almost all phase space plots are drawn to a specific state of the dynamical system by an attractor, a special sort of limit cycle. The limit cycle may be seen as a simple attractor using this definition. Chaotic systems create unlikely repulsions. As a result, a self-sustaining oscillator's internal energy source is a need. They are more stable to disturbances than conservative oscillators.

3.1.3 Phase

Physics and non-linear sciences utilize "Phase" differently. The state of the system in this phase space may be considered to be an identifiable phase point in non-linear sciences. In non-linear sciences, the system's time series plot depicts the phase point's progression across phase space. In other words, the phrases "phase transition" and "phase of oscillation" have varied meanings depending on the context. The amplitude and phase of an oscillation can be used to characterize it. When an oscillation is self-sustaining, the amplitude remains constant, but the phase can change at any time. One of the most intriguing things to consider is the stability of the phase point on the limit cycle or what may happen to the oscillation if the system is significantly disturbed. The phase point of the limit cycle is displaced when the system is perturbed. Rather than growing or decaying, the disturbance evolves in such a way that its amplitude shift is

reduced, yet its phase shift remains constant over time. An oscillator's phase may be changed by applying an external force, and the two can be brought into sync with each other.

3.1.4 Synchronization of Periodic Oscillators by External Force

Let's say that the frequency of oscillation of the oscillator is ω_0 and that of the external force is ω . The difference between these two frequencies $\omega - \omega_0$ is known as detuning. The effects of detuning caused by an external force in a rotating frame of reference are described below :

1. If detuning takes place without the application of a force, then the phase point oscillates with an angular velocity $\omega_0 - \omega$
2. It can be thought of as an object sliding down a slope whose speed increases with detuning.
3. A stable and unstable position on the equilibrium cycle is achieved in the presence of a force without detuning.

Phase locking can be defined as a state of the system during which there is a constant phase shift. It is one of the forms in which synchronization can be described. A non synchronous motion can have unbounded growth of phase difference whereas the phase difference is bounded in case of a synchronous motion. There is a constant phase shift between the oscillator and the external force such that

$$\phi(t) - \phi_e(t) = \text{constant} \quad (3.1)$$

Here the constant has a value equal to $\phi_0 + \delta\phi$. $\delta\phi$ depends upon the initial detuning.

In a plot of phase difference versus time, the region corresponds to a synchronization region if a horizontal line is encountered. Let the amplitude of forcing be fixed but the frequency is varied. Then initially in the synchronization region there would be zero detuning i.e. $\omega_0 = \omega$. Post this, if we see ω at the end of the synchronization region, then we can see how synchronization gets destroyed. If the detuning is increased from an initial state, then a constant phase shift occurs during a period of synchronization. Epochs of phase coherence can be observed in the systems as two oscillators which are always in synchronization can be considered as unified one. A phase slip might occur when the phase difference changes very fast by 2π . Repeated movement of the system into periods of constant phase difference and then into phase slips mean that a system oscillates synchronously with the external force for some time.

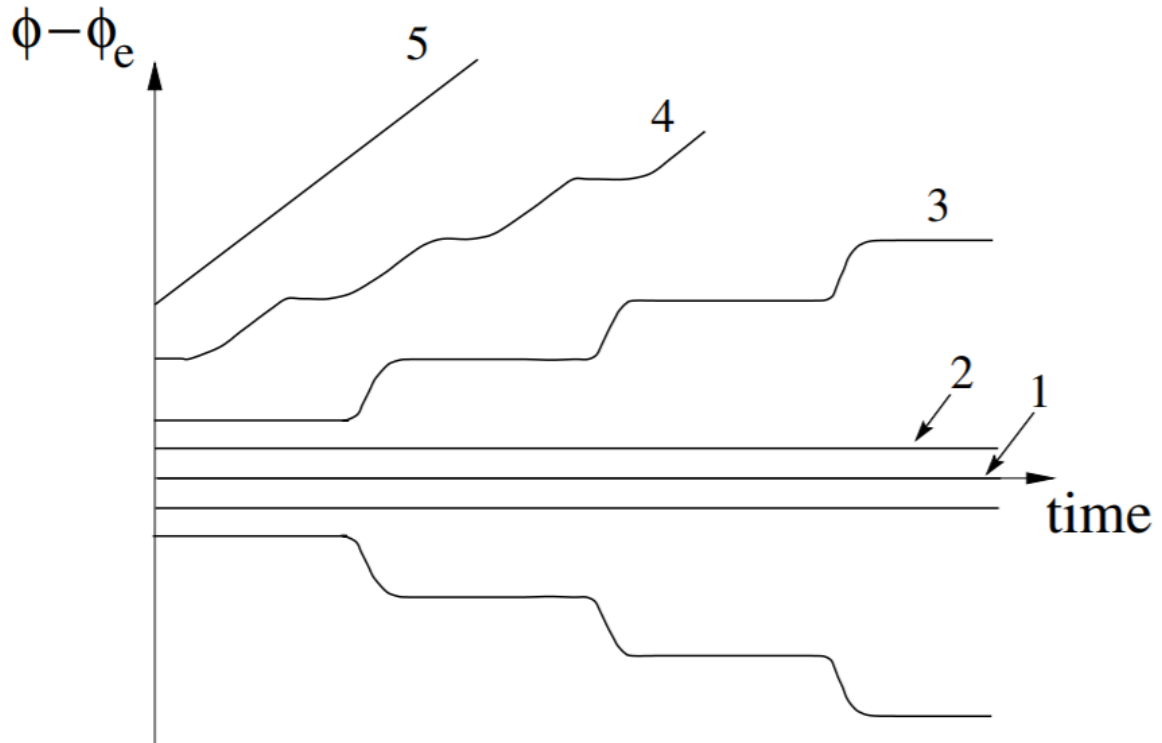


Figure 3.3: Dynamics of the phase at the synchronization transition. (Pikovsky et al. (2003)), Reproduced with permission

3.1.5 Two Interacting Oscillators

The discovery of synchronization was first done by observing two mutually coupled oscillators. There can be two ways in which synchronization is defined. One is frequency locking which corresponds to two systems that are non-symmetrical, i.e. both the oscillators influence each other, or one is more powerful. If one of the systems is very powerful than another, then it can be considered a case of external forcing, and then the system which is being driven is pulled towards the frequency of the driving system. However if both the oscillators influence each other, their frequency changes with time. Another type of synchronization that occurs is known as phase locking. In this type of synchronization, detuned frequency and strength of coupling determine how synchronization takes place and the role of how these systems are interacting is important. E.g. phase attractive or repulsive interaction in clocks can result in in-phase and anti-phase synchronization respectively. In the case of two uncoupled systems, when the following relation is obeyed

$$n\omega_1 \approx m\omega_2 \quad (3.2)$$

it is known as n : m synchronization. In this case the phases are also related to each other such that

$$|n\phi_1 - m\phi_2| < \text{constant} \quad (3.3)$$

3.2 Coupling of ENSO-Monsoon system

3.2.1 El Niño and Southern Oscillation (ENSO)

El Niño as a term was first used by the fishermen in Peru, which was associated with the warming of ocean waters near the coast during Christmas. In scientific terminology, the term is now used for a phenomenon which occurs in the eastern equatorial Pacific associated with the warming. However, there is no consensus on how much warming would qualify the event to be called an El Niño. An index Niño3, the average sea surface temperature (SST) anomalies in the region 90W-150W, 5S-5N is most commonly used as an index for El Niño. Southern Oscillation with El Niño is the see-saw of sea level pressure (SLP) or atmospheric mass over the east and west Pacific. The index to quantify Southern Oscillation is known as Southern Oscillation Index (SOI), the pressure difference between Darwin and Tahiti. El Niño Southern Oscillation, whose acronym ENSO, occurs about every 4 years with a band of 2-7 years. There were periods in the past associated with high-frequency oscillations, while at other times, there were periods that were marked by a lesser number of these events.

Bjerknes gave a physical explanation for the oscillation based upon observational data. His mechanism defines the state of the Pacific into two peculiar states, i.e. Normal and ENSO state. Even though the equatorial Pacific receives the same incoming solar energy during normal state, east is around 4-10 °C colder than the western Pacific. The eastern side in the normal state is associated with upwelling in the ocean from deeper layers, and hence the thermocline is shallow. This temperature gradient leads to a high pressure over the east and low pressure in the west driving easterlies further increasing upwelling and the gradient between the east and the west. Hence there is a positive coupled feedback at play. In contrast, during an El Niño state the east is warmer than the west. Hence, the thermocline deepens in the east, suppressing upwelling, weakening the easterly winds and reducing the east-west pressure gradient as it exists in the normal state. This weakens the winds and further deepens the thermocline, hence developing the previously developed feedback mechanism in the opposite direction.

3.2.2 Why is ENSO oscillatory?

Bjerknes mechanism explained the existence of two states but not why there was an oscillation between them. The variable which plays a vital role in the oscillation is the thermocline depth in the eastern equatorial the Pacific or the amount of warm water above thermocline. This amount of warm water is so huge that it cannot be a manifestation of flux exchanges with the atmosphere, instead it occurs because of wind-driven ocean dynamics. Whereas the wind and SST are tightly coupled to each other, thermocline is instead a slow response variable and is not in phase with either of them. For an oscillation to occur, there should be an element of the system that is not exactly in phase with the other element. For ENSO that element is thermocline depth which gives it an oscillatory behavior. Thermocline depth can also be understood as the heat content in the ocean driving this oscillatory behaviour.

3.2.3 Monsoon

Monsoon originates from Arabic for season and is characterized by reversal in the direction of wind in the regions of the world where this property is manifested. They are identified as regions where the reversal of winds is significant during the winter and summer months. Roughly the area is identified as between 25S - 35N, 30W to 170E, and the Indian landmass sits in between this region (Gadgil (2003)). The variations in wind and precipitation over seasonal scales form an important source of water for millions of inhabitants of the Indian subcontinent. The economy of South Asian countries is largely dependent on the Monsoon in the region. It occurs during June to September over large areas of Indian landmass with the east coast of the country being an exception. The reversal of winds and resulting Monsoon over the region forms an oscillatory behaviour that repeats a seasonal cycle every year.

3.2.4 ENSO-Monsoon relationship

The relationship of ENSO and Monsoon, that has been understood as a mean behavior, has been that an El Niño year is associated with droughts over India or weak Monsoon, and a La Niña is associated with floods over the subcontinent. This relationship however is not followed in all the samples and hence studying the relationship between the two is very important. Knowing whether the relationship is genuine beforehand can be helpful for the farmers over the Indian region as it can help them in crop management and other farming practices. It is also helpful for hydroclimate planning over the area. Using the wavelet coherence method Torrence and Webster (1999) show that the wavelet coherency between ENSO and ISMR is very high during the

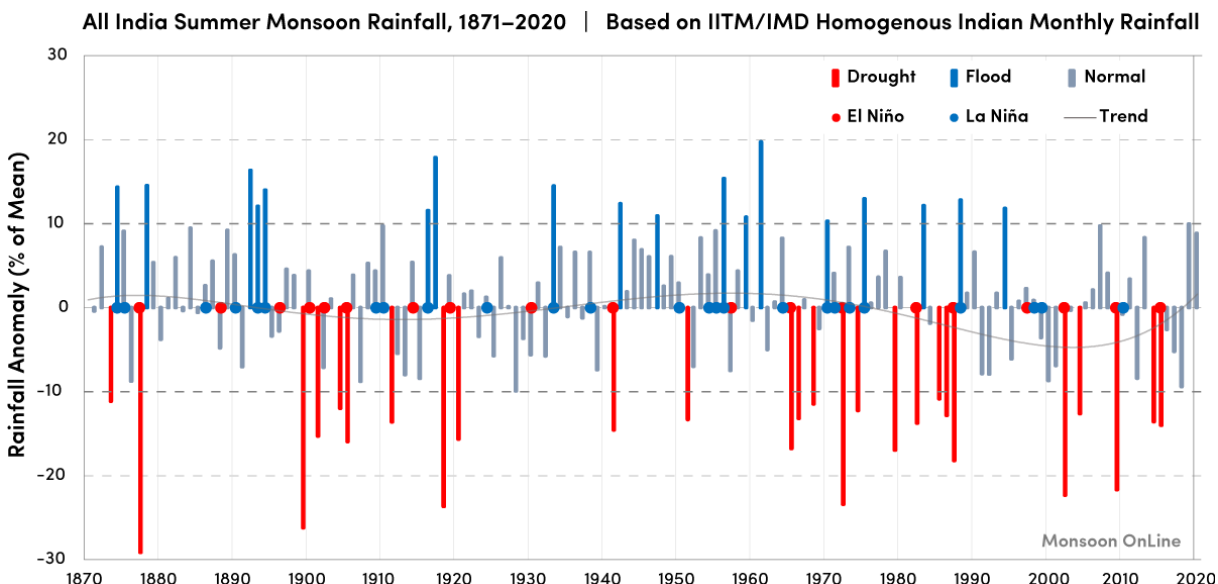


Figure 3.4: All India JJAS Rainfall and the relationship with El Niño/La Niña events, source: <https://mol.tropmet.res.in/monsoon-interannual-timeseries/>

years of high coherence in the 2-8 year band. Kumar et al. (1999) analyzed the ENSO-monsoon relationship employing sliding correlations of Indian Summer Monsoon Rainfall (ISMR) and El Niño Southern Oscillation (ENSO). They tried to argue that the relation between the two was breaking in recent times. They point to the possibility of Eurasian Warming strengthening the land-sea thermal contrast and leading to normal monsoons during ENSO years. In another study, Kumar et al. (2006) show that the ENSO events with the warmest SSTs in the central Pacific are more effective in forcing drought over the Indian landmass than the eastern Pacific El Niño events. Annamalai et al. (2007) studied the ENSO-Monsoon relationship in IPCC AR4 models and found varying behavior across models. Running correlations represent the relationship of low frequency oscillations between two signals and it could just be a stochastic artefact. This low-frequency relationship between ENSO and Monsoon is significant, and not a noise was shown by Gershunov et al. (2001). Wang et al. (2008) have shown the decreasing strength of ENSO-Indian Monsoon anti-correlation by studying the relationship of ENSO to various modes of monsoon variability. Goswami and Xavier (2005) have hypothesized a mechanism of how ENSO controls monsoon via the Length of Rainy Season (LRS). They find out that the mean rainfall over the Indian region during monsoon months can be affected by the LRS and LRS in turn depends upon the meridional Tropospheric Temperature gradient (δTT) which is reduced by an El Niño over the monsoon region. Kinter III et al. (2002) claim that the climatic shift in 1976 changed the ENSO-Indian Monsoon relationship. While ENSO was previously only related to the circulations in atmosphere over the Indian region, post 1976 it also started interacting with China's northeast region. While a number of studies in the 2000s talked about weakening the ENSO-Monsoon relationship, Xavier et al. (2007) pointed out the conclusions of previous studies to their definition of what constitutes the Indian Summer Monsoon Rainfall (ISMR). They devised a physical-based index of ISMR, which considered that an El Niño

would reduce the Length of Rainy Season (LRS) by inducing negative Tropospheric temperature gradients over Eurasia. This reduced length of the season was not taken into account by the previous studies, and if this would have been done, the relation of ENSO-Monsoon is still very robust, they claim. Webster and Yang (1992) show that ENSO and Monsoon are selectively interactive systems and that the relationship doesn't hold for all times and all cases. Ju and Slingo (1995) studied the interaction of ENSO-Monsoon system. They proposed a mechanism by which ENSO modulates the Asian Monsoon by changing the heating patterns over Indonesia and West Pacific. The inter-decadal phase of various indices of El Niño Southern Oscillation has a substantial impact on the ENSO-Monsoon relationship. In the future global warming scenario, more El Niños are likely to occur and likely to follow more droughts, and the ENSO-Monsoon relationship is expected to remain stable (Azad and Rajeevan (2016)). Kawamura (1998) gave a mechanism of ENSO-Monsoon coupling based on the physical linking of circulations and convection over the northern Indian Ocean.

3.2.5 Role of Indian Ocean Dipole on ENSO-Monsoon Coupling

Ashok et al. (2001) have shown that the effect of the Indian Ocean Dipole (IOD) and ENSO has been complementary during the 40 years from 1958-1997. They showed that whenever the ENSO-Monsoon relationship weakened, the IOD-Monsoon relationship strengthened. IOD was also shown to play a role in ENSO-Monsoon coupling. In another work, Ashok et al. (2004) tried to separate the effect of ENSO and IOD on the Indian Monsoon. They showed that IOD diminishes the impact of ENSO on the Indian Monsoon when both ENSO and IOD co-occur. Using the NCEP Climate System Forecast model, Achuthavarier et al. (2012) showed that prescribing the Indian Ocean SST in the model restores the anti-correlation of ENSO-Monsoon in the model showing the importance of the Indian Ocean in the ENSO-Monsoon relationship.

3.2.6 Role of Atlantic on ENSO-Monsoon Coupling

Chang et al. (2001) studied the role of Atlantic circulations in reducing the impact of ENSO on the Indian Monsoon. They found out that the poleward shift of jet stream over the North Atlantic was the reason behind the weakening relationship. This northward shift led to increased correlations to significant levels between western European air temperatures and Indian summer monsoon rainfall. These increased correlations are also manifested over eastern Europe, and the meridional temperature gradient were blamed for reduced ENSO influence on Monsoon. The physical mechanism by which North Atlantic SSTs impact Indian Monsoon was hypothesized by Goswami et al. (2006). Atlantic Multidecadal Oscillation produces nega-

tive/cold anomalies over Eurasia and the weaken meridional tropospheric temperature gradient resulting in early withdrawal of Indian Monsoon and decrease in the mean rainfall. On interannual time scales, this mechanism works via North Atlantic Oscillation (NAO) or Northern Annular Mode (NAM). These also setup cold temperature anomalies over Eurasia and weakens the Indian Monsoon. AMO can modulate the frequency of occurrence of NAO or NAM events and hence impact the monsoon. A similar mechanism was put forward by Lu et al. (2006). The variability of the ENSO-Monsoon relationship on multidecadal time scales was studied by Chen et al. (2010) using a 1000 years run of a CGCM. They point to the role of AMO, which occurs as a natural oscillation of AMOC in affecting the ENSO-Monsoon relationship on a multidecadal time scale. They postulate that AMO can weaken the ENSO-Monsoon relationship over decadal-multidecadal time scales. Wang et al. (2013) show that the Northern Hemispheric Summer Monsoon has intensified since the 1970s. They point towards mega ENSO, AMO and asymmetrical global warming as the reasons for these intensifications.

3.2.7 Role of Solar Irradiance on ENSO-Monsoon Coupling

Mehta and Lau (1997) studied the role of solar irradiance on ENSO-Monsoon relationship and found that at 11 years time scale, there is no significant relationship between Indian Monsoon and Solar Irradiance or ENSO and Solar Irradiance. However, they find out that Indian Monsoon and Solar Irradiance are in-phase at multi decadal time scales while ENSO and Solar Irradiance are out of phase to each other. The relationship of the ENSO-Monsoon system at interannual time scales is also affected by their multidecadal variability with Solar Irradiance.

3.2.8 Role of Greenhouse gas warming on ENSO-Monsoon coupling

Ashrit et al. (2001) used a coupled general circulation model to study the role of greenhouse gas warming on the ENSO-Monsoon relationship. They find out increased ENSO events in the future and increasing mean and variability of Indian Monsoon. They point to a weakening impact of ENSO on India monsoon, possibly by the warming of landmass over Eurasia.

3.2.9 Role of Basic State in ENSO-Monsoon coupling

Turner et al. (2005) found out that the systematic error in the equatorial Pacific mean made ENSO-Monsoon teleconnection in the model poor. They applied flux corrections over Pacific and Indian Oceans and found out that the model's ENSO-Monsoon relationship was well rep-

resented.

3.2.10 ENSO-Snow-Monsoon relationship

Yang (1996) found out that the Eurasian Winter Snow Cover (EWSC) increased more predominantly during El Niño winters than during La Niña winters and its signal can also be found in the Southern Oscillation Index (SOI). EWSC and Indian Monsoon have an inverse relationship as shown in the previous studies but Yang (1996) showed that the Snow-Monsoon relationship broke during ENSO events suggesting the vital role played by ENSO and strong ENSO-Monsoon coupling.

3.2.11 Role of PDO and interdecadal oscillations in ENSO-Monsoon coupling

Krishnamurthy and Goswami (2000) showed that if the tropical Pacific is in a warm phase of the interdecadal oscillation, the El Niños are more likely to be associated with droughts, and La Niña might not have a relation. In contrast, opposite might happen in the case of a cold phase of the interdecadal oscillation. Krishnamurthy and Krishnamurthy (2014) also find that the warm phase of PDO is associated with a rainfall deficit over India and its role in ENSO-Monsoon coupling. The coupling strengthens during warm phases in that during a warm phase of PDO impact of El Niño strengthens, and during a cold phase of PDO, the effects of La Niña strengthen. The role of PDO impacting the Indian monsoon has already been explained in detail by Krishnan and Sugi (2003).

3.2.12 Indian Summer Monsoon influence on ENSO

Until now, only the role of ENSO over Monsoon was discussed; however Kirtman and Shukla (2000) show that Monsoon can also lead to variability of ENSO using a 50-year simulation of AGCM. They postulate that weak monsoons lead to weaker trade winds in equatorial tropical Pacific and increased monsoon variability increase the variability of ENSO. They also show that ongoing ENSO events are intensified by weak monsoons and vice-versa. This dual effect of the Monsoon-ENSO relationship makes the case of ENSO-Monsoon coupling considered from the point of view of two oscillators interacting with each other rather than an oscillator behaving in a certain way by external force (ENSO).

3.3 ENSO-monsoon phase coherence during the historical period (1871-2016)

That volcanic aerosols could have a role in deciding the ENSO-Monsoon relationship was first proposed by Maraun and Kurths (2005). They present a non-linear time series analysis method which they applied to study the phases of ENSO and Monsoon. Basically, they argued that the ENSO-Monsoon relationship should not be seen from the point of view of running correlations (Kumar et al. (1999)) or linear analysis methods. Rather non-linear methods should be used to study the relationship and that the association occurs in epochs rather than being always followed. They identified distinct epochs 1886-1908 and 1964-1980 during which the ENSO and Monsoon were coupled to each other in contrast to periods 1921-1935 and 1943-1963 where there was almost no synchronization. They were for the first time able to identify new types of coupling called 2:1 coherence during 1981-1990, 1908-1921 and 1935-1943, during which monsoon oscillated with double the phase speed of ENSO. They argue that the high temporal resolution of the data makes them capable of identifying the onset of phase coherence with accuracy. Hence, they were able to postulate that periods of ENSO-Monsoon coupling co-occurred with the strong volcanic eruptions. The two periods of good coupling which they identified were both associated with two strong volcanic eruptions i.e. Krakatoa in 1883 and Agung in 1963.

The phase coherence analysis uses of the phase-locking principles as discussed previously (Pikovsky et al. (2003)). The algorithm to conduct a Phase Coherence method as followed by Maraun and Kurths (2005) is as follows:

- The data chosen is monthly ISMR data from IMD and Niño3 SST data-sets. They are passed through a low pass filter to dampen the intra-annual oscillations. A function damping frequencies $> 0.7/\text{year}$ is chosen by Maraun and Kurths (2005).
- The derivatives of the filtered time series are estimated and then smoothed with a 13 month running mean. The phase space plot of the derivative time series shows an attractor around which the oscillator Niño3 would oscillate, hence justifying the use of principles of synchronization.
- The resulting series is then passed through a Hilbert transform, and the instantaneous phases are then calculated. Only the phases that fulfill the criteria that the amplitude is greater than 0.8 are considered to be qualified as well defined. This criterion makes sure that the swing or motion of the oscillator to a particular direction is complete or atleast 0.8 times the amplitude for it to be considered in the phase coherence analysis.
- The instantaneous phases are then unwrapped by adding 2π after every oscillation.

- The unwrapped phases are then subtracted to get the phase difference plot on which the plateaus show periods with phase coherence.

The analysis of Maraun and Kurths (2005) was done only until 2003 and it has been reproduced in this work to understand the role of volcanic aerosols on ENSO-Monsoon coupling. The phase coherence analysis is extended to 2016 as can be seen in figure 3.5 and a period of free coupling which is intrinsic to the ENSO-Monsoon system during 2006-2010 is found out.

We further carry out the phase coherence analysis from the IPSL PMIP3 historical simulations from 850-1850 and find out periods of ENSO-Monsoon coupling both free as well as forced by volcanic eruptions. The data for Niño3 is taken as average SST over Niño3 region and surface pressure anomalies over Central India (74.5E - 86.5E, 16.5N - 26.5N) are taken as precursors for Indian Summer Monsoon Rainfall. Pressure is chosen as a variable to conduct the analysis as rainfall is a derived variable in the models and inferring conclusive results from model generated rainfall can be tricky.

In addition to the phase coherence analysis a composite analysis was done over the ENSO variability data (Li et al. (2011)), South Asian Summer Monsoon Index (SASMI, Shi et al. (2014)) and PDO index (macdonald2006pacific) over the last millennium for 9 out of top 25 volcanic events from Sigl et al. (2015) since -436 AD for which the data is available for all the three proxy data-sets. As a result, it can be seen that the monsoon index SASMI reduces in the year after the eruption, and the ENSO index increases after the volcano, showing a propensity for drought and El Niño, respectively.

3.4 Phase coherence analysis using the IPSL PMIP3 last millennium simulation

Tejavath et al. (2019) have analysed the Paleoclimate Model Intercomparison Project Phase 3 (PMIP3) simulations of various models for the robustness of Indian Monsoon in PMIP3 simulations (Fig. 3.15). It can be seen that the ENSO-Indian Monsoon anti-correlation is captured only in IPSL model simulations which is comparable to the anti-correlation seen in observational datasets from the instrumental era. Hence we use the IPSL model simulations of the last millennium (850-1850) to conduct the phase coherence analysis of ENSO and IM systems. The paleo-experiments were run as a branch off of the initial conditions from the PI control and prescribed annually varying orbital parameters, trace gases, volcanic aerosols and solar irradiance parameters. Ozone, aerosols, vegetation, ice sheets, topography and coastlines are kept the same as the preindustrial conditions. The problem of predictability as studied by Lorenz can be divided into two categories; first being the predictability of the first kind which is highly dependant on the initial conditions and the second being predictability of the second kind which

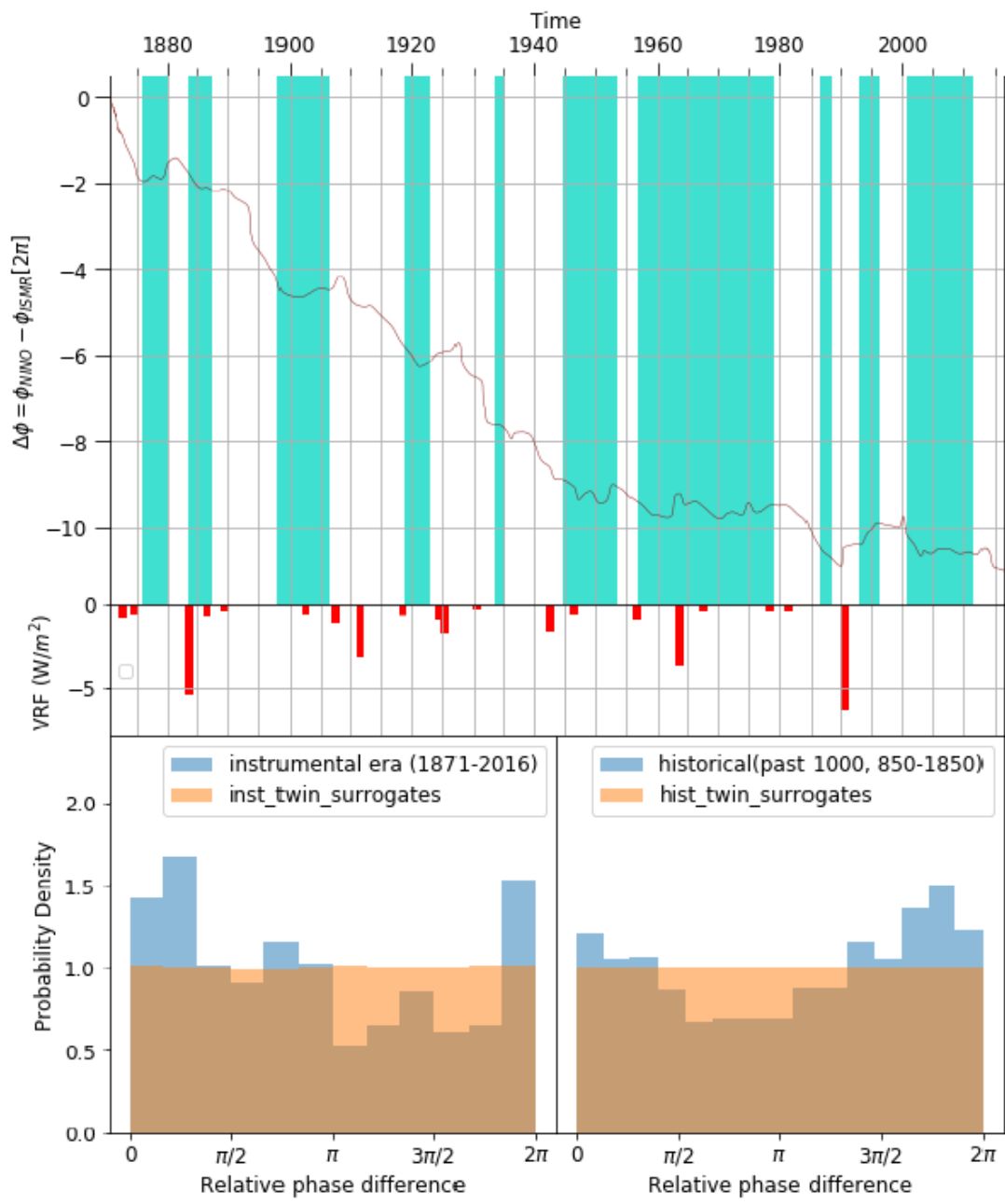


Figure 3.5: ENSO and IM Phase Coherence Analysis for the instrumental era (1871-2016) [Top]. Statistical Significance of instrumental-era and last millennium phase Coherence[Bottom]

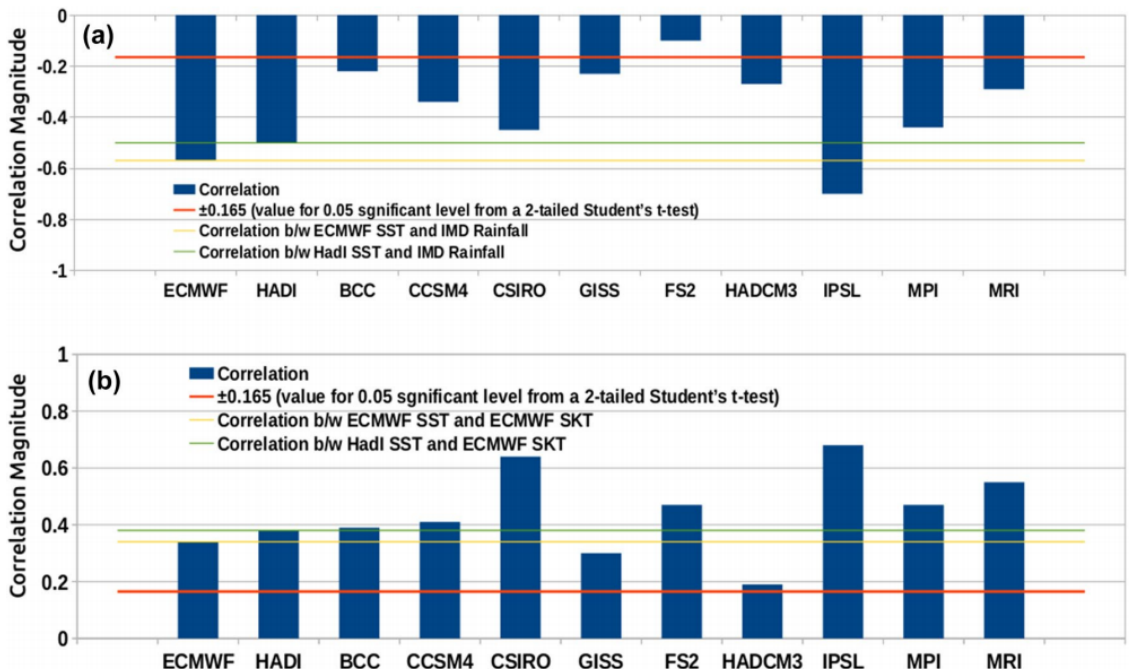


Figure 3.6: Coefficient of correlation between (a) all India rainfall and Niño3.4, (b) Surface air temperature on Indian landmass and Niño3.4 from historical simulations (Tejavath et al. (2019)), Reproduced with permission

aims to predict the evolution of time averaged statistical properties of the climate. It is the predictability of the second kind that we are dealing with when using PMIP3 climate simulations. Since IPSL model shows a good ENSO-IM anti-correlation as compared to other models it is most suited to conduct an analysis on the relationship between ENSO and IM.

3.5 Statistical Significance of Phase coherence analysis

The statistical significance of phase coherence analysis is performed by using twin surrogates as the null distribution. Twin Surrogates (Thiel et al. (2006)) preserve the non-linear properties of the time series and are state of the art in surrogate time series generation. The algorithm to generate twin surrogates is as follows:

- The time series is first embedded to generate a n-dimensional representation of the system. The embedding is performed using a time delay parameter (calculated using mutual information) and an embedding dimension (calculated using false nearest neighbours method)
- Recurrence matrix is then constructed from the embedded signal, and the states which correspond to twins (meaning the state vectors sharing the same recurrences) are identi-

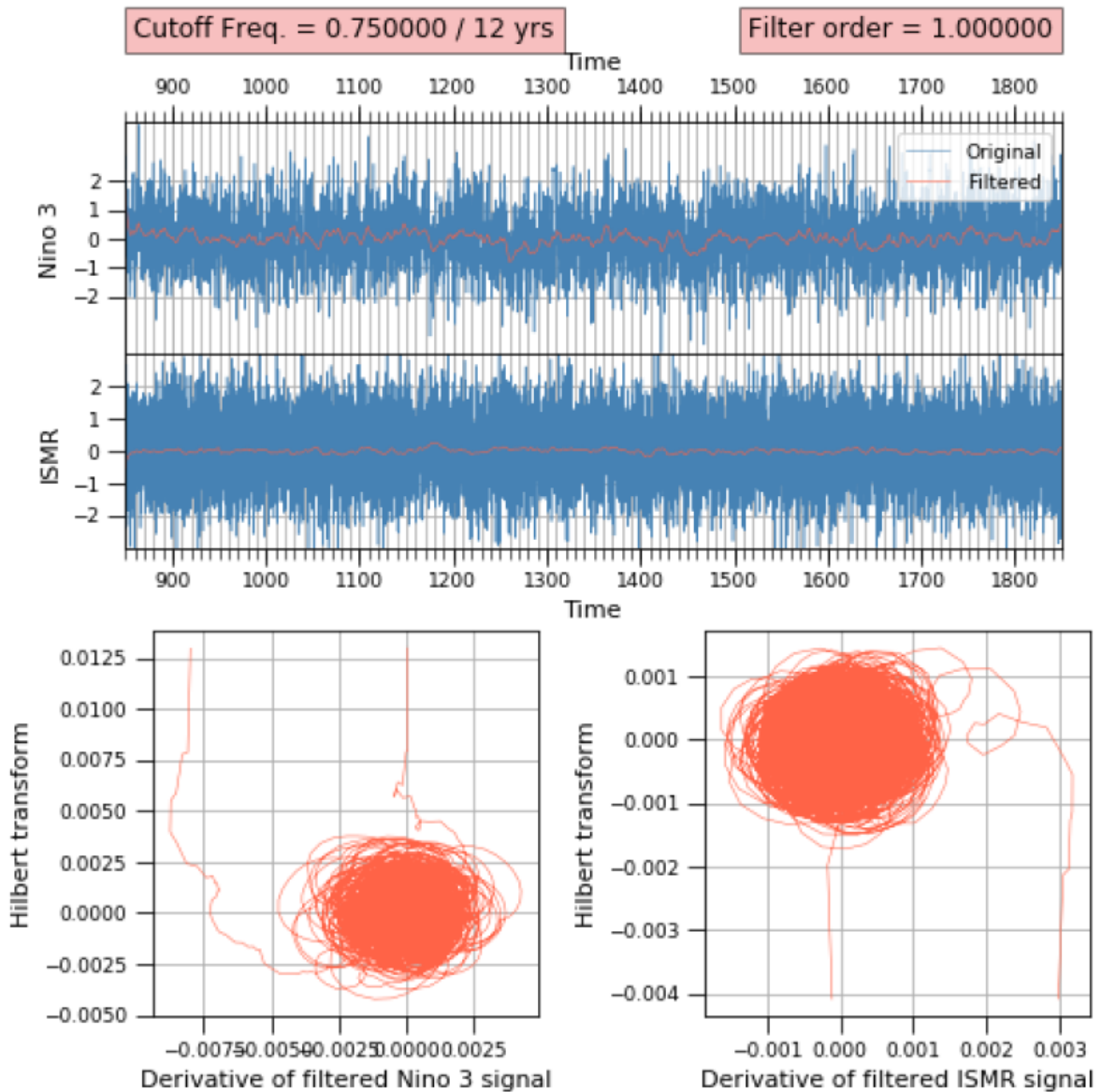


Figure 3.7: ENSO, IM filtered time-series and their respective phase space plot during last millennium: Time-series of Niño3 and IM indices during 850–1850 based on the last millennium IPSL PMIP3 simulations in blue and the filtered time-series in orange (top panel). The trajectory in complex plane of the Niño3 index and its Hilbert transform (bottom left panel), and the IM index and its Hilbert transform (bottom right panel) show oscillations of Niño3 and IM around a single attractor. The trajectory in complex plane demonstrate ENSO and IM to undergo self-sustained oscillations on a single attractor, respectively

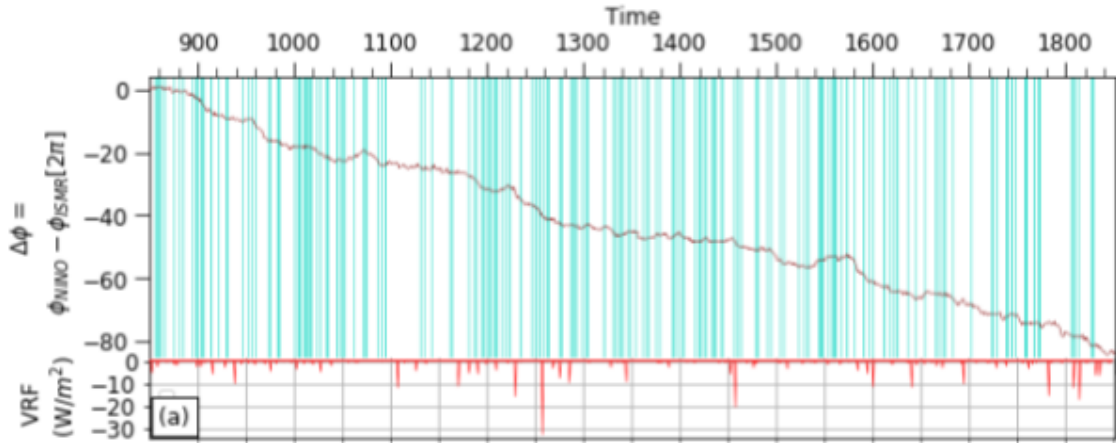


Figure 3.8: ENSO and IM phase coherence from IPSL PMIP3 model runs during the last millennium. The ENSO-IM phase difference is shown in the top figure, while the volcanic radiative forcing during the last millennium is shown in the bottom plot (850-1850 AD). The backdrop is coloured green to indicate statistically significant epochs.

fied.

- Twin Surrogate series is then generated by initially starting from a random index in the time series as the first index of the twin surrogate. This is followed by adding to the twin surrogate series values from the original time series as they would occur while following the trajectory in the phase space.
- If a twin is encountered, then jump over to that state and continue from that state in the time series.
- If the last index is encountered, start from a random index again until the length of the series is encountered.
- Repeat the above steps to generate more surrogates

Five thousand surrogates time series of ENSO and IM are generated to conduct the phase coherence analysis. The distribution of the phase differences of the original time series and the phase differences from the null distribution (twin surrogates) are then plotted. A Kolmogorov-Smirnov test of the two distributions reveals that they are non-identical, and comparison (of distributions) with the instrumental PCA reveals the similarity of the distributions.

An Event Synchronization Analysis of the phase-coherent events from the phase coherence analysis and the volcanic eruptions also reveals a statistically significant synchronization between the two systems. Event Synchronization (Quiroga et al. (2002)) between two event series determines whether an event series leads or lags the other time series. For this purpose, let's assume we have two-time series A and B. One by one, events in A are visited, and the number of events in B that follow the events in A, within a dynamic time delay, are counted

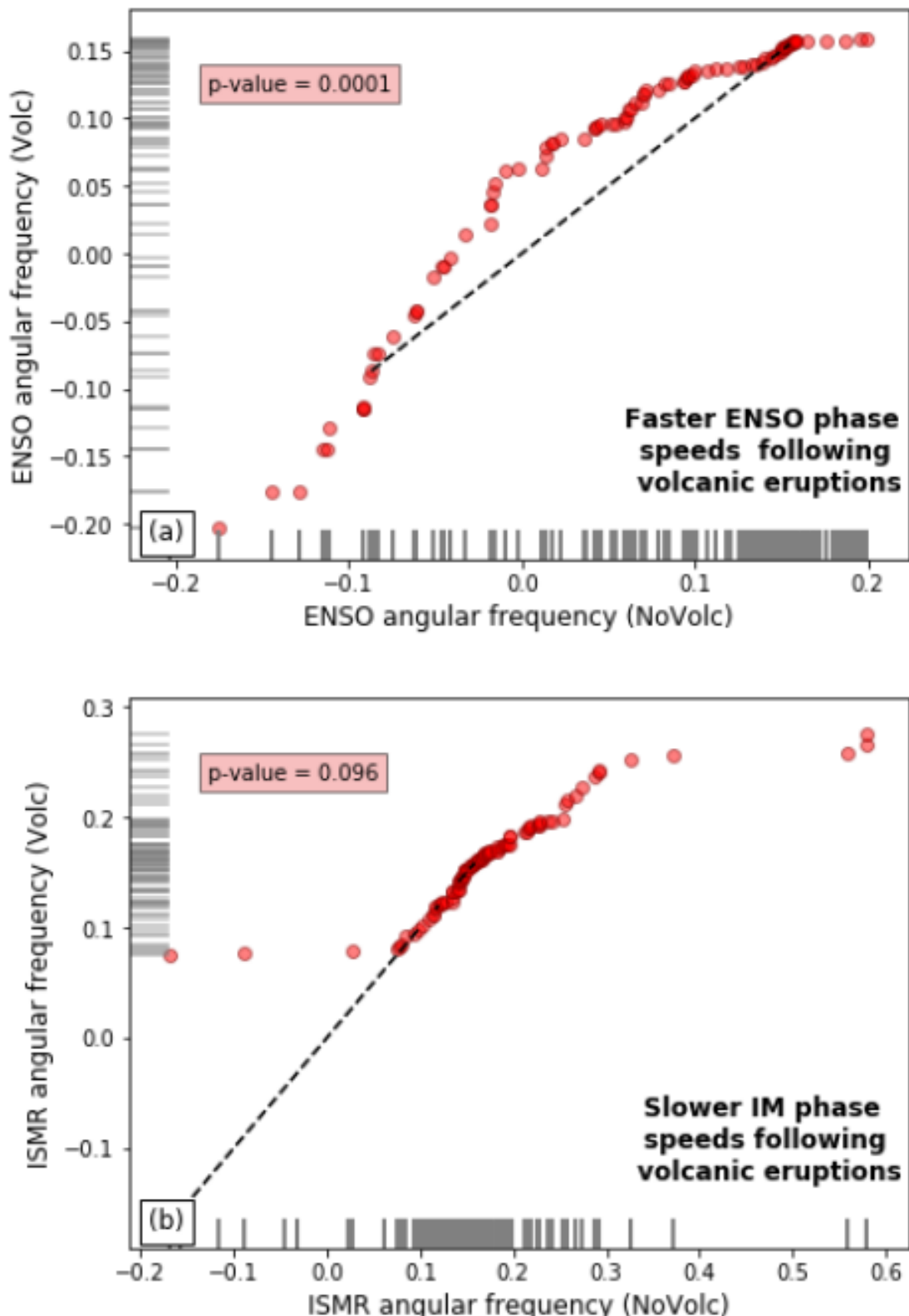


Figure 3.9: Comparison of Volc and NoVolc distributions of ENSO and IM angular frequency using quantil-quantile plots. Volc phase speeds are bootstrapped up to year 4. The remaining corresponds to NoVolc

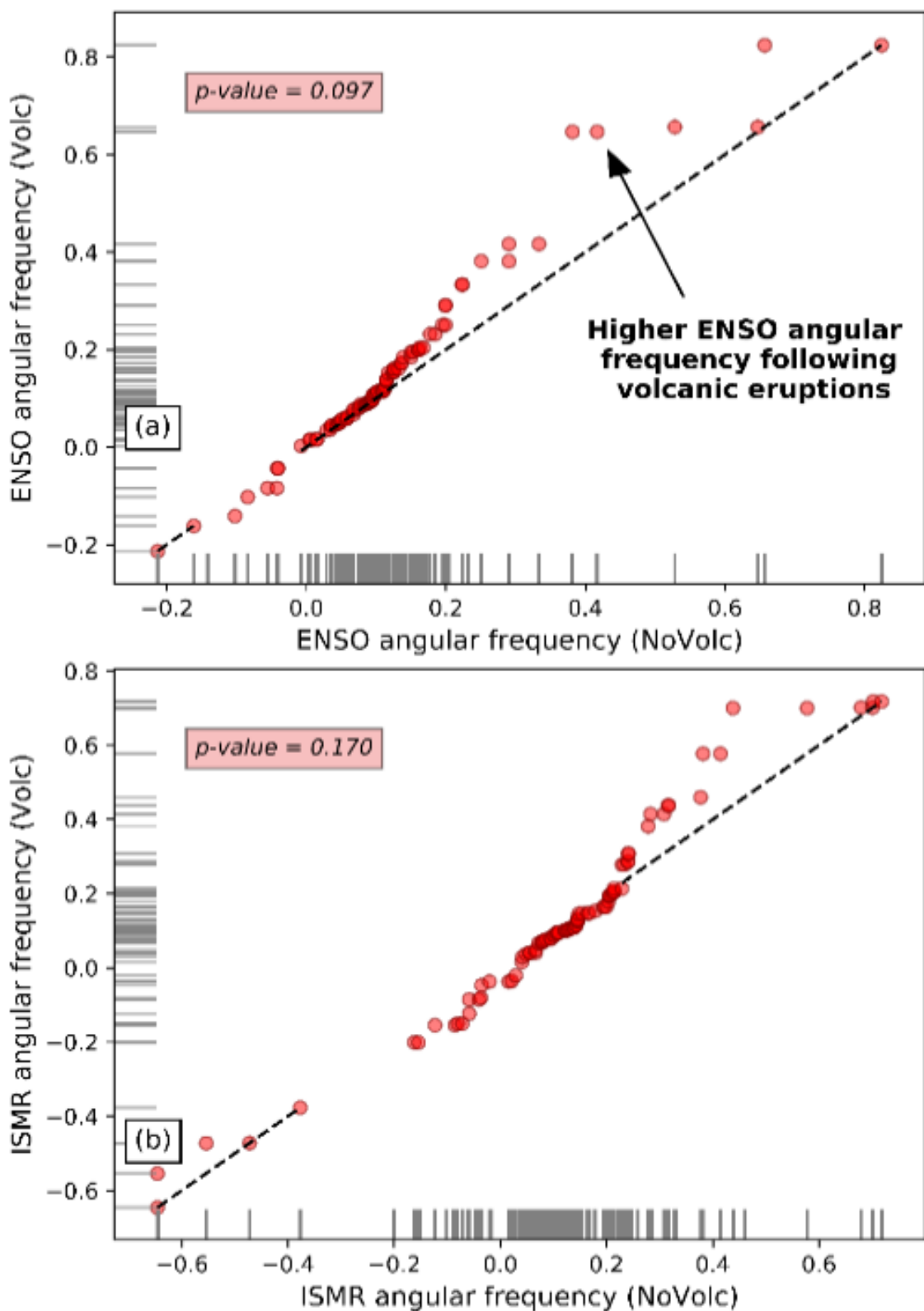


Figure 3.10: (Caption next page.)

Figure 3.10: (Previous page.) LVE-induced changes in ENSO and IM oscillation angular frequencies in the previous millennium. Volc and NoVolc are bootstrapped similar to Figure 3.9

and summed to the total event synchronization number. Surrogates of the two series are then constructed, and the event synchronization number again calculated. If the actual event synchronization index is greater than the 95%ile of the null distribution, we call the two systems A and B to be in synchronization. In our example, the phase-coherent periods and volcanic events are synchronized.

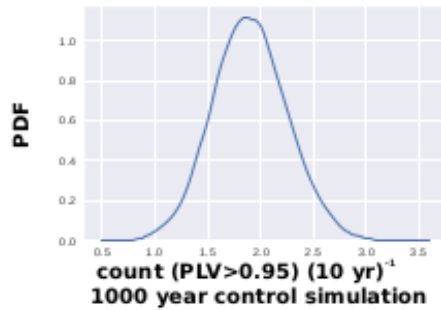
3.6 Dynamical mechanism of volcanism induced ENSO-Indian monsoon coupling

Angular frequency was obtained by taking the first derivative of phase obtained from Hilbert Transforms to understand the mechanism behind the coupling of ENSO and Indian Monsoon oscillatory systems following volcanic eruptions. The phase was obtained from Phase Coherence Analysis. Quantile-Quantile plots statistically significant higher ENSO angular frequencies following large volcanic eruptions. The angular frequency series was binned in two categories, i.e. Volc and No-Volc. All the angular frequencies within 4 years of the eruptions were classified as Volc and the rest were classified as No-Volc. Similarly, for Indian Monsoon, the angular frequencies were classified into Volc and No-Volc. No significant increase or decrease in angular frequency was observed for the Indian Monsoon. Hence, the coupling between ENSO and the Indian Monsoon takes place due to an increase in phase speed / angular frequency of ENSO oscillatory system. Out of ENSO and IM, ENSO is a slow oscillator with 2-7 years period and, IM is an interannual oscillator. By making an analogy to the oscillators of Huygens, it can be seen that if the slow oscillator's phase speed increases, the two oscillators can come into synchronization (Figure 3.16-3.17).

Phase speed or angular velocity is computed at every step as a derivative of phase with respect to time from Figure 3.8. The phase speed is computed from the phase coherence analysis for the observational datasets and the last millennium IPSL PMIP3 simulations. The phase speeds are binned into Volc and NoVolc as the periods up to 4 years from strong volcanoes identified as Volc and the remaining time series as NoVolc. Q-Q plot is constructed from the Volc and NoVolc distributions of ENSO-IM phase speeds for observational (Figure 3.9) and IPSL PMIP3 simulations (Figure 3.10) datasets. It can be seen from the two figures that the angular frequency of ENSO increases after strong volcanic eruptions. On the other hand, IM phase speed does not change (insignificant) in the last millennium simulations and decreases in the instrumental era.

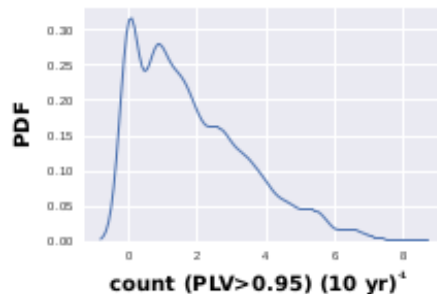
PDF of counts (decadal) of Phase Coherence (PLV>0.95) in PI control and historical simulations during last millenium from PCA of monthly data

PI control

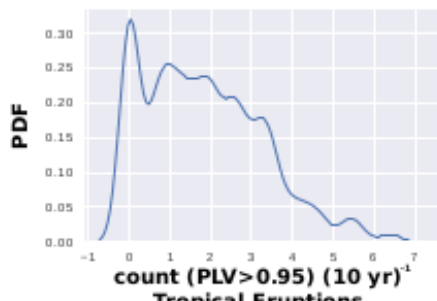


a

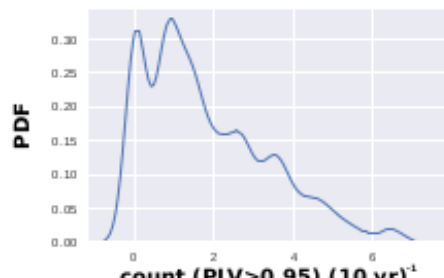
**IPSL PMIP3 last millennium simulation
(850-1850)**



b



c



d

Figure 3.11: Probability Distribution functions of Phase Locking Value for PI Control (1000 years) and Historical run from IPSL PMIP3 simulations. Monte Carlo analysis is done with $N=10000$ for both PI control and historical runs and 10 year samples are taken out from the complete dataset. For historical subsampling only those samples that satisfy the presence of a volcanic eruption are chosen. (a) PI Control (b) correspond to the historical (last millenium) wherein the 10 years are choosen with the condition that volcanic eruption should have occurred in that period, (c) same as (b) but for Tropical eruptions, (d) same as (b) but for extra-tropical eruptions.

Seen from a dynamical systems perspective, if there are two oscillating systems with one having a higher phase speed and the other having a lower phase speed, they tend to go in a coupled state if the phase speed of the faster (slower) oscillator reduces (increases). Similarly, ENSO is a slow oscillator with a cycle varying from 2 to 7 years, and the Indian monsoon is an interannual oscillation. The analysis demonstrates a speeding up of ENSO, which explains the coupling from a dynamical systems perspective. Finally, a computation of phase-locking value for the control and last millennium simulation of the IPSL PMIP3 model shows the volcanic imprint on ENSO-IM coupling (Figure 3.11). Moreover, the separation of tropical and extra-tropical eruptions shows that tropical eruptions are more effective in coupling the two systems relative to extra-tropical volcanic explosions.

3.7 Conclusions

This chapter describes phase coherence analysis as an advanced methodology to quantify instantaneous phase coupling between two oscillatory systems. It then goes on to establish that the ENSO and IM are oscillatory systems on which the theories of non linear dynamics can be applied. This is established for the instrumental period from the observational datasets and the last millennium from the outputs of the PMIP3 simulations. Robust statistical significance using twin surrogates is established between ENSO and IM in the last millennium. Event synchronization is used to fingerprint the role of large volcanic eruptions on the ENSO-IM coupling. Finally, a dynamical mechanism is found out which establishes that the phase speed of ENSO increases after large volcanic eruptions and, from non-linear dynamics perspective, leads to the coupling of ENSO and IM.

The next chapter discusses experiments conducted using IITM ESM and the analysis carried out using paleoclimate proxy simulations to fingerprint the role of large volcanic eruptions on ENSO-IM coupling.

Chapter 4

Volcanic fingerprint on ENSO-monsoon coupling: Climate model simulations & paleoclimate proxy records analysis

As the Earth system evolves and adapts to inter-system feedback, the climate is governed by various phenomena and variability across many scales (both space and time). Using Earth System Models (ESMs) gives a better understanding and quantification of physical, chemical, and biological processes that influence the rates of change of elements in the Earth system and throughout its many components (such as the atmosphere, ocean, land, cryosphere, and biosphere). Mathematical equations define physical and natural laws that control Earth System dynamics, and ESMs are global numerical models that follow and solve these laws. It is possible to build numerical simulations of ESM coupled systems using either finite difference techniques or Spectral/Galerkin methods, in which the numerical equations are integrated in time. However, ESMs are computationally difficult and time-consuming because of the large number of computations required to integrate state-of-the-art models. Significant progress in ESM development has been made possible in the last few decades thanks to breakthroughs in High Power Computing (HPC) and computational methodologies.

To better understand the effects of human-induced perturbations (e.g., increased greenhouse gas and aerosol emissions, land-use and land-cover changes, etc.) on the climate system, ESMs have become increasingly popular in recent years. Environmental, agricultural, water supply, natural resources, ecosystems, biodiversity, economic, and social well-being are all at

risk because of climate change. GHG concentrations in the atmosphere have increased rapidly since the turn of the twentieth century due to human activity. Direct measurements and remote sensing from satellites and other platforms show the warming of the climate system since the 1950s, and many of the observed changes have been unprecedented in decades or millennia (Stocker (2014)).

4.1 IITM Earth System Model

The CMIP models have shown conclusively that human-induced GHG forcing influences the growing trend in global mean temperatures (Flato et al. (2014)). On the other hand, it is challenging to assess the effects of climate change on regional scales accurately. IPCC model simulations and future predictions of South Asian monsoon rainfall show a wide range of variations (Krishnan et al. (2016), Sharmila et al. (2015)). These variations pose huge challenges to policy makers as well as the development of adaptation strategies. With this realisation in mind, it is imperative to enhance human capacity for all hard challenges related to global warming and climate change science. The Indian Institute of Tropical Meteorology (IITM) developed an Earth System Model (ESM) to address the science of climate change, including the detection, attribution, and future forecasts of global and regional climate. This ESM is focused on the South Asian monsoon. It was conceived by transforming a current state-of-the-art seasonal prediction model—the Climate Forecast System version 2—into a model that could be used to study long term climate variability and change. The first model (IITM-ESM version 1) was developed at the Centre for Climate Change Research, IITM, Pune (CCCR–IITM) (Swapna et al. (2015)). It underwent a significant revision, resulting in a climate model capable of addressing the science of global climate change (Swapna et al. (2018)). For the first time, the IITM-ESMv2 has participated in the CMIP model intercomparison effort and will contribute to the IPCC AR6 assessment report.

Using the NCEP Global Forecasting System (GFS) model, the atmosphere component of the IITM-ESMv2 is configured at a triangular truncation of 62 waves in the horizontal (2° grid) and finite difference in the vertical with 64 sigma-pressure hybrid layers with the top model layer extending up to 0.2 hPa in the vertical. Integrations of the model and atmospheric radiation calculations are done every hour, with a time-step of 10 minutes. An updated version of the Simplified Arakawa-Schubert (SAS) method is used to parameterize cumulus convection in the model (Han and Pan (2011)). Saha et al. (2010) provide more information on the portrayal of atmospheric physical processes. The Noah land surface model (LSM) with four layers is used in the IITM-ESMv2 to simulate the land surface processes (Ek et al. (2003)).

The GFDL Modular Ocean Model Version 4p1 makes up the ocean component of IITM-ESMv2 (MOM4p1, Griffies et al. (2009)). Using the Boussinesq approximation with a rescaled

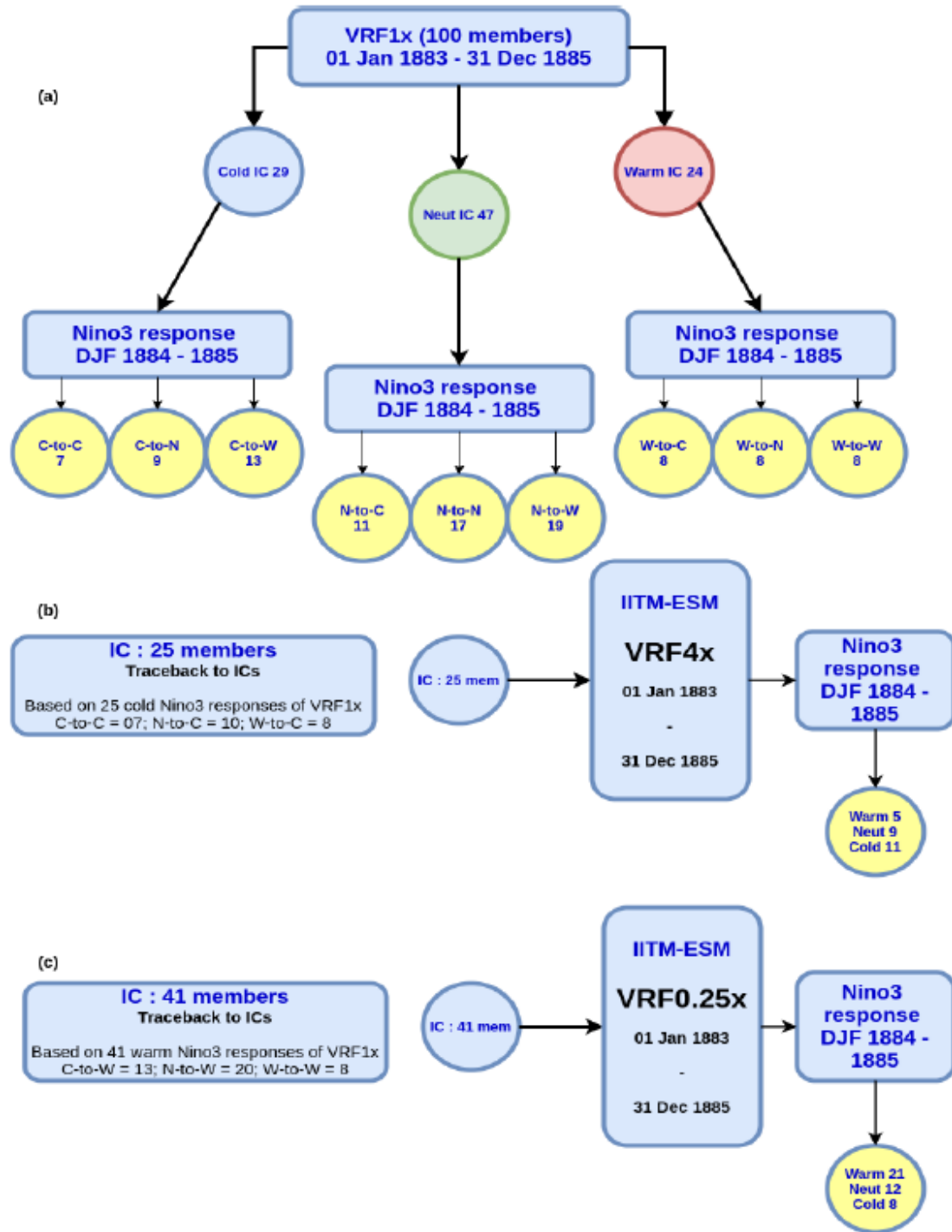


Figure 4.1: Diagram illustrating the flow chart for the IITM-ESM simulations carried out to find the influence of volcanic explosions on ENSO-Indian monsoon coupling

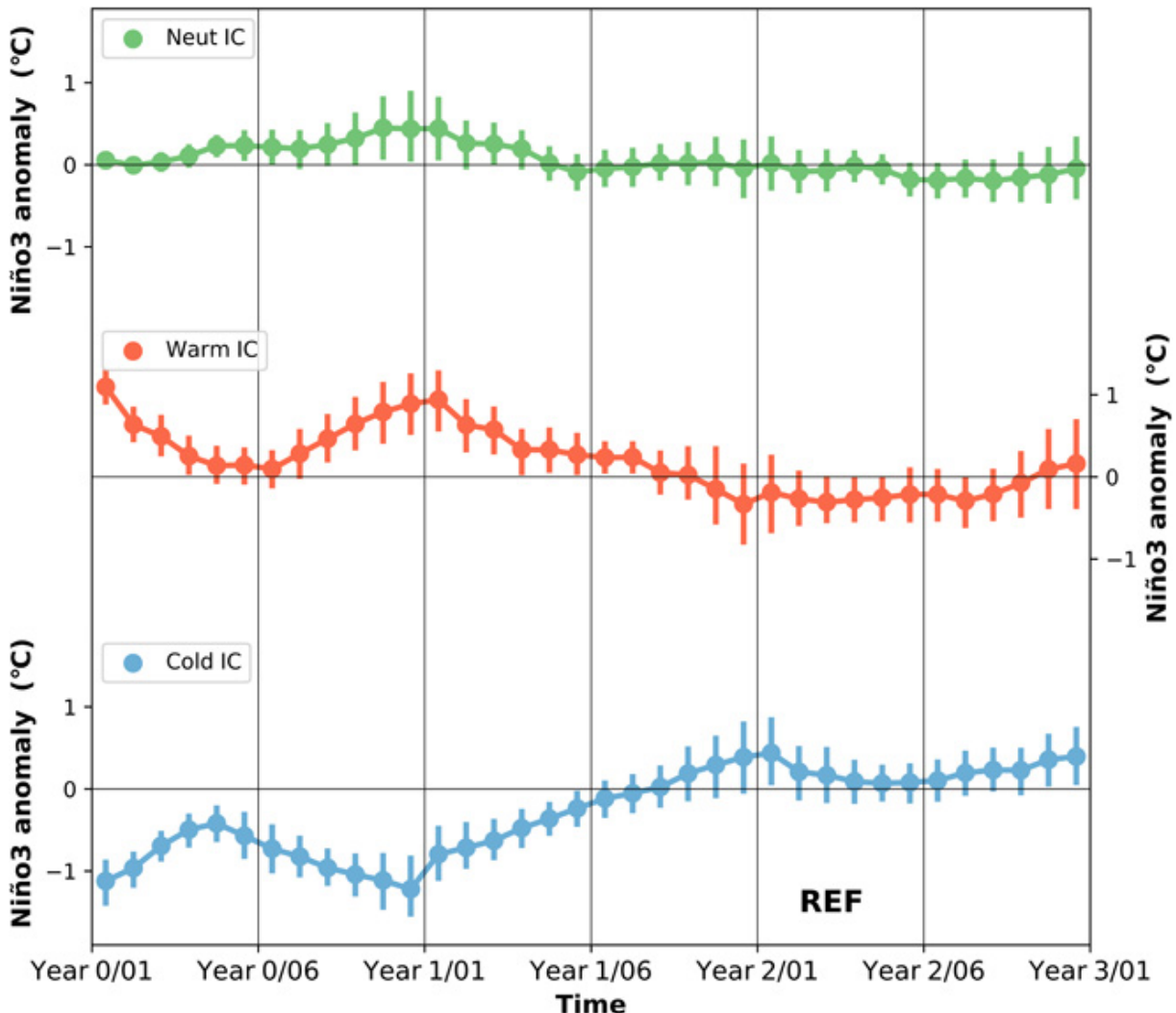


Figure 4.2: Plots of SST anomaly distributions from the 100-member REF ensembles without volcanic forcing (i.e., based on the pre-industrial control simulation) from January of year 0 through December of year 2 are displayed. Realizations start with 47 Neutral ICs, 24 warm and 29 cold ICs compose the 100 members of the group.

geopotential vertical coordinate with 50 levels, the MOM4p1 hydrostatic model simulates the flow of water. As you move northward, the zonal resolution drops to 0.33° , while the meridional resolution rises to 1° . According to Large et al. (1994), the KPP surface boundary layer technique is used to compute the vertical diffusivity, vertical viscosity, and transport of nonlocal matter as a function of flow velocity. MOM4p1 additionally includes interactive modules for ocean biogeochemistry and marine ecosystem processes. In IITMESMV2's ice component, the Sea Ice Simulator (SIS, Winton (2000)) has three vertical layers, one snow and two ice, as well as five ice thickness categories.

CFSv2 operational seasonal prediction model was transformed into a long-term climate model at the CCCR-IITM to answer climate change-related research questions. It is necessary to incorporate some crucial components into a climate model to meet the need for an ESM for

long-term climate research. After adding the GFDL MOM4P1 ocean component with biogeochemistry in CFSv2, the initial version of the ESM was built using extended simulations (more than 100 years) and comprehensive model validation (Swapna et al. (2015)).

Global radiation energy balance at the top-of-the-atmosphere (TOA) and at the Earth's surface must be properly represented in climate models for credible assessments of climate change simulations. The IITM-ESMv1 had a significant radiation imbalance of 6 W/m² near the TOA, making this a complex problem to solve. Many modifications were made to reduce radiation imbalances in the IITM-ESMv2, which resulted in a radiatively balanced system. To be considered acceptable, the radiation imbalance at the TOA in the IITM-ESMv2 is less than 0.8 W m², which is consistent across several CMIP models (Forster et al. (2013)). Improvements in IITM-ESMv2 were primarily due to the incorporation of heating from viscous dissipation of turbulent kinetic energy (TKE) into the model. Additional enhancements to the IITMESMv2 include: (a) realistic Arctic sea ice distribution (b) replication of the Atlantic Meridional Overturning Circulation (AMOC) (c) IITM-ESMv2's mean monsoon precipitation across India compared to IITM-ESMv1 (d) The Indian Ocean Dipole (IOD) and the Indian monsoon rainfall (e) CMIP6's incorporation of time-varying aerosol characteristics (natural and anthropogenic) and land-use land-cover changes.

Natural (e.g. dust, sea salt, volcanic emissions) and anthropogenic (emissions of sulphate, nitrate, organic carbon, black carbon, etc.) aerosols and their radiative impacts on the climate system are included in IITMESMv2. Anthropogenic aerosol forcing has been found to influence radiation, monsoon rainfall, and regional climate in recent research (Krishnan et al. (2016), Bollasina et al. (2011), Ramanathan et al. (2005)). Aerosols, unlike GHGs, have a considerable spatial and temporal variability. Rainfall variability in South Asia is significantly impacted by internal monsoon dynamics. Large, explosive volcanic eruptions can alter ENSO and the monsoon rainfall cycle via stratospheric aerosol forcing (Liu et al. (2020), Ning et al. (2020), Khodri et al. (2017)). That's why we need solid evidence linking changes in regional monsoon precipitation to the aerosol forcing we're seeing. The IITM-ESMv2 is a valuable tool for addressing the link between aerosols and monsoons. It is also possible to model the impacts of land-use and land-cover changes (LULC) on the climate system using the IITM-ESMv2.

4.2 Volcanic footprint on ENSO-monsoon coupling in IITM-ESM

An ensemble of 100 IITM-ESM simulations starting from different initial conditions forced with Krakatoa Volcanic Radiative Forcing (VRF), which is proportional to the global mean aerosol optical depth (AOD), are performed as shown in Figure 4.1a. When compared with the reference (NoVolc) simulations (Figure 4.2), we can see an early El Niño developing when ini-

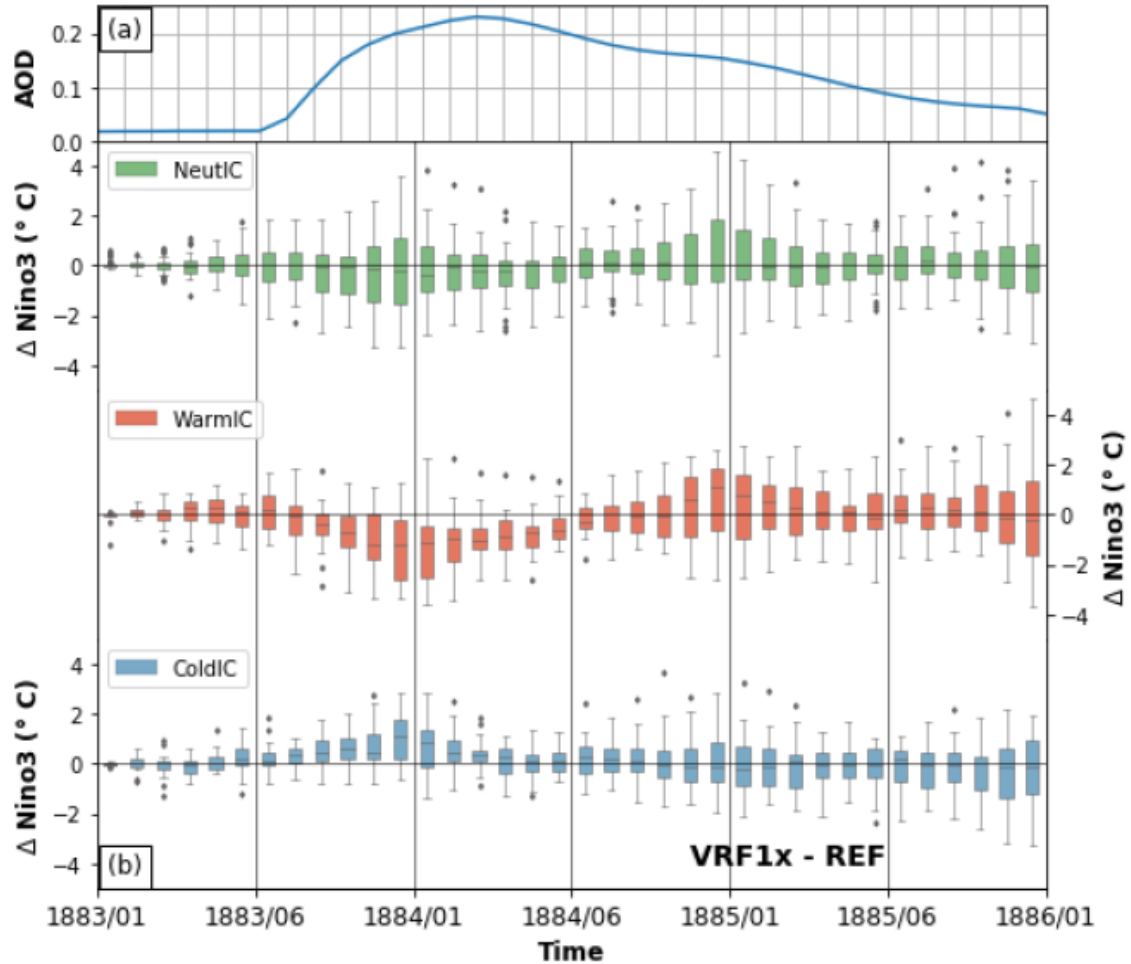


Figure 4.3: ENSO modulations forced by LVE under varied initializations: Progress from January 1883 till the end of December, 1885 (a) AOD at mid-latitudes across the world (b) Box-whisker graphs illustrating the distribution of $\Delta \text{Niño}_3$ changes calculated from the difference between the VRF1x and REF ensembles.

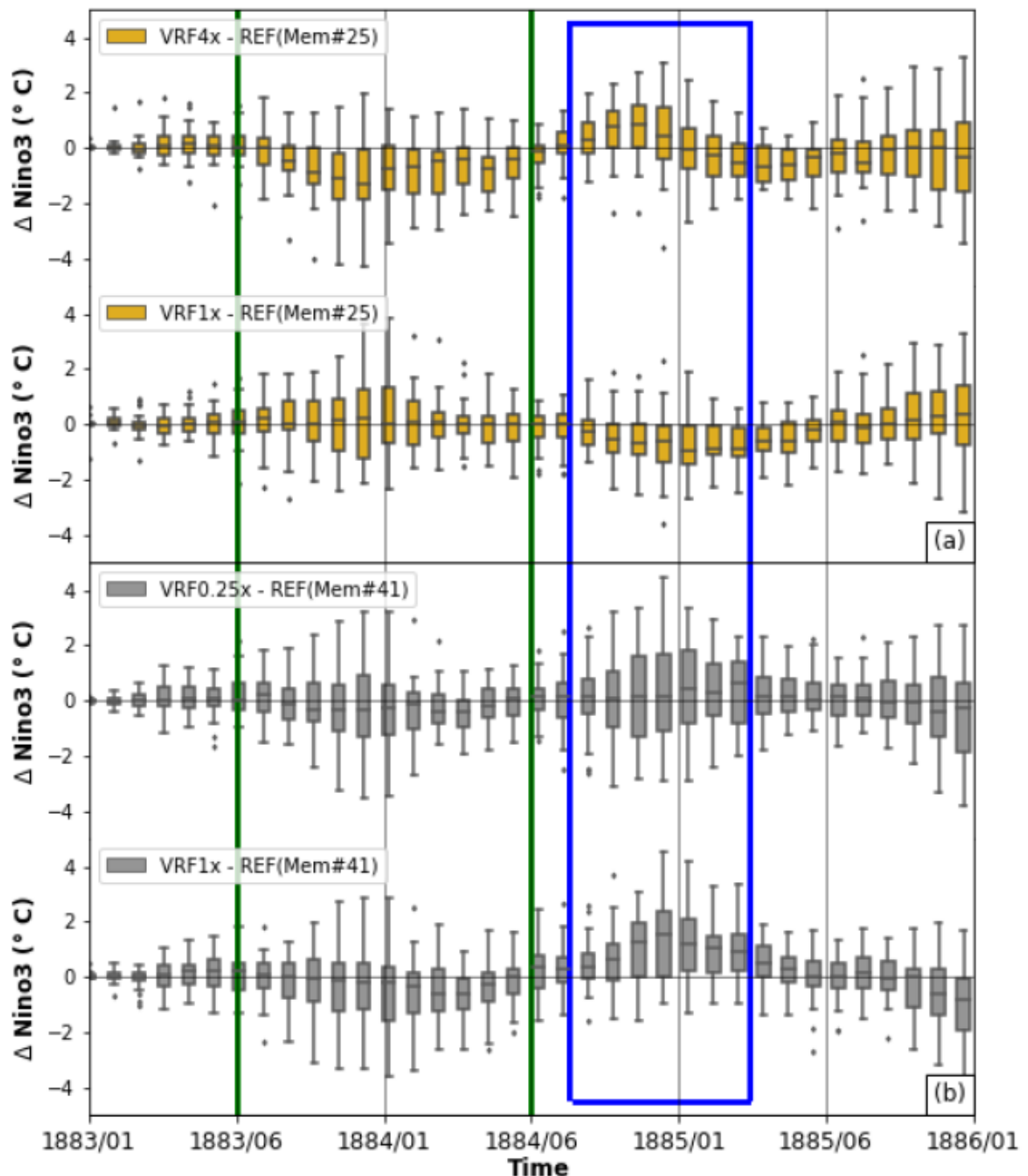


Figure 4.4: Box-whisker plots illustrating the distribution of $\Delta \text{Niño}_3$ fluctuations from January 1883 to December 1885 showing ENSO's reaction on the intensity of the LVE

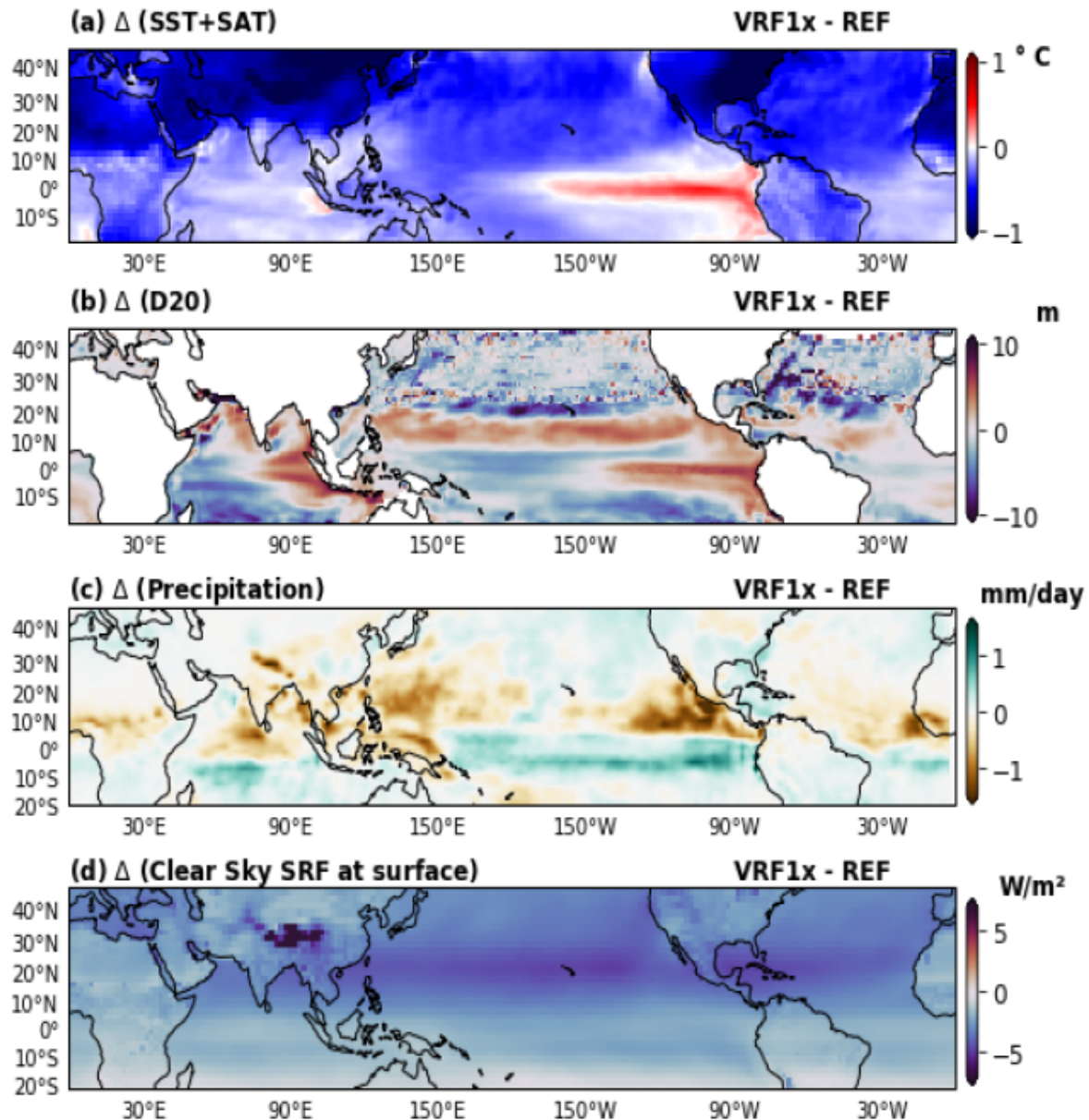


Figure 4.5: Spatial maps of VRF1x - REF generated by ensemble mean of 100 members of Krakatoa VRF realisations in tropical Indo-Pacific and monsoon domain

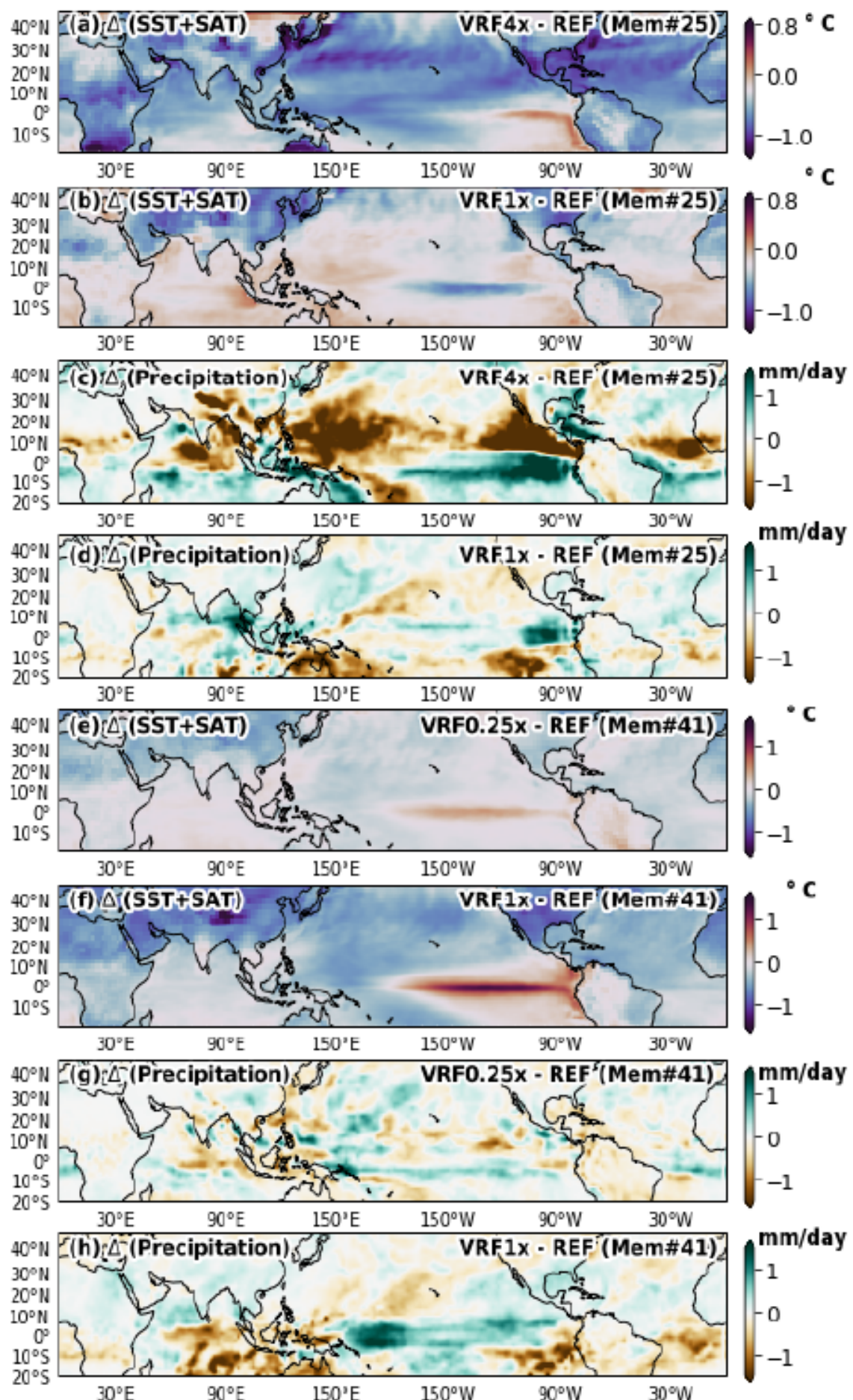


Figure 4.6: (Previous page.) Response of the tropical Indo-Pacific region to varied magnitudes of volcanic activity

tialized from cold IC, late El Niño in case of warm IC and near-neutral conditions when starting with neutral ICs (Figure 4.3). Increase in phase speed / angular frequency when the IITM-ESM is forced with Krakatoa VRF (Figure 4.3). The experiments are further repeated such that for the cases that transitioned to warm ENSO conditions with 1x VRF, IITM-ESM was rerun with the same initial conditions but with 0.25x VRF (Figure 4.1c). Similarly, for the cases that had transitioned to La Niña under 1x VRF, IITM-ESM was run again but with VRF increased to 4x and exact initial conditions (Figure 4.1b). A tendency for the ENSO system to transition towards the warm state in case of enhanced forcing and reduced warming in case of reduced forcing is noted (Figure 4.4). Spatial maps of VRF1x - REF show warming in the Pacific (Fig. 4.5) associated with deepened thermocline in the eastern Pacific and eastern Indian Ocean. Reduced clear-sky shortwave radiative forcing at the surface and reduced precipitation over India in the year following the Krakatoa eruption is also observed (Figure 4.5). The response of surface air temperature and precipitation to the various configurations of the experiments is shown in Figure 4.6. It can be seen that the states which were previously in a state of cold central Pacific under 1x VRF transition to an El Niño like state forced by 4 VRF.

Consequently, the Indian monsoon transitions from normal conditions to a state of drought (Figure 4.6). Conversely, under reduced forcing, i.e. 0.25x VRF, the warming gets suppressed in the central Pacific, and there is no definite signal over the Indian monsoon region. These experiments show that the system's state can play a vital role in determining the ENSO-IM coupling by deciding the ENSO state. Volcanic radiative forcing also plays a crucial role in determining the phase coupling between ENSO and IM.

4.2.1 Mechanism of ENSO-IM coupling from IPSL PMIP3 outputs

The mechanism for ENSO-IM coupling has been attempted to be understood by the composites of various fields from the IPSL PMIP3 model simulations. It can be seen that immediately after the volcanic eruptions, i.e. in the year (+1), there is a net positive radiative forcing at the eastern equatorial Pacific. This is due to the Bjerknes feedback. If we provide uniform heating across the Pacific in neutral conditions, the east will get heated less than the west. This is due to the upwelling along the eastern shore that will bring up the cold water from the deep ocean. This results in the development of an east-west gradient of temperature. Opposite effect would result if we uniformly cool the Pacific as with a volcanic eruption. East-West gradient will develop but now, with the east getting warmed up and the west cooling down. This feedback mechanism explains the El Niño-like anomaly in the eastern Pacific following a volcanic eruption as shown

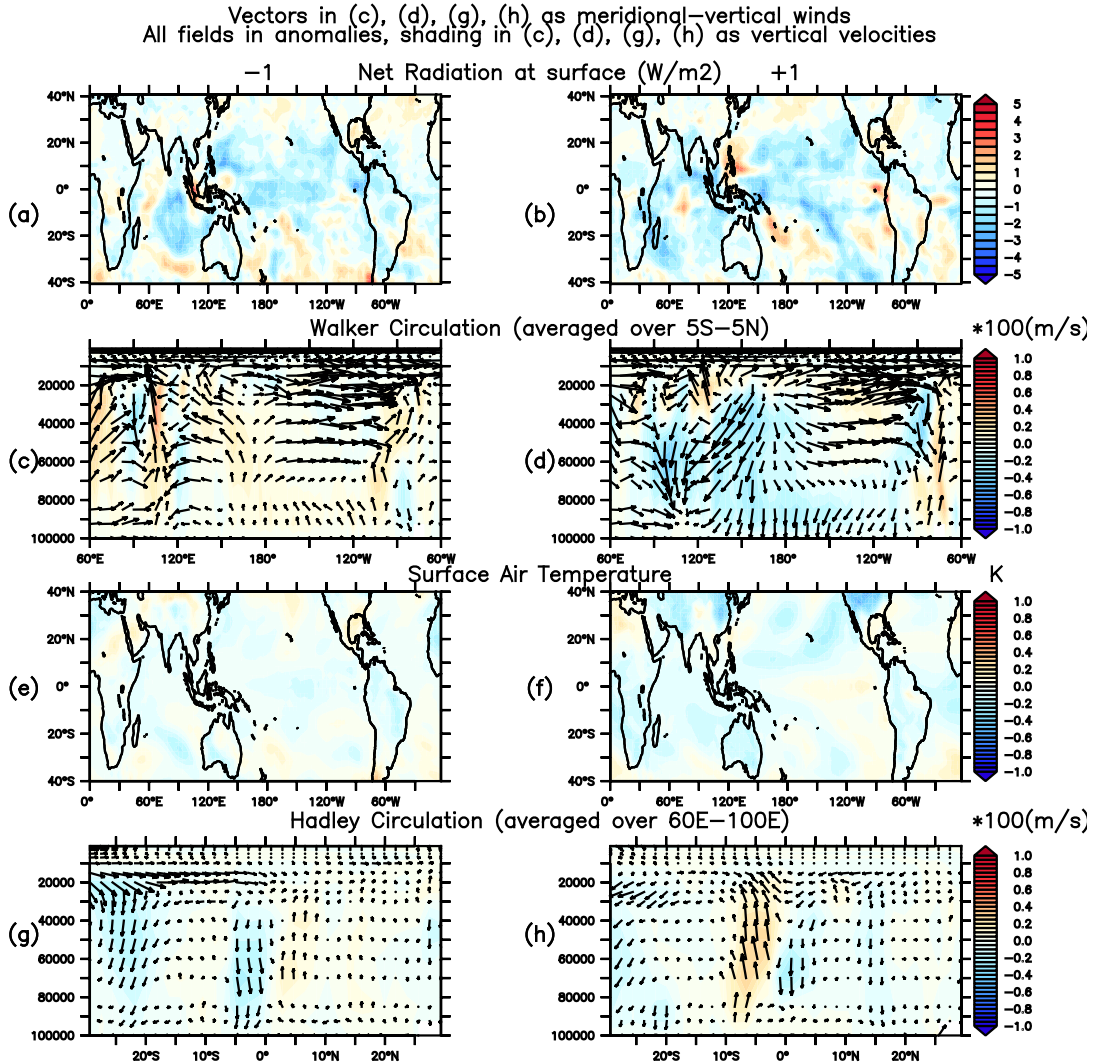


Figure 4.7: Composite of Net Surface Radiation, Walker Circulation(5S-5N averaged), Surface Air Temperature and Hadley Circulation (60E-100E averaged) for large volcanic eruptions (mag>1.0 W/m²) for years -1 and +1 relative to the volcanic eruption

in the Figure 4.7 for the year after the eruption. The Walker circulation breaks down, eventually leading to a break down of the Hadley circulation weakening Indian Monsoon.

In the subsequent years following the volcanic eruptions, there is a high probability of a La Niña (Sun et al. (2019)). This can also be seen in the composite analysis from the last millennium simulations of the IPSL model. The Indian Monsoon strengthens as a result, and hence the coupling strengthens. Year +2 shows signatures of the La Niña associated with strengthening monsoon winds as a mark for enhancing coupling. That La Niña results from the volcanic eruption induced forcing and not internal variability is explained in detail in Sun et al. (2019)

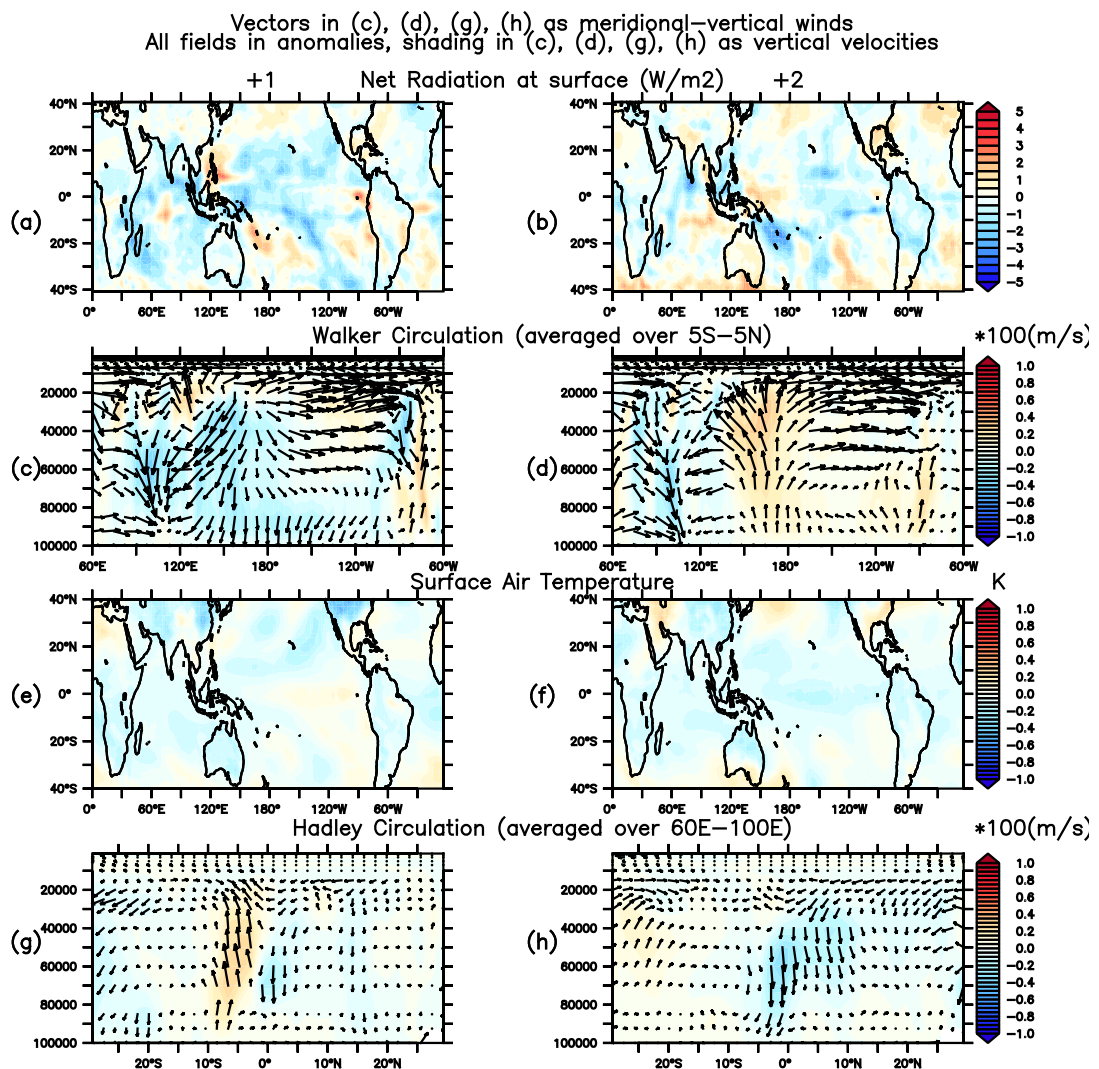


Figure 4.8: Composite of Net Surface Radiation, Walker Circulation(5S-5N averaged), Surface Air Temperature and Hadley Circulation (60E-100E averaged) for large volcanic eruptions (mag>1.0 W/m²) for years +1 and +2 relative to the volcanic eruption

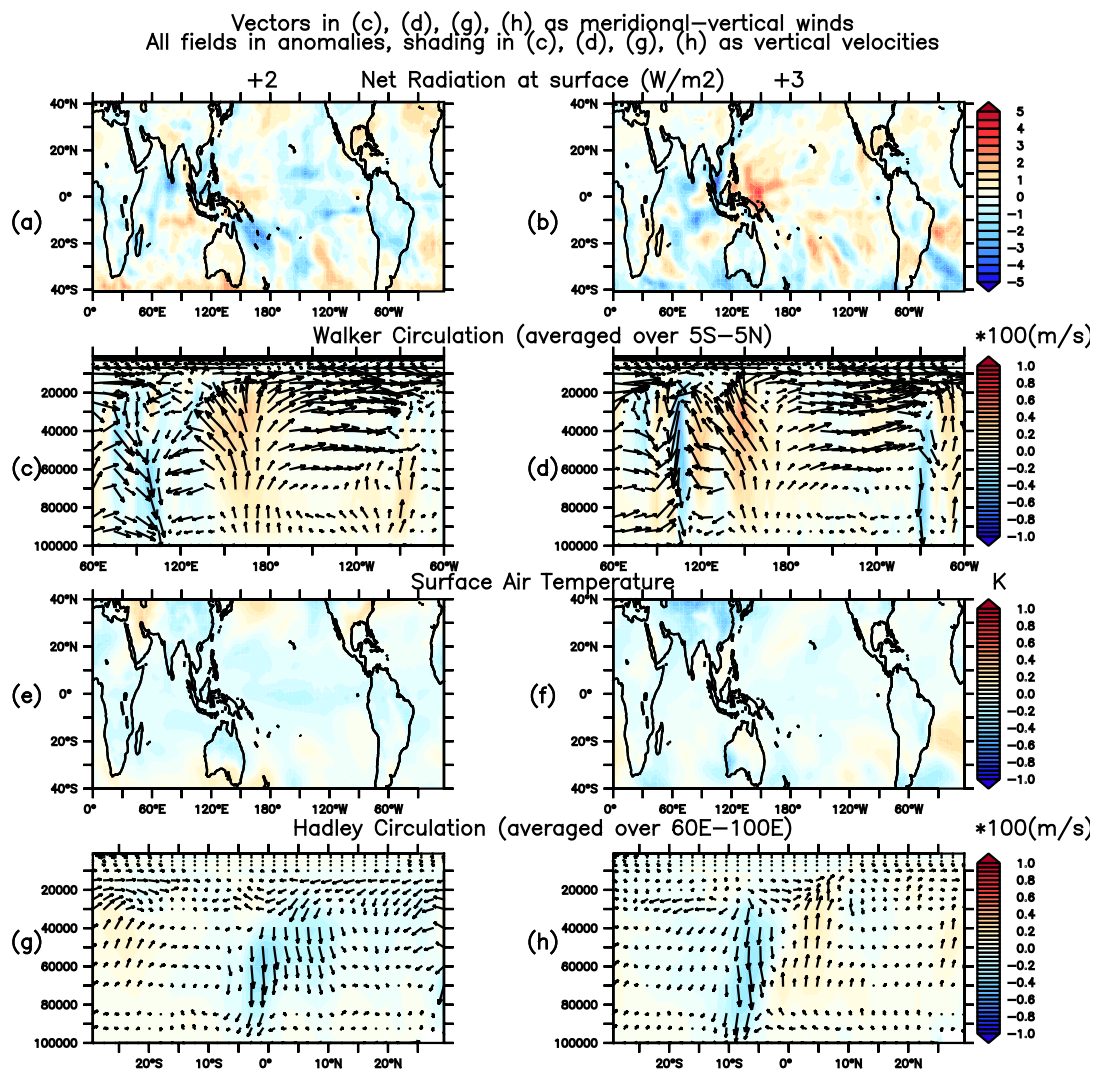


Figure 4.9: Composite of Net Surface Radiation, Walker Circulation(5S-5N averaged), Surface Air Temperature and Hadley Circulation (60E-100E averaged) for large volcanic eruptions ($\text{mag} > 1.0 \text{ W/m}^2$) for years +2 and +3 relative to the volcanic eruption

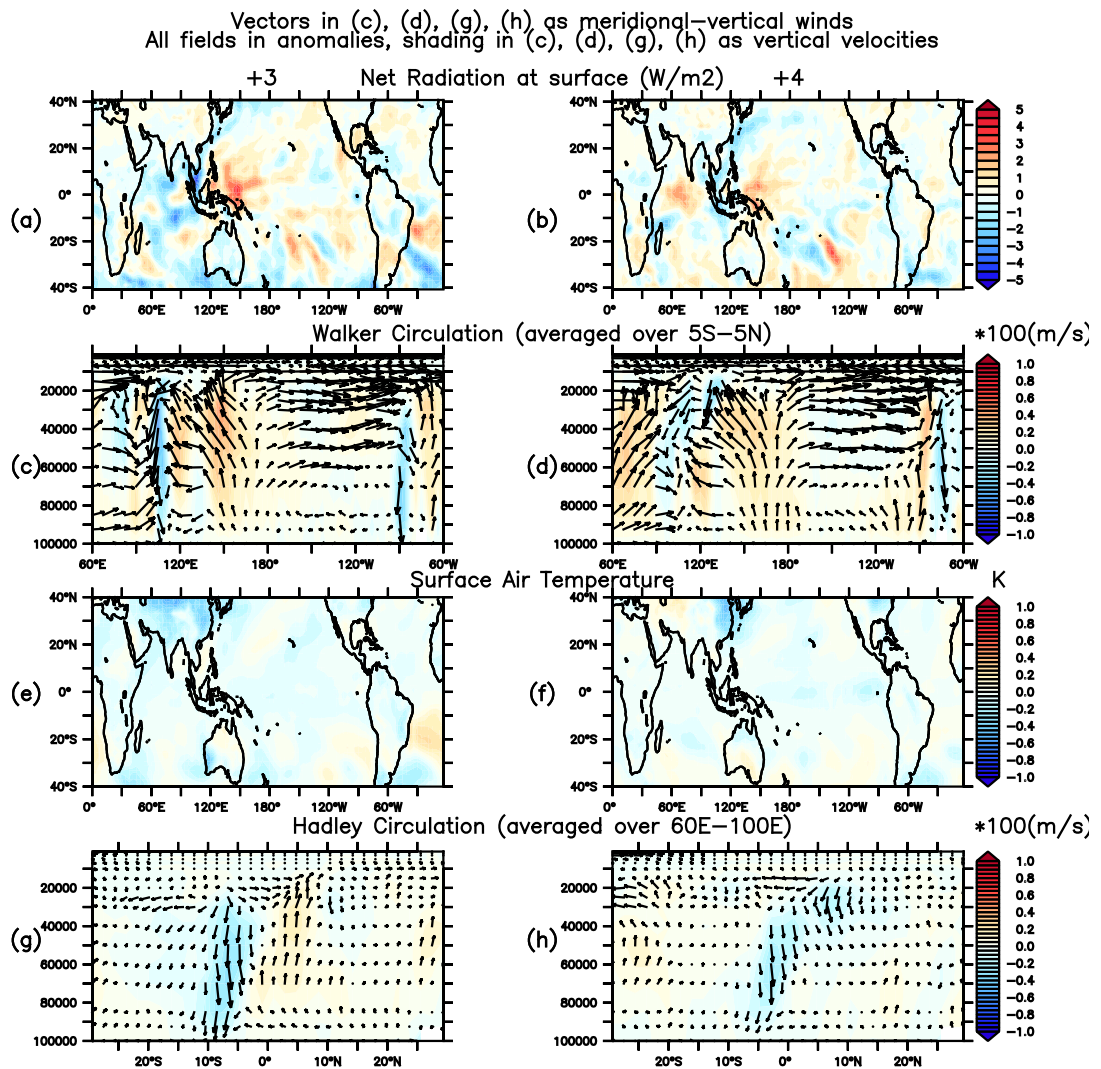


Figure 4.10: Composite of Net Surface Radiation, Walker Circulation(5S-5N averaged), Surface Air Temperature and Hadley Circulation (60E-100E averaged) for large volcanic eruptions ($\text{mag} > 1.0 \text{ W/m}^2$) for years +3 and +4 relative to the volcanic eruption

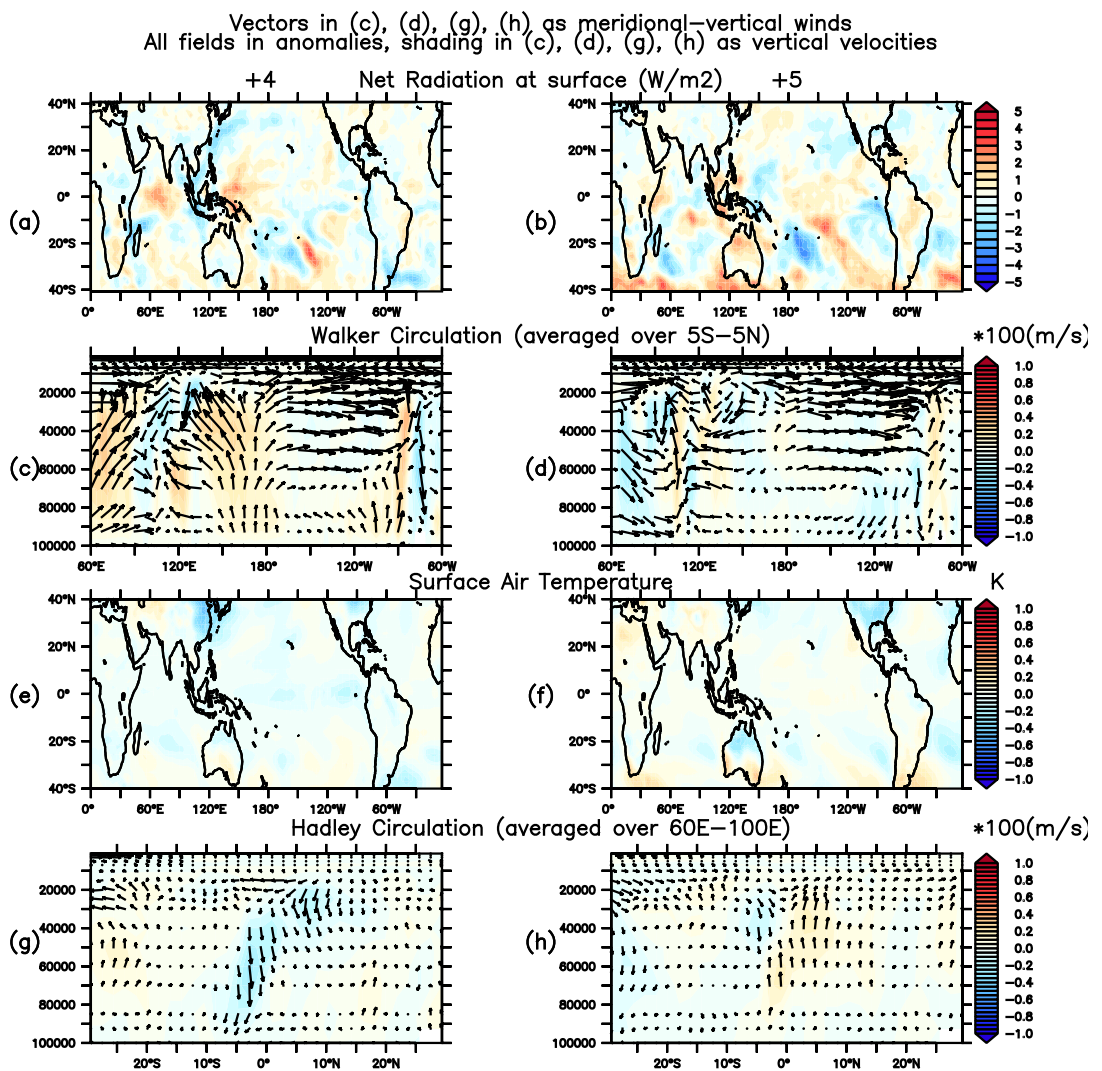


Figure 4.11: Composite of Net Surface Radiation, Walker Circulation(5S-5N averaged), Surface Air Temperature and Hadley Circulation (60E-100E averaged) for large volcanic eruptions (mag>1.0 W/m²) for years +4 and +5 relative to the volcanic eruption

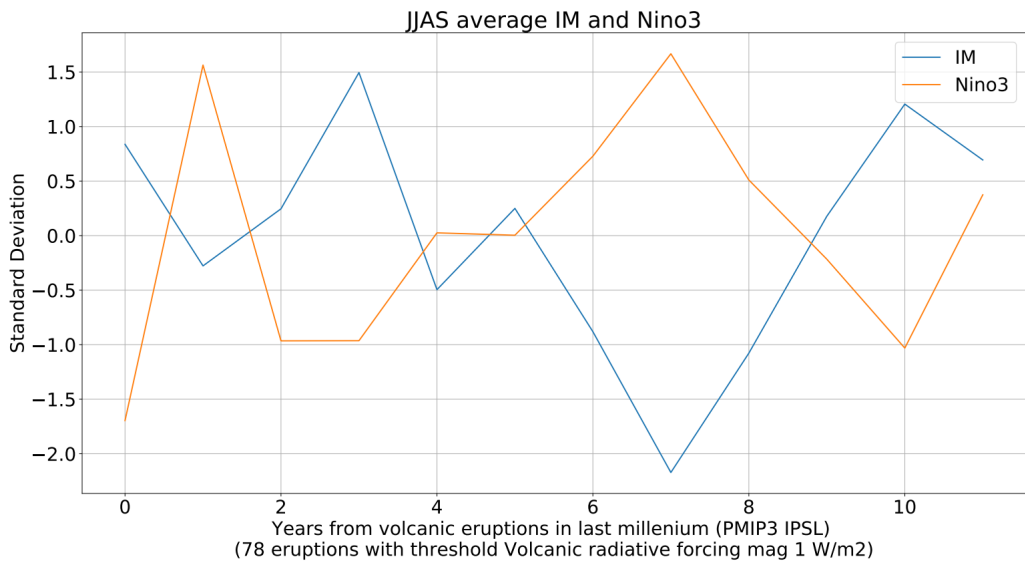


Figure 4.12: Composite time series of Nino3 and IM after an eruption

4.3 Paleoclimatic evidence of volcanism forced ENSO-monsoon coupling

This section illustrates the various paleoclimatic proxy datasets used in the analysis (Table 4.1). The correlation coefficients between ENSO and Indian Monsoon between different epochs in the historical period and last millennium deduced from the phase coherence analysis as phase coherent periods is shown in Table 4.2.

Table 4.1: Datasets used

Index	Variable/Proxy	Source	Period
HEN	Nino3 SST	HadISST (Rayner et al. (2003))	1871 – 2016
HIM	All India Rainfall	India Met. Dept. (Kothawale and Rajeevan (2017))	1871 – 2016
EN1	ENSO Proxy	North American tree rings (Li et al. (2011))	900 - 2000
EN2	ENSO Proxy	Tree-rings Asia, New Zealand, North & South America (#2222) (Li et al. (2013))	1300 - 2000
EN3	ENSO Proxy (Nino3)	Global paleoclimate reconstructions using tree-rings, ice-cores, coral, sediments & others (Mann et al. (2009))	500 – 2000
EN4	ENSO Proxy	Laguna Pallcacocha sediment (Moy et al. (2002))	Past 12000 years before 1950

Continued on next page

Table 4.1 – continued from previous page

Index	Variable/Proxy	Source	Period
EN5	ENSO Proxy	Tree rings “TEX-MEX” region North America (D’Arrigo et al. (2005))	1408-1978
EN6	ENSO Proxy (Unified proxy)	Multiple sources (McGregor et al. (2010))	1650–1978
EN7	ENSO Proxy (Southern Oscillation Index)	Tree rings from North America and Indonesia (Stahle et al. (1998))	1706-1977
EN8	ENSO Proxy	Network of tropical records from circum-Pacific (Emile-Geay et al. (2013))	1000-2000
EN9	ENSO Proxy (Nino3)	Tree-ring data from Mexico and Texas (Cook et al. (2008))	1300-2006
EN10	ENSO Proxy	Tree rings, corals, ice cores & documentary evidences (Gergis and Fowler (2009))	1525 - 2000
EN11	ENSO Proxy (Southern Oscillation Index)	Precipitation reconstructions in Indo-Pacific and Galapagos (Yan et al. (2011))	50 – 1955
EN12	ENSO Proxy	Global proxy records (743) (Dätwyler et al. (2019))	1000 – 1990
EN13	ENSO Proxy	Annually resolved multi-proxy records (40) from Tropics (Wilson et al. (2010))	1540 – 1998
EN14	ENSO Proxy	Multiple records from Pacific basin (13) (Braganza et al. (2009))	1525 – 1982
IM1	$\delta^{18}\text{O}$ anomaly	Stalagmites from Dandak cave (19°00N, 82°00E) in core monsoon zone (Sinha et al. (2007))	600 – 900
IM2	Precipitation	Stalagmites from Jhumar (18° 52N, 81° 52E) and Wah Shikar (25° 15N, 91° 52E) caves (Sinha et al. (2011))	600 – 2008
IM3	$\delta^{18}\text{O}$ anomaly	Gridded Monsoon Area Drought Atlas (MADA) for South Asia from network of tree rings (Cook et al. (2010))	1300 – 2004
IM4	Precipitation	Stalagmites from Sahiya cave (30° 36N, 77° 52E) (Sinha et al. (2015))	96 – 2000

Continued on next page

Table 4.1 – continued from previous page

Index	Variable/Proxy	Source	Period
IM5	IM Proxy over Central India Precipitation	Multiple tree rings and documentary records (Shi et al. (2018))	1470 – 2013
IM6	IM Proxy South Asian summer monsoon	Index & Reconstructed SASMI using multiple ENSO, PDO and AMO reconstructions (Shi et al. (2017))	895 – 2000
IM7	IM Proxy South Asian summer monsoon Index	Tree ring chronologies (15) (Shi et al. (2014))	900 – 1996
IM8	IM Proxy Palmer Drought Severity Index	Tree ring records from Manali (32°13N, 77°13E) (Sano et al. (2017))	1767 – 2008
IM9	IM Proxy Monsoon rainfall anomaly	Tree ring chronology from Kerala, South India (Borgaonkar et al. (2010))	1481–2003
IM10	IM Proxy $\delta^{18}\text{O}$ anomaly - Precipitation	Stalagmites from Uttar Kannada District of Karnataka, India (Yadava et al. (2004))	1666 – 1996
IM11	IM Proxy - May–Sept precipitation reconstruction	Tree rings, documentary evidences, ice-core records, instrumental observations (Feng et al. (2013))	1470 – 1999
PDO1	PDO Proxy	Global paleoclimate reconstructions using tree-rings, ice-cores, coral, sediments & others (Mann et al. (2009))	500 – 2000
PDO2	PDO Proxy	Reconstructed from instrumental records & tree ring chronologies (Biondi et al. (2001))	1661-1992
PDO3	PDO Proxy	Tree ring chronologies from Asia (70) (D'Arrigo and Wilson (2006))	1565 – 1988
PDO4	PDO Proxy	Tree ring chronologies from California and Alberta (MacDonald and Case (2005))	993-1996

Table 4.2: Pearson correlation coefficients for different volcanically induced epochs in the last millennium, their data sources and number of paleoclimatic reconstructions confirming significant correlation

Epoch	Pearson Correlation Coefficient(p-value)	Data Source/Description	# of combinations of paleoclimatic data (ENSO and IM) confirming significant correlation
1888-1898	-0.259 (0.004)	Observational data from 1871-2016 (see Table S1 / HEN, HIM).	
1965-1975	-0.264 (0.003)		Not Applicable
1871-2016	-0.079 (0.0008)		
1888-1898	-0.56	Reconstructions of 14 ENSO (Table S1 / EN1, ..., EN14) and 11 IM (Table S1 / IM1, ..., IM11) indices.	33
1715-1725	-0.45		25
1630-1640	-0.67		12
1401-1411	-0.79		7
1715-1725	-0.64(0.0)	Variations of Nino3 and IM time-series from the IPSL PMIP3 last-millennium experiment (27)	
1630-1640	-0.59(0.0)		Not Applicable
1401-1411	-0.65(0.0)		

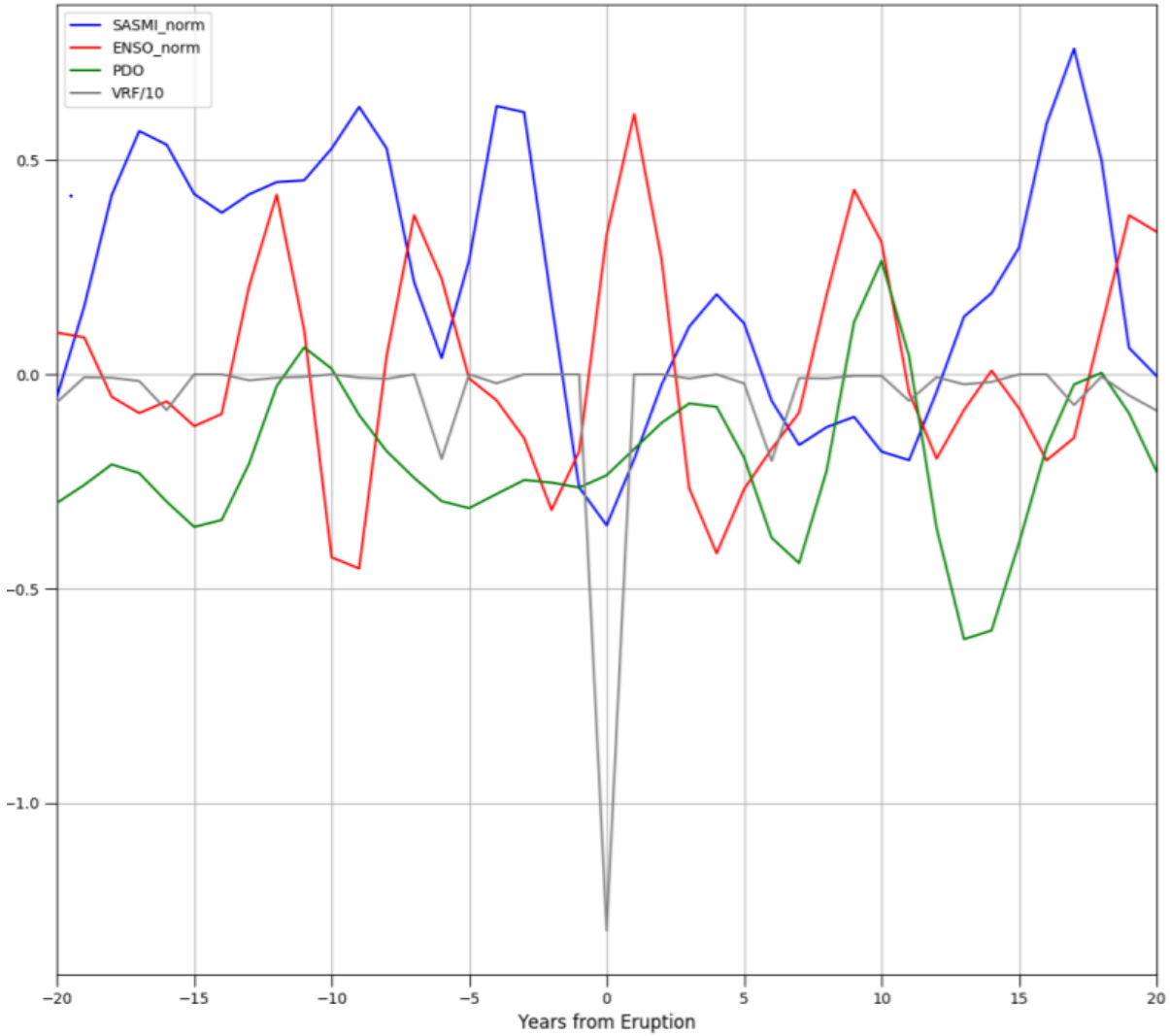


Figure 4.13: Superposed epoch analysis on proxy paleoclimatic data-sets for ISMR, ENSO, PDO and volcanic radiative forcing

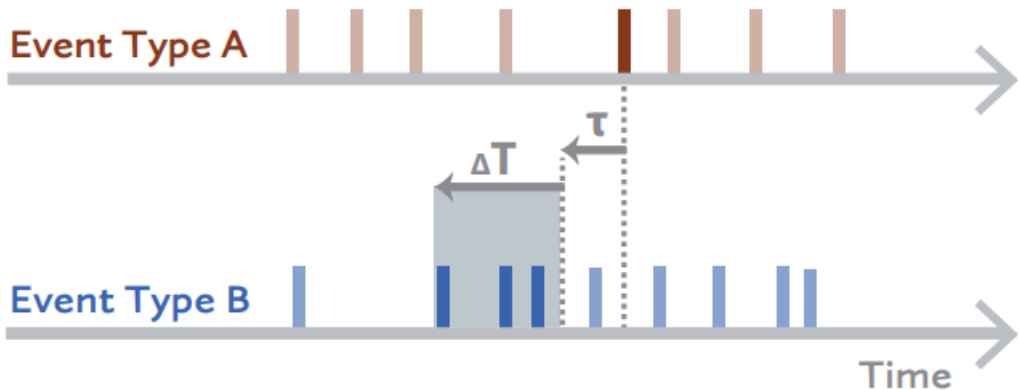


Figure 4.14: Figure illustrating event coincidence analysis for assessing statistical interrelationships between two events time series A and B. Reproduced from Donges et al. (2016) with permission

4.3.1 Event Coincidence Analysis

Event Coincidence Analysis is based on Donges et al. (2016). It counts coincidences between two different event types, let's say A and B. These coincidences are then tested for their statistical significance using twin surrogates. There are two series, and we want to try whether B precedes A (Figure 4.14). We define a coincidence interval as the maximum window within which event A should occur after B has occurred. Counting in this way for different coincidence intervals, precursor coincidence rates and trigger coincidence rates can be computed. Please refer Donges et al. (2016) for details on the equations. It can be seen from Figure 4.15 using three ENSO proxies and three Indian Monsoon proxies, using precursor coincidence rate, that there is a significant chance of El Niño and Indian monsoon drought in the year following the volcanic eruptions.

4.3.2 Bayesian Analysis

The paleoclimatic reconstructions from the last millennium were used for Bayesian analysis of phase coincidence using ENSO and Indian Monsoon. Various combinations of 14 ENSO and 11 IM reconstructions for the last millennium show enhanced probabilities of coupling conditional to a volcano in the previous year (Figure 4.16). Next, a question arises whether the coupling will happen every time a large volcanic eruption occurs. Bayesian analysis is conducted to calculate ENSO-IM coincidence probabilities up to year 4 following the volcanic eruption to test for the coupling further in time following the volcanic eruptions. We can see enhanced probabilities up to year four following the volcanic explosions (Figure 4.17). However, the coupling probability

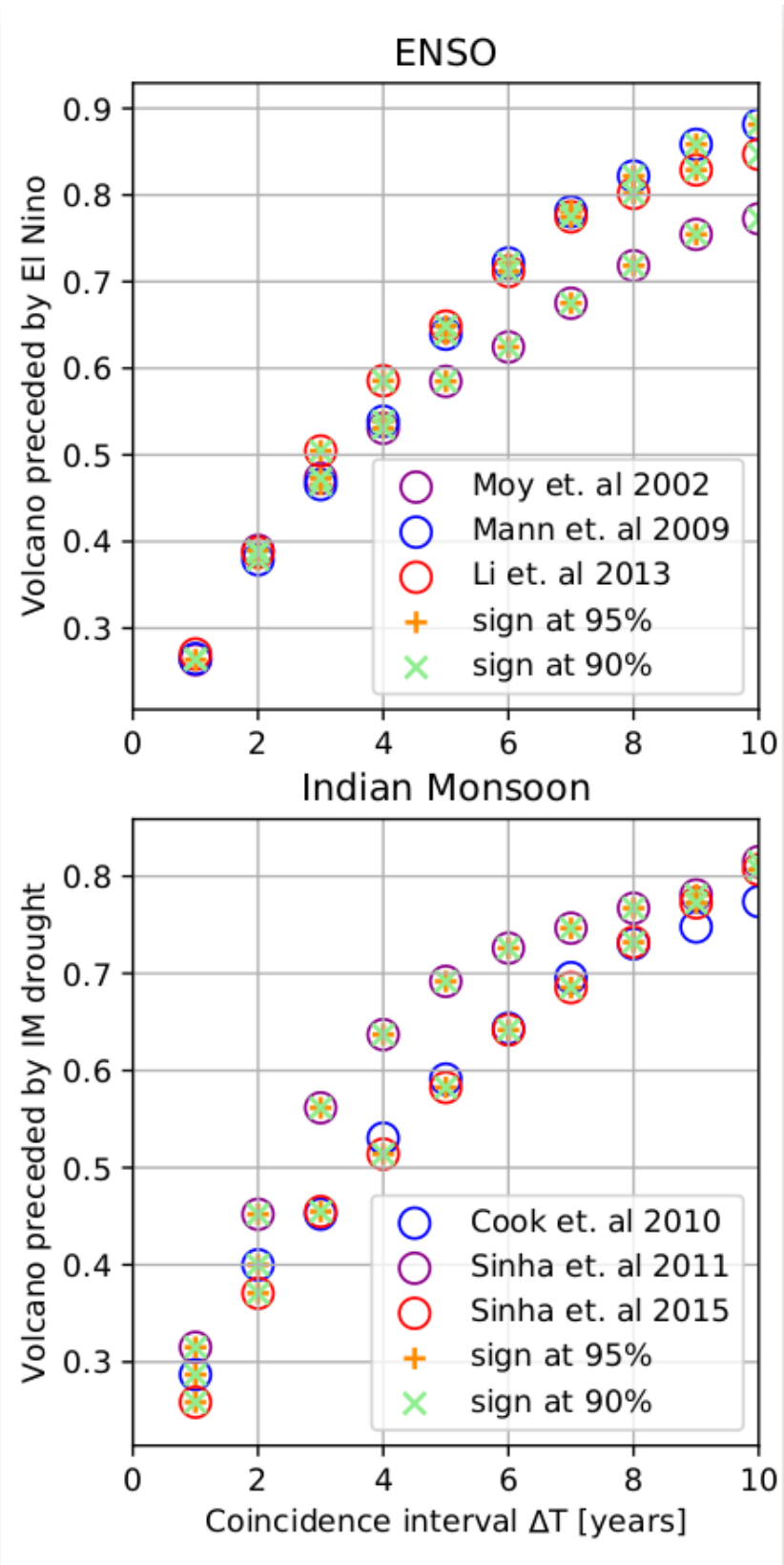


Figure 4.15: Event Coincidence Analysis (Precursor coincidence rate) for ENSO (top) and Indian Monsoon (bottom). The Event Coincidence Rates are such that volcano precedes ENSO and IM drought

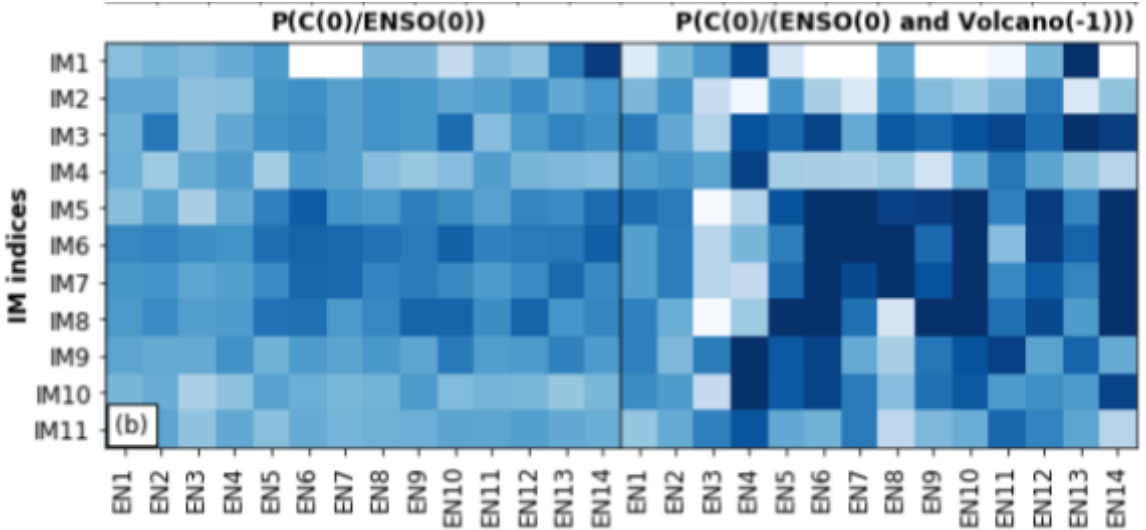


Figure 4.16: Conditional probability analysis of ENSO and IM coincidence subject to (left) ENSO (0), (right) ENSO (0) and Volcano (-1).

reduces as we move away from the volcanic eruption. The Bayesian conditional probabilities for different lags from the volcanic eruptions and different PDO datasets (PDO1..PDO4) are also computed. A consistent enhancement in the ENSO-IM coupling probabilities when supported by PDO and volcano compared to when conditioned only by the volcano is observed. When conditioning with PDO also, it is observed that the coupling probability reduces as we move away from the volcanic eruption; however probabilities remain high as compared to when not conditioned on PDO (Figure 4.18-4.21). These results corroborate the hypothesis that large volcanic eruptions induced ENSO-IM coupling.

4.3.3 Northern Hemispheric Land Cooling

The impact of volcanic eruptions on the Indian Monsoon region was further assessed by compositing the surface air temperature anomalies for the last millennium following volcanic eruptions relative to the period before the eruptions (Figure 4.22). We can observe a cooling of up to 0.5 degrees following the volcanic eruptions. Cooling of the landmass can weaken land-sea thermal contrast and hence suppress Indian Monsoon. The composite of Northern Hemispheric land surface temperature anomalies for strong volcanic eruptions ($\text{mag(VRF)} > 3.7 \text{W/m}^2$) shows strong cooling over India and the Northern Hemisphere. The data used is paleo-climatic reconstructions by Cook et al. (2013).

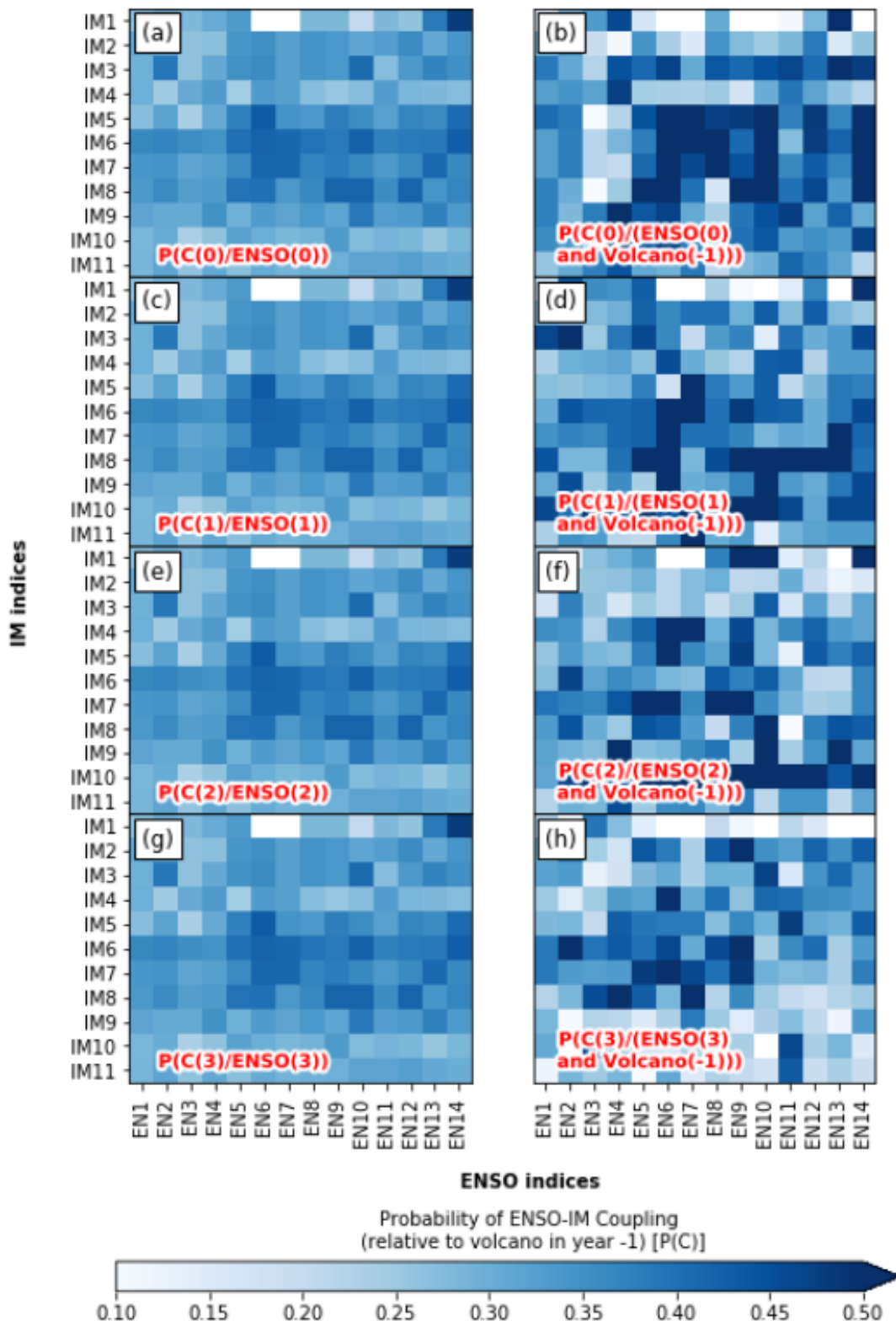


Figure 4.17: Conditional probability analysis of ENSO and IM coincidence subject to (left) ENSO (0), (right) ENSO (0) and Volcano () for different years relative to the LVE

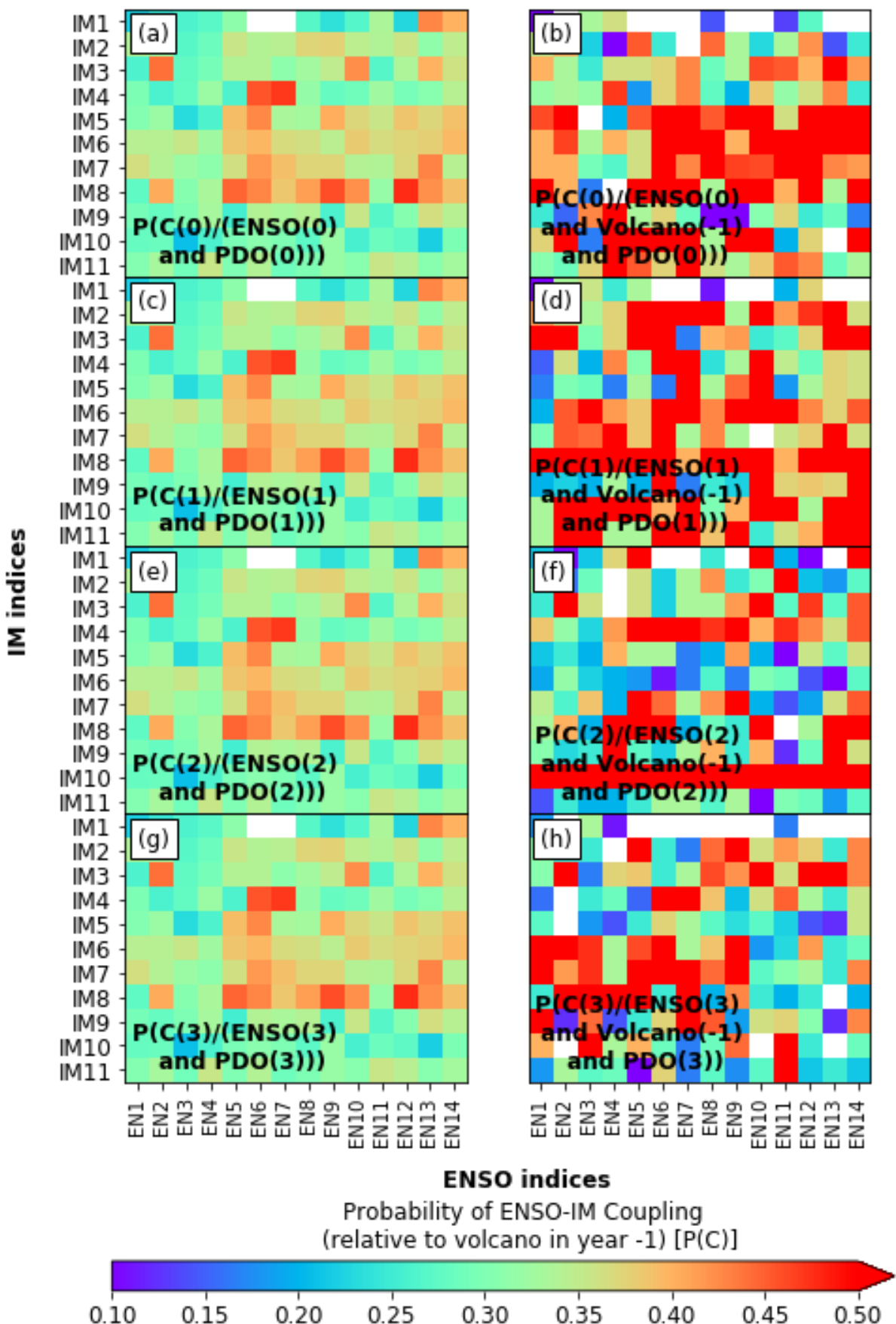


Figure 4.18: Similar to Figure 4.17, except that the conditioning is also done using the PDO index based on Mann et al. (2009)

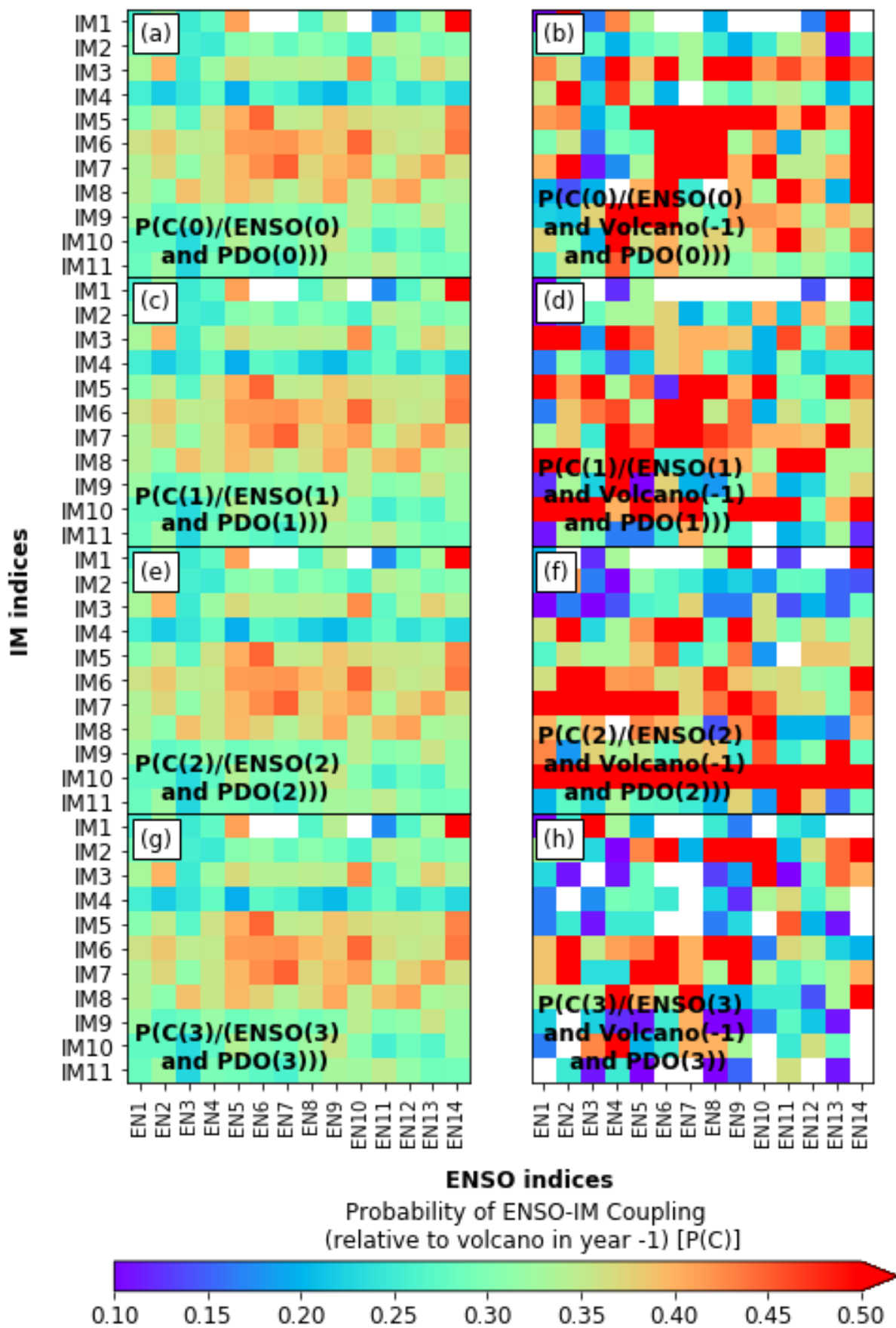


Figure 4.19: Similar to Figure 4.18, except that the PDO index is based on MacDonald and Case (2006)

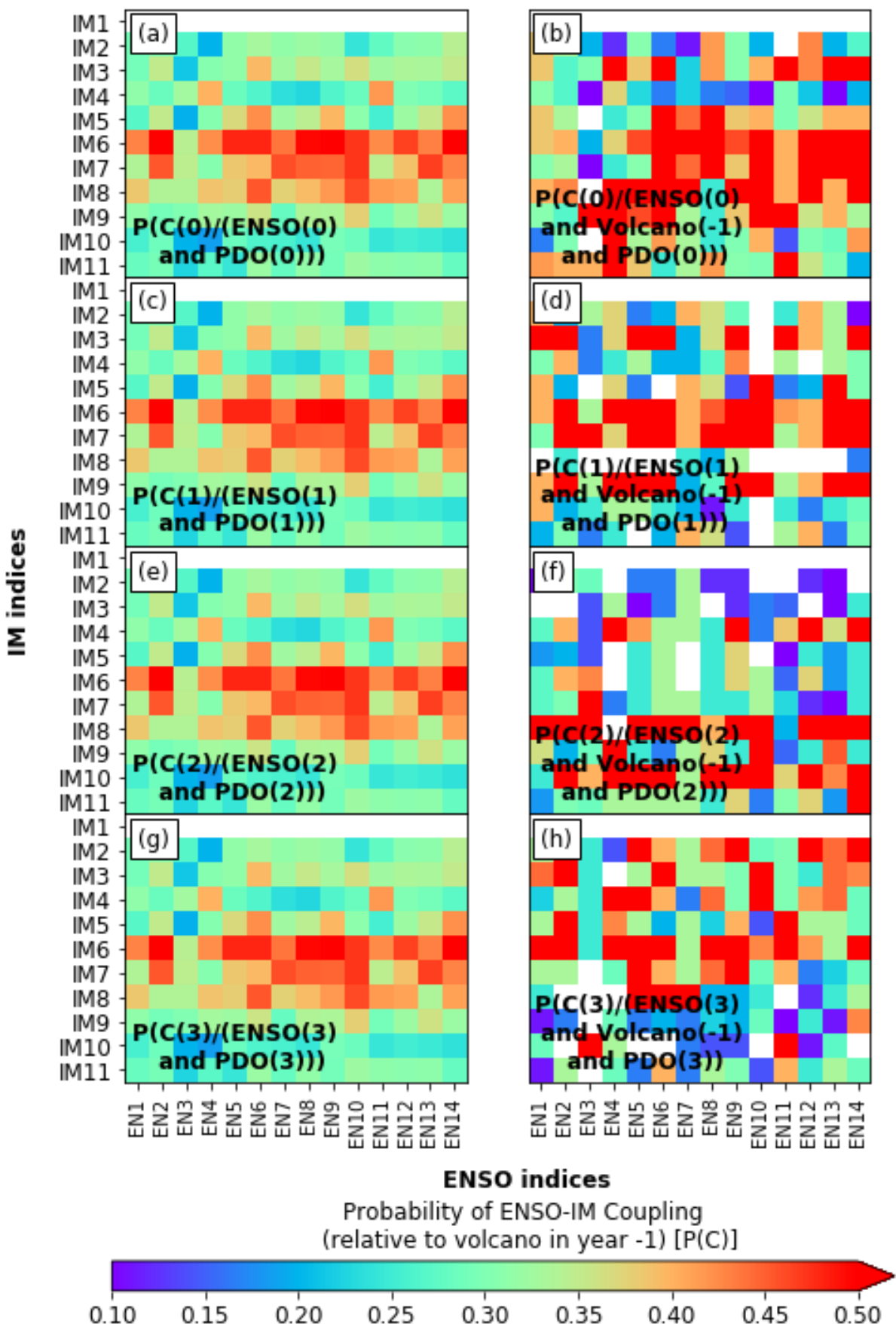


Figure 4.20: Similar to Figure 4.19, except that the PDO index is based on D'Arrigo and Wilson (2006)

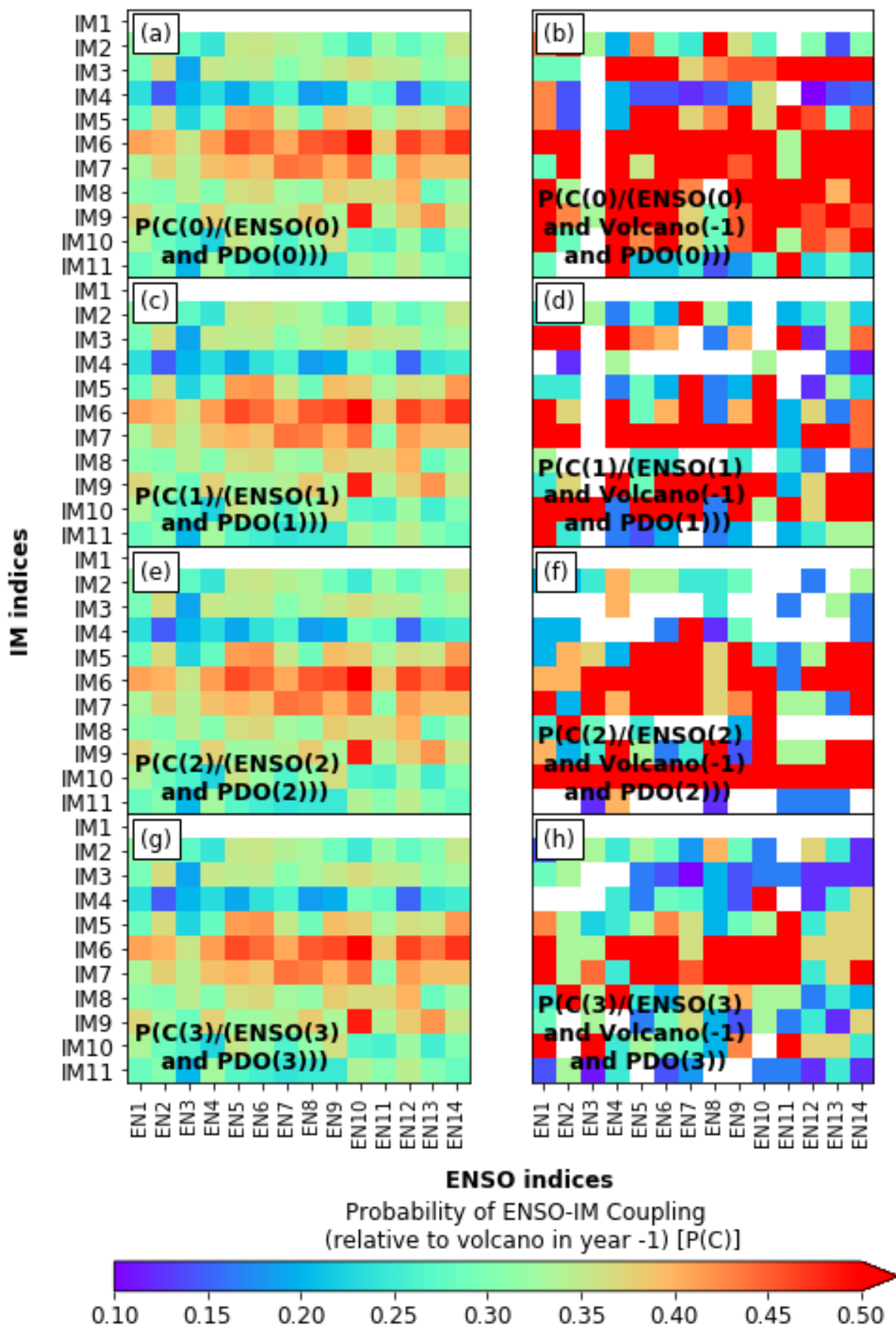


Figure 4.21: Similar to Figure 4.20, except that the PDO index is based on Biondi et al. (2001)

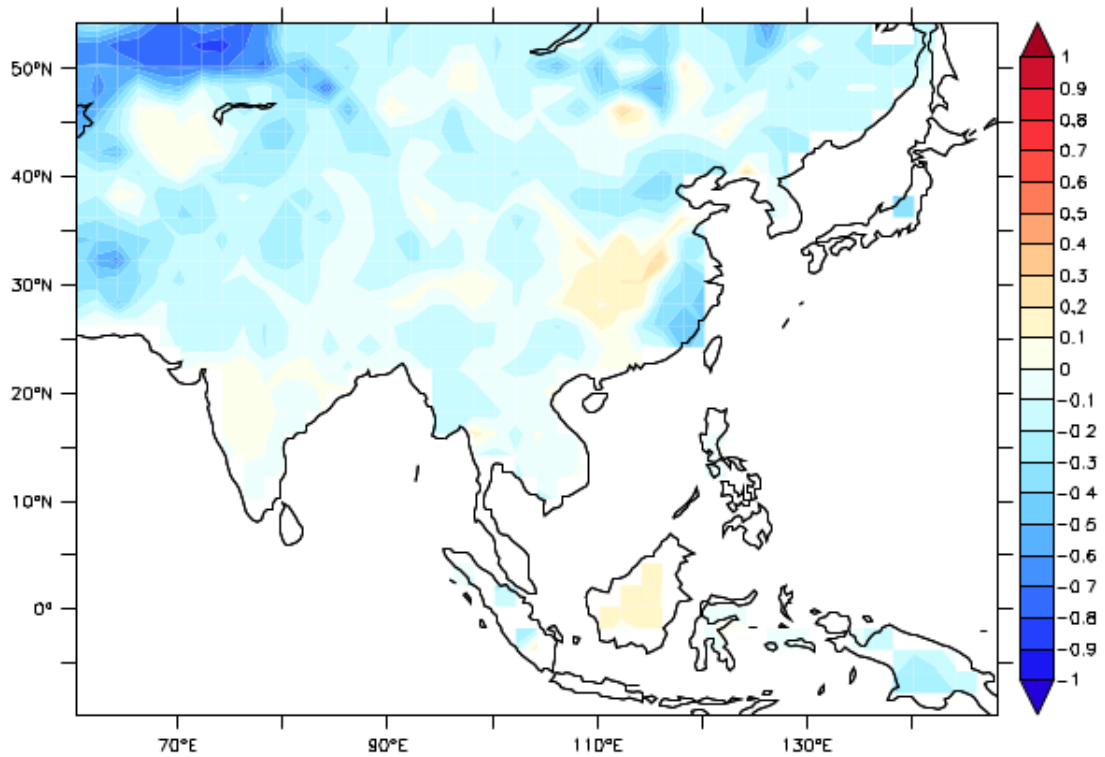


Figure 4.22: Response of summer temperatures in the Northern Hemisphere to very strong volcanic eruptions in the last millennium. The volcanoes are selected as top 25 from Sigl et al. (2015). Surface air temperature data from the last millennium is from Cook et al. (2010)

4.4 Climate Network Analysis

The case of Krakatoa (1884) volcanic eruption and the phase-locking that followed is a typical one in which, immediately following the eruption, there was no El Niño in the Pacific; rather the 5-6 years following the eruption were associated with La Niñas and wet monsoons. It was only in the El Niños of 1896 and 1899 that droughts were observed over India. The 20 year period following this eruption (1884-1903) is an epoch of high anti-correlation between ENSO and Indian Monsoon, and the phase-locking is very strong. In contrast, the period following Agung (1964) eruption was immediately followed by a strong El Niño and a drought in 1965, and the extended period until 1982 was associated with strong phase synchronization between ENSO and IM. Therefore, it is important to understand the different couplings manifested during these two epochs and why they occurred.

A climate network analysis similar to the one done by Tsonis et al. (2006) was performed 3 years before the eruptions and 3 years after the eruption (including the year of eruption). The data of monthly surface air temperatures from historical IPSL CMIP5 simulation was used for this analysis. Degree centrality is plotted in Figure 4.23, which clearly shows that following the Krakatoa eruption, India and its surrounding regions (maritime continent) were not a part of the climate network. However, when we observe degree centrality following Santa Maria (1902) and Agung (1963) eruptions, the Indian landmass and the maritime continent have a high degree centrality. These cues from the climate network analysis lead us to believe that the state of the system plays a role in the coupling as the Pacific Decadal Oscillation positive phase was stable to declining during the Krakatoa (1884) eruption. In contrast, during the other two volcanic explosions, it was moving towards a positive phase.

4.5 Conclusions

The analysis conducted using targeted IITM-ESM simulations and paleoclimate proxy records are analysed in this chapter. It is found that following the volcanic eruptions, there is an enhanced probability of ENSO-IM coincidence from Bayesian analysis of proxy records. The enhanced coincidence probabilities persist at least until four years following the volcanic eruptions. Large ensemble IITM-ESM simulations point to the Indian monsoon drought and El Niño in the Pacific in the year following a large volcanic eruption. The role of the state of the system in the Pacific and the strength of volcanic eruptions are also tested by separate simulations of IITM ESM. Existing cold sea surface temperature anomalies in the Pacific are conducive to coupling relative to warm anomalies. Increased strength of volcanic eruptions further contributes to the coupling. This chapter concludes the work on understanding the role volcanic aerosols in

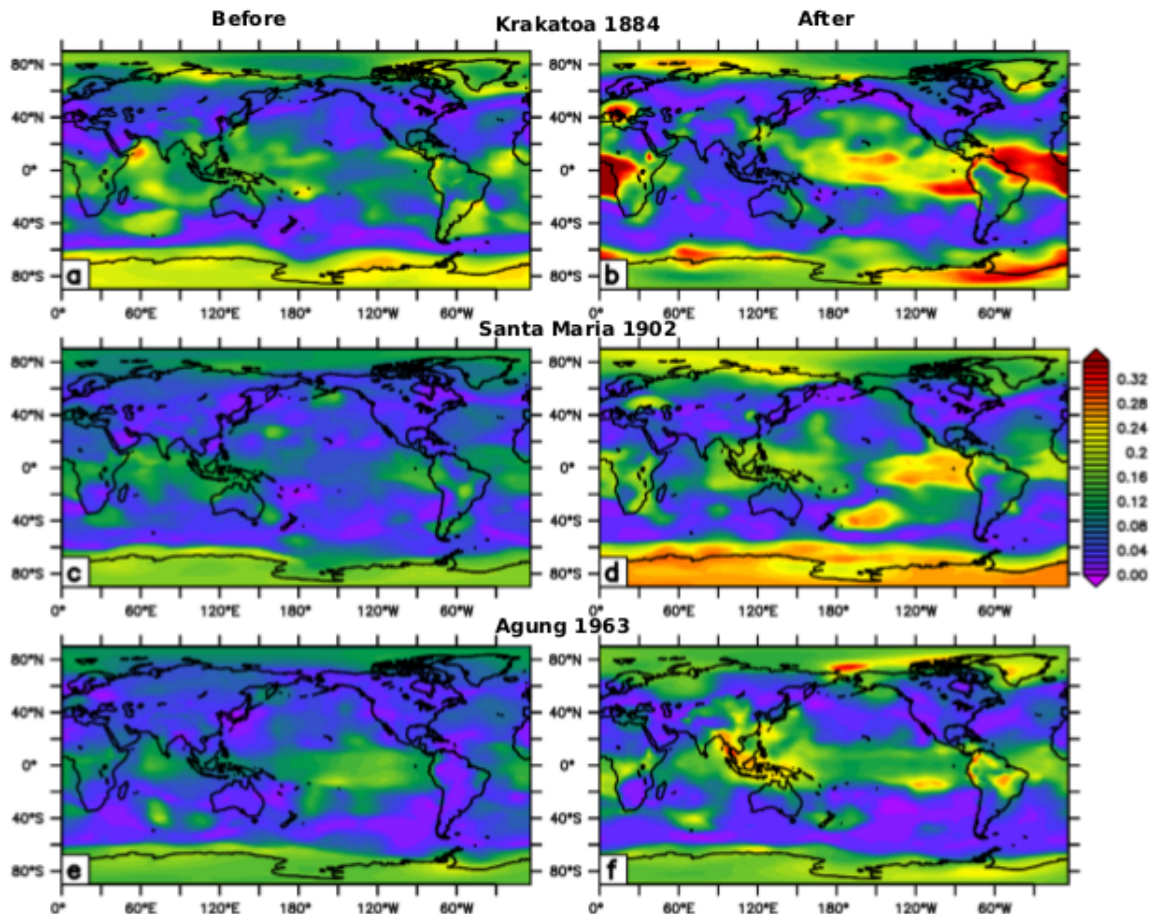


Figure 4.23: Climate Network Analysis: Degree Centrality of the Climate Network (Tsonis) from the monthly surface air temperature (tas) from the CMIP5 IPSL-CM5B-LR historical simulation. The left panel (a, c, e) shows the degree centrality before the eruption (-3, -2, -1 years relative to the eruption) and the right panel shows the network after the eruption (0, 1, 2 years relative to the eruption). It can be seen that the Indian landmass/Indian Ocean areas are not a part of the system/not in the network from b after Krakatoa 1884 eruption. Tsonis et al. (2006)

tropical ocean-atmosphere-land coupled system.

The next chapter discusses the variability caused by mixed natural-anthropogenic aerosols on the South Asian monsoon via changes in land-atmosphere interactions.

Chapter 5

Role of anthropogenic aerosols on the tropical ocean-atmosphere-land coupled system and South Asian monsoon and associated aerosol-land-atmosphere interactions

Niyogi et al. (2007) stated that the Indian summer monsoon response to aerosols may be investigated via the lens of aerosol-land-atmosphere interactions. Although earlier research has sought to add information on the understanding of how aerosols change hydroclimate, there have been limited studies explicitly concentrating on the interactions between aerosols, land, atmosphere and the Indian monsoon (e.g. Singh et al. (2019), Krishnan et al. (2016)). Furthermore, all of the research relied solely on observations or models or was limited to remote or local aerosols. Past modeling studies have been structured as long-term spin-up simulations with constant forcing and no-forcing (control) experiments to decouple the influence of aerosols in the atmosphere. Because aerosols exhibit a substantial forcing, the researchers conclude that using them to improve the prediction of numerical weather systems is a good idea. It has been shown in the survey by Sanap et al. (2015) and others (Kedia et al. (2014), Srivastava and Ramachandran (2013), Kaskaoutis et al. (2012a), Dey et al. (2008)) that the dust-coated with anthropogenic aerosols is the most likely mixed state of aerosols over the Indian region.

As evidenced by observational studies, this diverse state is responsible for the aerosol radiative forcing over the region. Amongst modeling or observational studies, only limited research has used a variety of aerosols in different forms. A multi-model multi-observational effort is required to demonstrate the potential predictability due to aerosols for extending beyond the limited theoretical modelling research. Furthermore interactions between aerosols, land, and the atmosphere, which are critical components of the coupled ocean-atmosphere-land Indian summer monsoon system, have received little attention.

5.1 IITM Earth System Model experiments

Developed from the seasonal forecast system CFSv2, the IITM-ESM is a model of the Earth's system. Several modifications and enhancements have been made, including better radiative balance at the top of the atmosphere, the incorporation of additional components for land use-/land cover, aerosols, and a revised cumulus parameterization method (Swapna et al. (2018), Swapna et al. (2015)). The model's faithfulness for the South Asian Monsoon simulations, as well as its sensitivity to volcanic eruptions, has been demonstrated (Singh et al. (2020), Swapna et al. (2018)). The model is composed of an atmospheric component based on the GFS, an ocean component based on the MOM4p1, a land surface component based on the NOAH-LSM, and aerosols prescribed using the MACCv2-SP parameterization. MACCv2-SP generates aerosol optical properties for models that do not include interactive aerosols but want to simulate the realistic radiative impacts of aerosols. It is designed for models that do not include interactive aerosols but still want to simulate the realistic radiative effects of aerosols. Using the IITM-ESM model, sensitivity experiments with and without anthropogenic aerosols have been conducted. Hindcast simulations for the year 2002 are produced. The year 2002 is chosen as it was one of the worst droughts in recent times. It had the largest dust aerosol optical depth over North Indian plains. All the models at that time were unable to simulate the seasonal monsoon suppression. The initial conditions of the atmosphere, ocean, and land are prepared for these hindcasts. Thirty ensemble members (Milinski et al. (2020)) are run, with each simulation commencing at 00z on the days 21 April, 22 April, 23 April...20 May through 15 October with and without anthropogenic aerosols. A high enough number of ensembles is required to interpret the signal from the sensitivity trials and balance out the model's internal variability (Milinski et al. (2020)). This ensures a high signal-to-noise ratio from the ensemble averages (Sterl et al. (2007)).

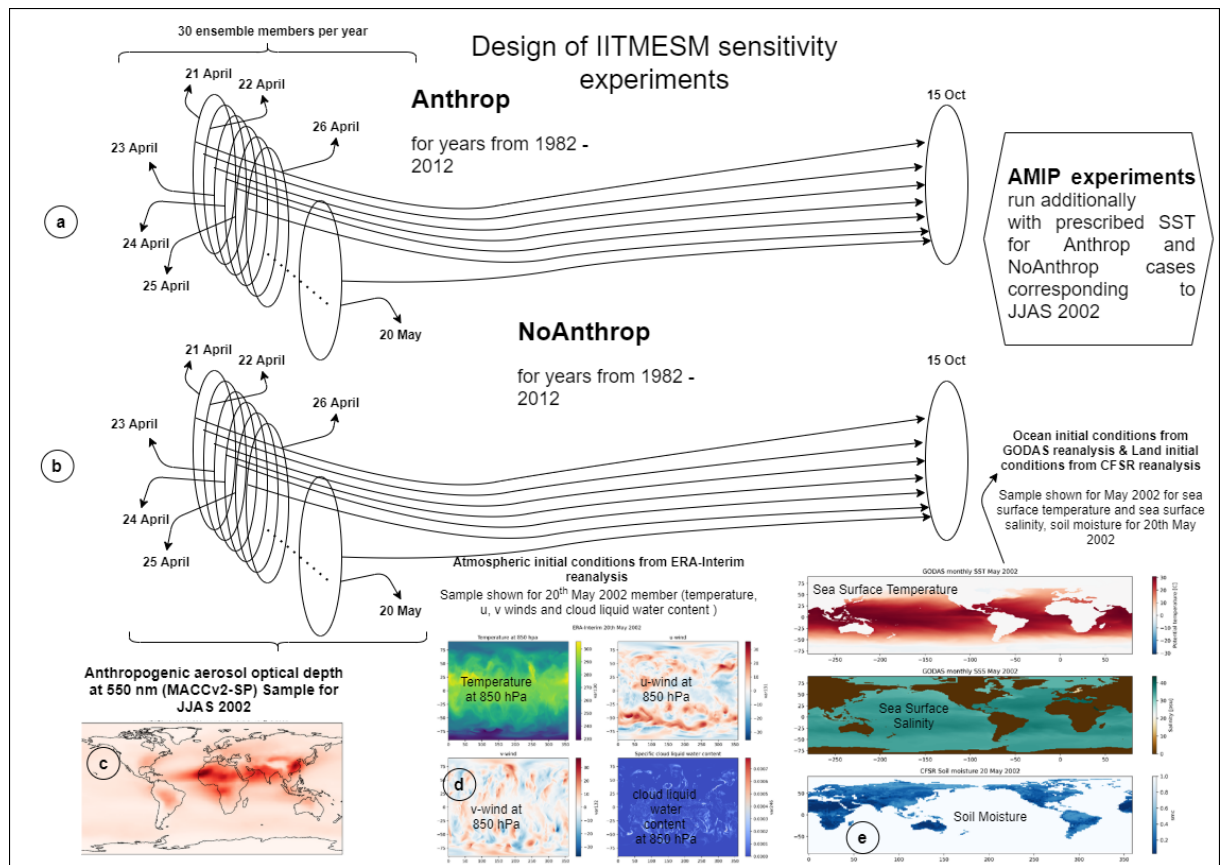


Figure 5.1: Design of IITM-ESM experiments

5.2 Initial conditions for the atmospheric model of IITM-ESM

The ERA-Interim reanalysis data are utilized to initialize the atmospheric conditions. The atmospheric component of IITM-ESM is executed at T62 spectral-spatial resolution. The code for generating the data for initializing the atmospheric conditions was derived from

<https://github.com/tmiyachi/data2gfs>. IITM-ESM utilizes the following variables for the initial conditions: geopotential height, temperature, u and v horizontal velocity vectors, specific and relative humidity, cloud liquid and ice water content, ozone mass mixing ratio, and the logarithm of surface pressure. These variables are also required by the GFS and are used in the IITM-ESM. The gridded reanalysis dataset is interpolated to the 64 sigma hybrid vertical levels of IITM-ESM and then mapped to the spectral space.

5.3 Initializing ocean model in IITM-ESM

To build the model's ocean initial states, monthly GODAS reanalysis is used. The latitude-longitude gridded dataset must first be converted to the tripolar grid of the ocean. Codes from <https://github.com/COSIMA/ocean-ic> were utilized to produce the ocean conditions, which were modified for this purpose. Next, it is necessary to use temperature and salinity variables from the reanalysis dataset to create a one-degree tripolar gridded dataset that would be used as an input to the ocean model.

5.4 Initial states of the land surface in IITM-ESM

The land model in IITM-ESM is based on reduced Gaussian grids, and regular latitude-longitude datasets are used as the starting point. It is necessary to obtain the data for land conditions (low resolution) from the CFS reanalysis (CFSR), which is located at: <https://www.ncei.noaa.gov/data> and is also available at: <https://www.ncei.northwest.gov/data/climate-forecast-system/access/operational-analysis/initial-conditions-low-resolution/>. T126 and T382 resolutions are available for CFSR reanalysis, although T126 is the default resolution. As a starting point for this procedure, the T126 resolution surface initial condition files are downloaded, which are provided as gridded latitude-longitude datasets. The data is then interpolated to the gridded latitude-longitude corresponding to the spectral T62 resolution, resulting from the previous step. It is possible to construct a reduced Gaussian grid from the ordinary latitude-longitude dataset in the same way as

some of the variables that are read directly in reduced Gaussian gridded format are. A modified version of the code from <https://github.com/jswhit/gfstonc> was used to read the surface binary files from CFSR, and the code was changed from there. A detailed description of the various grids may be found at <https://sites.ecmwf.int/docs/atlas/design/grid/>. Inhouse codes were used to transform the regular gridded latitude-longitude data to reduced Gaussian grids.

5.5 Aerosols and Chemistry Model Intercomparison Project (AerChemMIP)/CMIP6 outputs

The Aerosols & Chemistry Model Intercomparison Project (AerChemMIP) is a model inter-comparison project (MIP) under the Coupled-Model Intercomparison Project (CMIP6). The AerChemMIP project's objective is to understand better the impact of chemical species and aerosols on air quality and the climate. As a result, AerChemMIP prescribes targeted sensitivity tests using aerosols and chemistry forcings identical to those used in all of the models participating in the activity. From AerChemMIP, we use three experiments from five distinct models to test our hypotheses. The following are the details of the targeted simulations that were utilized in this study:

- piClim-control: In this experiment, ocean-atmosphere-land models are simulated with pre-industrial (1850) forcings and run for 30 years.
- piClim-aer: This is the same as piClim-control, with the exception that the 2014 aerosols are used.
- piClim-2xdust: This is the same as piClim-control, with the exception that dust emissions are doubled when compared to pre-industrial levels

The meteorological initial conditions used correspond to the year 2014.

5.6 Instrumental/reanalysis datasets

The observational datasets utilized include gridded precipitation from stations distributed throughout the Indian mainland, satellite gridded precipitation product 3B42v7 from the Tropical Rainfall Measuring Mission, and the gridded precipitation from stations scattered across the Indian landmass (TRMM). These datasets are used to validate IITM-ESM simulations and determine whether or not there are any improvements resulting from including the impacts of anthropogenic aerosols in the model's calculations. Furthermore, for the following products, area-

averaged time series across the core monsoon zone (14-28N, 74-87E) for daily data for the years 2003 to 2018 are generated:

- Vegetation products derived from the GLEAM reanalysis, including the normalized difference vegetation index (NDVI) and the enhanced vegetation index (EVI).
- Aerosol optical depth (AOD) measured at 550nm by MERRA-2 reanalysis
- In addition to ERA5 reanalysis data on evaporation and transpiration, surface temperature, relative humidity, zonal and meridional wind, surface pressure, precipitable water and sea-surface temperature-based indices such as Arabian sea temperature are used.

5.7 Coupling metrics of land and atmosphere

Because of the amount of accessible energy, wet soil can help moisten the atmosphere by increasing evapotranspiration. In turn, this results in cooling of the land as well as a reduction in sensible heat flux, which in turn reduces the temperature of the atmosphere. The moistened air and hindered boundary layer development have a reciprocating impact on cloud formation and precipitation, which is caused by the moistened air and inhibited boundary layer development. A wide range of land-atmosphere coupling metrics, each of which quantifies the changes in land-atmosphere interactions, have been computed following <https://www.pauldirmeyer.com/coupling-metrics>. Some of the important ones are explained below:

5.7.1 Terrestrial Coupling index

When it comes to soil moisture, the terrestrial coupling index (TCI) is defined as the product of the correlation of surface heat fluxes and soil moisture and the temporal standard deviation of soil moisture. Using TCI, locations where input to the atmosphere has the potential to have a large influence, are highlighted, whereas regions where actual feedback is small, are excluded. For example, hot deserts have a negligible impact on the amount of moisture in the atmosphere, and their contribution is insignificant. Soil moisture has a significant and direct influence on precipitation, though the feedbacks via evapotranspiration are trimmer and more subtle. For example, there is an inverse relationship between soil moisture and temperature, a direct relationship between soil moisture and near-surface humidity, and an inverse relationship between soil moisture and temperature. Let's look at the surface fluxes from the land surface to the atmosphere. The two-segment connection is composed of soil-state fluxes to surface fluxes, and surface fluxes to atmospheric conditions and precipitation, respectively. The terrestrial segment is responsible for variations in soil moisture and evapotranspiration. During the growing

season, fluctuations in soil moisture influence how much water is in the soil, and changes in evapotranspiration serve as a reaction.

5.7.2 Memory of soil moisture

Soil moisture affects the atmosphere by affecting the outflow of energy at the surface, therefore spreading the latent and sensible heat energy components of the atmosphere. Changing amounts of water in the soil create variability in these fluxes, affecting the humidity and temperature at the soil surface. Anomalies in soil moisture from one month to the next are carried over. The delayed autocorrelation of soil moisture, as a result, assesses the persistence or recall of anomalous soil moisture conditions. The knowledge gained from variations in soil moisture quantity over a single season will have a significant impact on the state of the environment and the ability to anticipate it on both seasonal and yearly time frames. It is possible to utilize autocorrelation as an indicator of soil moisture memory, and the lag at which the autocorrelation falls below $1/e$ is referred to as soil moisture memory. It is usually the case that soil moisture memory is more in dry environments. When the rainy season begins, soil moisture memory is often low in the area where it begins. Changes in soil moisture memory have far-reaching implications for the use of soil moisture states for generating seasonal to sub-seasonal forecasts, and predicting future soil moisture conditions.

5.7.3 The atmospheric component of land-atmosphere coupling

The coupling between land & atmosphere can be divided into two parts: the first is the relationship between soil moisture and surface fluxes, which is referred to as the terrestrial component of land-atmosphere coupling. The second is the connection between surface fluxes and the atmospheric boundary layer, referred to as the atmospheric leg of land-atmosphere coupling. Surface fluxes must be linked to atmospheric variables such as low-level cloud cover, near-surface temperature, and humidity to establish a connection between the fluxes on the ground and atmospheric states. The atmospheric leg of the land-atmosphere coupling is the term used to describe this interaction. Significant values of the atmospheric component of the land-atmospheric coupling indicate a stronger feedback relationship between the two environments.

5.7.4 Information theory-based metrics

- Mutual Information: The term "correlation" refers to any statistical link between two or more variables that may be expressed as an index of covariation of two variables. On the other hand, Covariation does not always suggest a relationship between two factors, although it may serve as an indication pointing in that direction. When determining the relationship between two variables, the Pearson product-moment correlation coefficient is most frequently utilized. It is suitable for continuous and consistently distributed data, which implies that outliers may cause it to misinterpret the data. In nonlinear connections, the correlation will misrepresent the relationships, which is why it should be avoided whenever possible. In actuality, the vast majority of our surroundings are non-linear and not evenly dispersed regularly. As entropy (the proclivity of random processes to lose energy or order) is defined, Shannon established the mathematical basis for what is known as mutual information (the ability to share knowledge between two parties) (MI). When it comes to its adoption as the suitable generalization of the correlation coefficient, there have been several roadblocks, including computing problems and issues with precise calculation when dealing with tiny datasets.
- Multivariate Mutual Information: When a link exists between the combined information from many other variables to one variable, the Multivariate Mutual Information (MMI) is used to measure how much uncertainty has decreased due to the relationship.

5.8 Causal discovery using PCMCI

In causal discovery, the process of inferring the causal structure of a closed system from observational data is the objective. PCMCI is a two-part method in which PC stands for Peter and Clark, and MCI stands for Mutual Conditional Independence (Di Capua et al. (2019)). This approach has a low rate of false positives and a high ability to discover causal links, making it an excellent alternative to other methods of causality identification. Granger causality and the majority of other causal methods, tend to allow for the testing of higher-dimensional data. PCMCI, on the other hand, allows for the analysis of higher-dimensional data since it reduces the number of connections evaluated in the causal network by utilizing PC. Another problem with Granger causality is that it can only be used to analyze specific elements in isolation from other factors. On the other hand, partial correlation is used for the MCI phase of PCMCI, which ensures that all variables are investigated at the same time, and dissociating interactions between correlated variables is a substantial benefit.

5.9 The IITM-ESM's response to the introduction of anthropogenic aerosols

Figure 5.2 depicts the IITM-ESM's response to introducing anthropogenic aerosols for the months of monsoon drought year 2002. It is to be noted that July was responsible for the monsoon failure during that year. The year is also associated with El Niño in the Pacific Ocean and the highest burden of dust aerosols over the Northern Indian plains (Figure 5.4) for any year in the past. The spatial pattern of the anthropogenic aerosols remains the same with an increasing interannual trend (Figure 5.5). Previous studies have suggested the plausible role of mixed natural-anthropogenic aerosols in modulating the radiation and circulation over the Indian region (Kaskaoutis et al. (2012a), Kedia et al. (2014), Sanap et al. (2015)). For the year 2002, if the month of July is removed from the monsoon season, the summer monsoon would flip to a normal state. None of the models employed in the year 2002 was able to simulate the monsoon drought even after a strong ENSO teleconnection (Gadgil et al. (2005)). It can be seen from Figure 5.2 that the precipitation suppression can be partially attributed to the combination of natural-anthropogenic aerosols. Compared with the observational anomaly with a maximum negative grid point rainfall suppression of -10 mm/day, the mixed natural-anthropogenic aerosols show a reduction of -2 mm/day. This is consistent with the underlying physics and the understanding that aerosols are a small forcing in a large scale system. When present in the significant amounts forming the mixed state, which can modulate radiation, it can contribute to the modulations of monsoon precipitation over South Asia. The atmosphere only version of the model also shows more considerable precipitation reduction, as shown in Figure 5.3

5.10 Coupling metrics between the land and the atmosphere for Anthrop minus NoAnthrop IITM-ESM simulations

For July 2002, the coupling metrics of land-atmosphere interactions from IITM-ESM show that the central Indian region has similar zones of strong land-atmosphere coupling to that identified by Koster et al. (2004) (Figure 5.6). Different land-atmosphere coupling metrics for the Anthrop minus NoAnthrop simulations are generated and plotted for July 2002, as shown in Figure 5.6. It should be noticed that the box whisker plots of the land-atmosphere coupling metrics for Anthrop and NoAnthrop simulations show that there is a statistically significant decrease in the coupling metrics due to anthropogenic aerosols. The medians of the distributions of coupling metrics over core monsoon zone and p-values corresponding to the Mann-Whitney test are indicated on the figure. It can be clearly seen there is a suppression of land-atmosphere coupled feedbacks due to mixed natural-anthropogenic aerosols. The results are shown utilizing

South Asian monsoon 2002

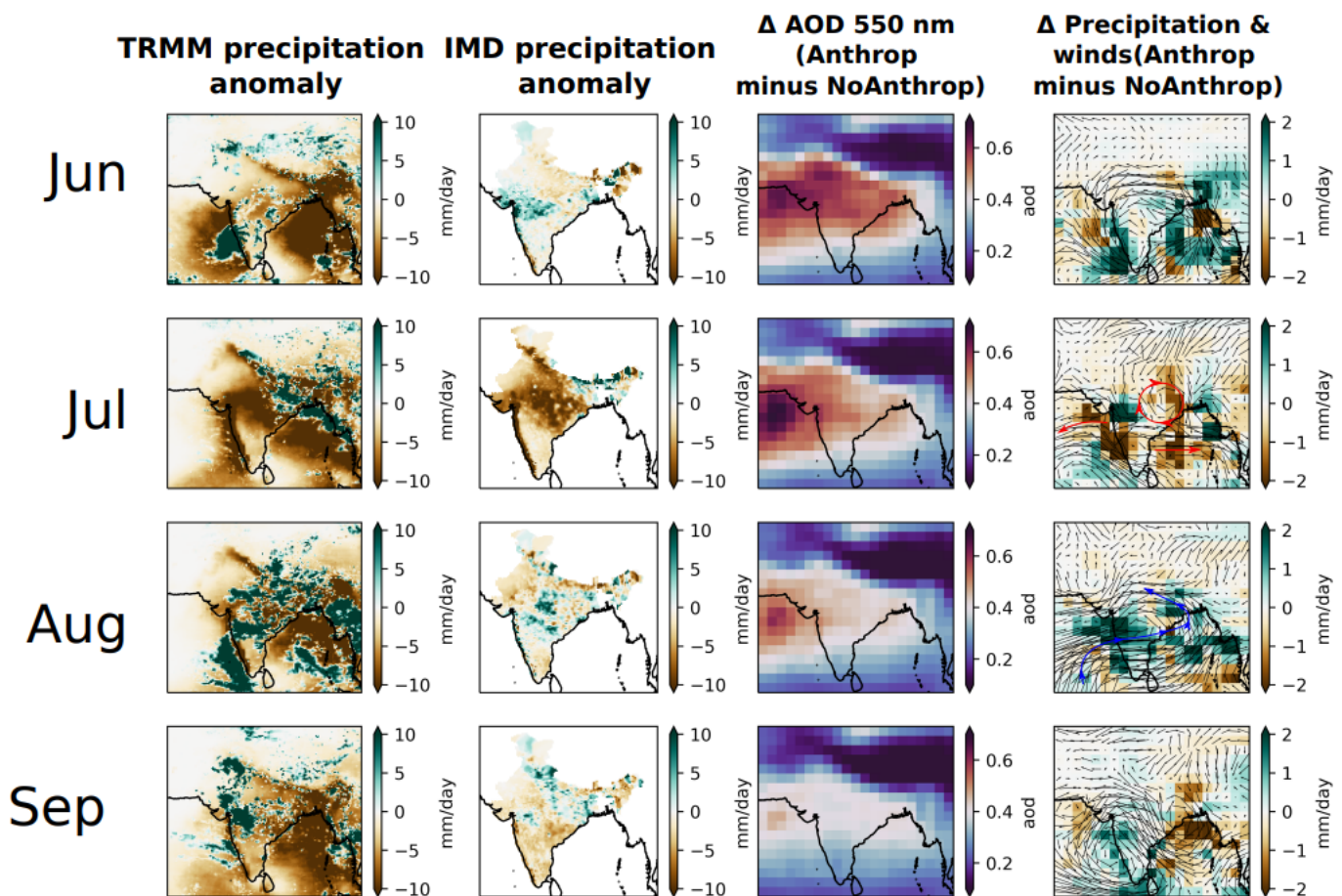


Figure 5.2: Suppression of precipitation due to mixed natural-anthropogenic aerosols in IITMESM for July 2002. July was the month in monsoon drought of the year 2002 that was responsible for the failed monsoon and also corresponds to the maximum ever dust aerosol loading over the Northern Indian plains

Anthropogenic aerosol response
IITMESM-GFS atmosphere only simulation for JJAS 2002

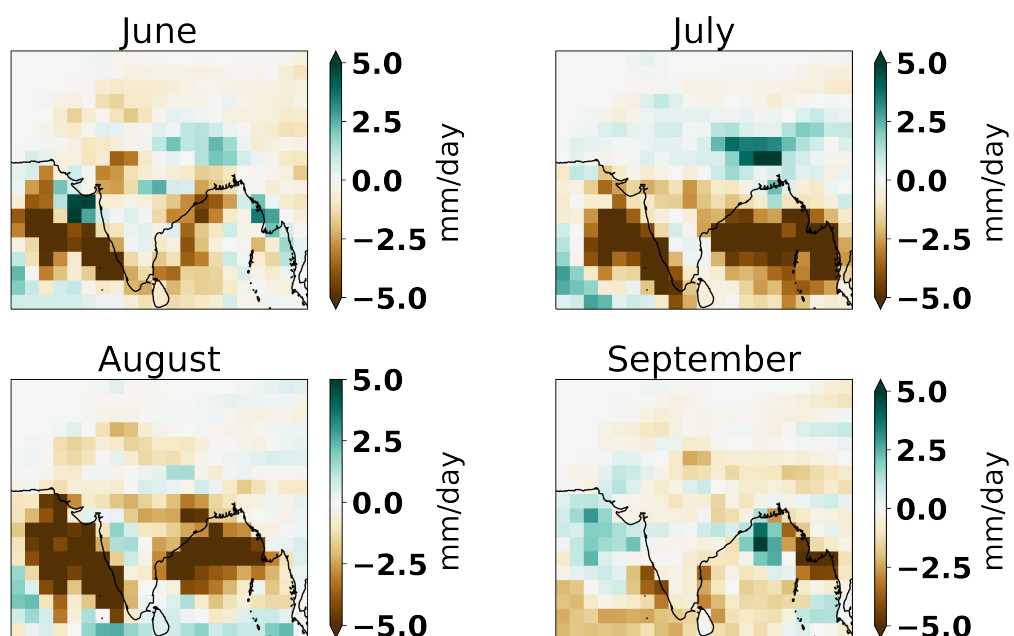


Figure 5.3: Similar to Figure 5.2, but from the atmosphere only version of IITM-ESM with and without anthropogenic aerosols

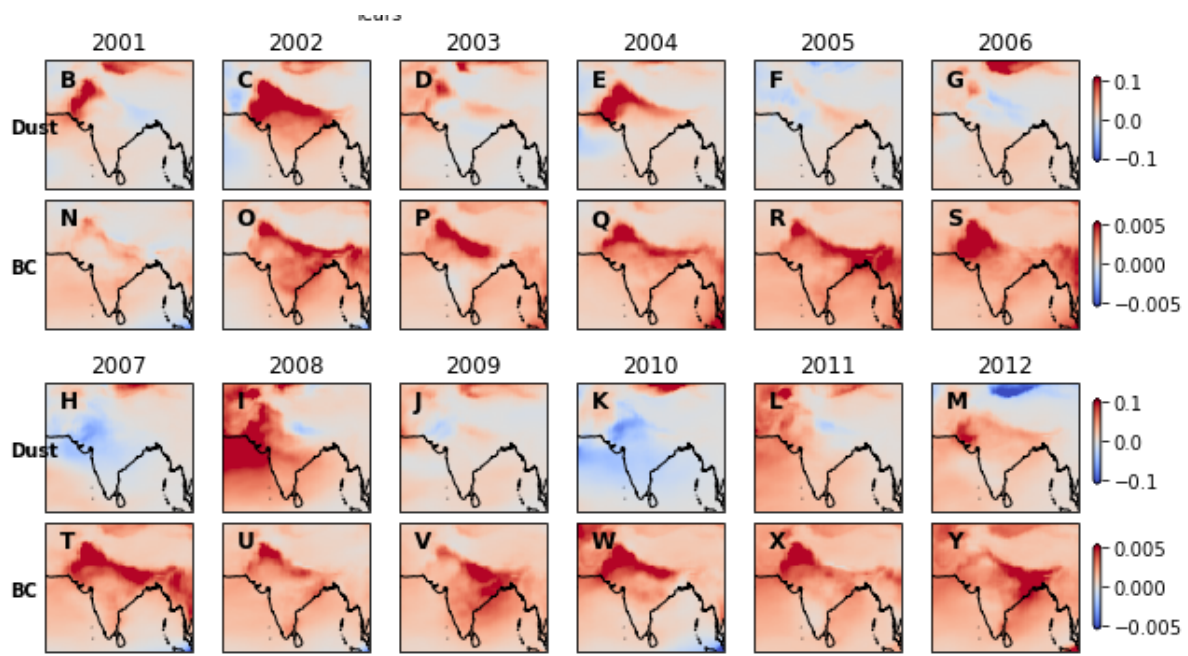


Figure 5.4: (B-M) According to the MERRA-2 reanalysis, the anomaly in the dust aerosol optical depth when compared with the climatology (2000-2020). (N-Y) Except for black carbon (BC) aerosols, this is the same as (B-M). Figure shows analysis from the year 2001 because the instrumental datasets from AERONET that are used to evaluate reanalysis aerosols over India are only available from that year.

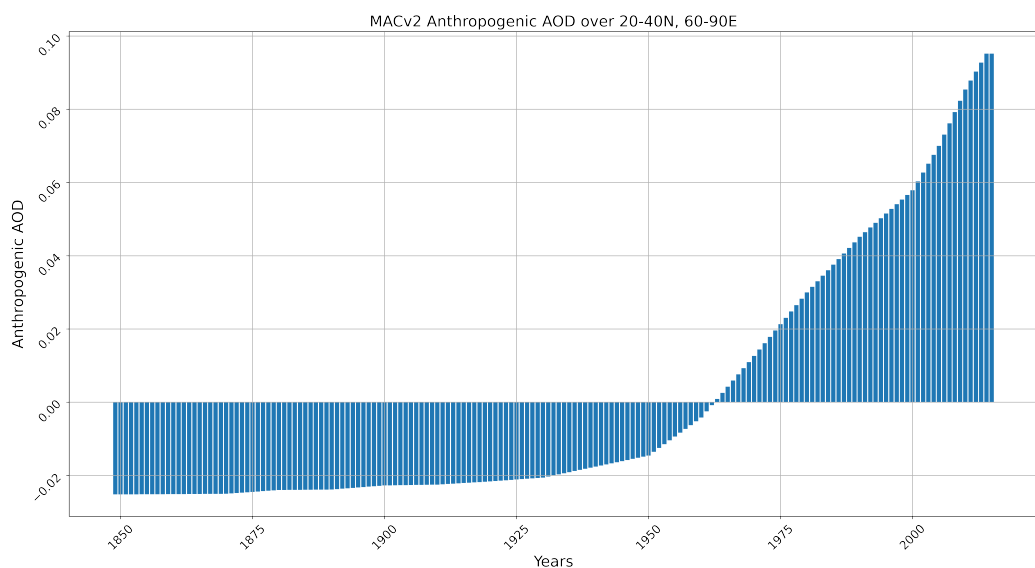


Figure 5.5: Aerosol optical depth due to anthropogenic emissions at 550 nm averaged for the South Asian domain (5-40N, 60-100E) for each year from 1850-2014 from MACv2-SP dataset

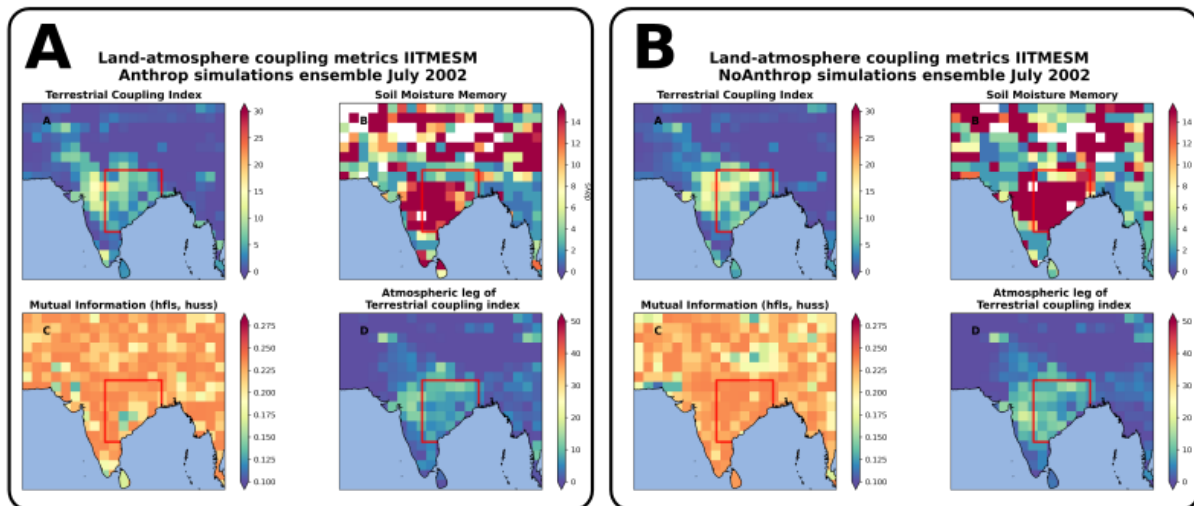
Terrestrial coupling index, Soil Moisture memory, mutual information and atmospheric leg of terrestrial coupling index. The terrestrial coupling index represents the feedbacks from precipitation to soil moisture to evaporation and then back to precipitation. The atmospheric leg is similar to the terrestrial coupling index; however, the difference is that the feedback loop is via surface specific humidity rather than soil moisture. Mutual information between surface latent heat flux and surface specific humidity quantifies a part of the atmospheric leg of terrestrial coupling index. Soil moisture memory quantifies the control of soil moisture on the overlaying atmosphere. A decrease in all these coupling indices indicates weakening of the coupled feedbacks.

5.11 Indian monsoon response to aerosols in AerChemMIP-CNRMESM-CMIP6 outputs

The IITM-ESM sensitivity experiments have provided the data for investigating the function of aerosols in modifying the Indian monsoon via land-atmosphere interactions. One drawback of IITM-ESM simulations, on the other hand, is that the model does not include dynamic aerosols. Instead, the aerosols are prescribed in the radiative transfer scheme via optical characteristics (aerosol optical depth, single scattering albedo, and asymmetry parameter). Additional analysis using AerChemMIP outputs, which are available as a dedicated Model Intercomparison Project (MIP) activity outputs from CMIP6 to understand aerosols are also analysed. The dataset for IPSL, MIROC6, NORESM, UKESM, MPI-ESM and CNRMESM are available from the ESGF portal (<https://esgf-node.llnl.gov/search/cmip6/>). These models are evaluated for their ability to simulate all India summer monsoon in the historical period (Figure 5.7) and aerosols over the region (Figure 5.9). It is found that CNRMESM is the model which realistically represents historical monsoon and aerosol optical depth over the South Asian region. Different experiments from the AerChemMIP, which are used as available, are listed below:

- AER: This experiment consists of all the aerosols corresponding to the year 2014
- Control (C): This is same as the preindustrial control simulation corresponding to 1850 conditions
- 2xdust: This experiment corresponds to the control simulation with the difference that dust aerosols are doubled

Taylor diagram is constructed for the core monsoon zone precipitation for historical simulations from five CMIP6 models (IPSL, NASA-GISS, UKESM, MPIESM, CNRMESM) corresponding to the period 1901-2014, which is the common period for which the observed gridded



Anthropogenic aerosols led statistically significant decrease in land-atmosphere coupling metrics over core monsoon zone (18-27N, 77-88E) for July 2002

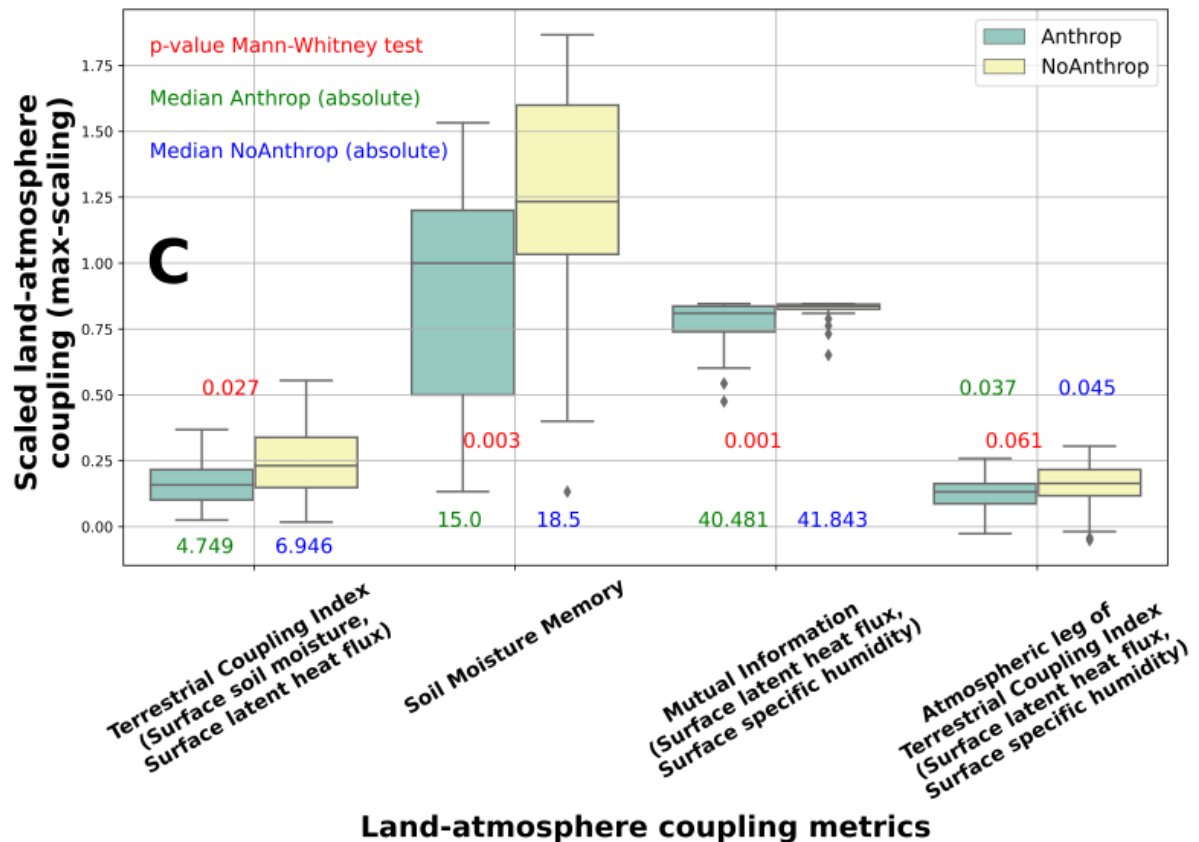


Figure 5.6: From the output of the IITM-ESM corresponding to July 2002, the absolute values land-atmosphere coupling metrics for the ensemble mean of Anthrop and NoAnthrop simulation. Mann-Whitney test is performed over the distributions of the coupling metrics from two simulations. The p-values and medians are annotated in the C

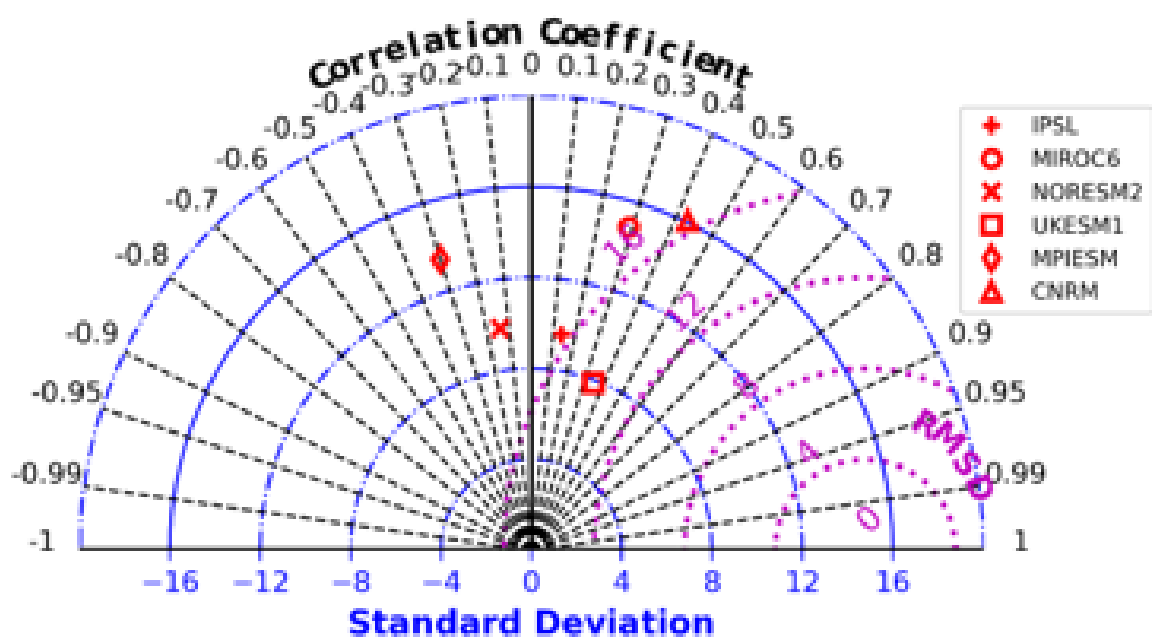


Figure 5.7: Taylor plot showing the comparison of historical simulations of different CMIP6 models and instrumental all India summer monsoon rainfall

Aerosol Optical Depth 550 nm AER & MERRA-2 MJAS 2014

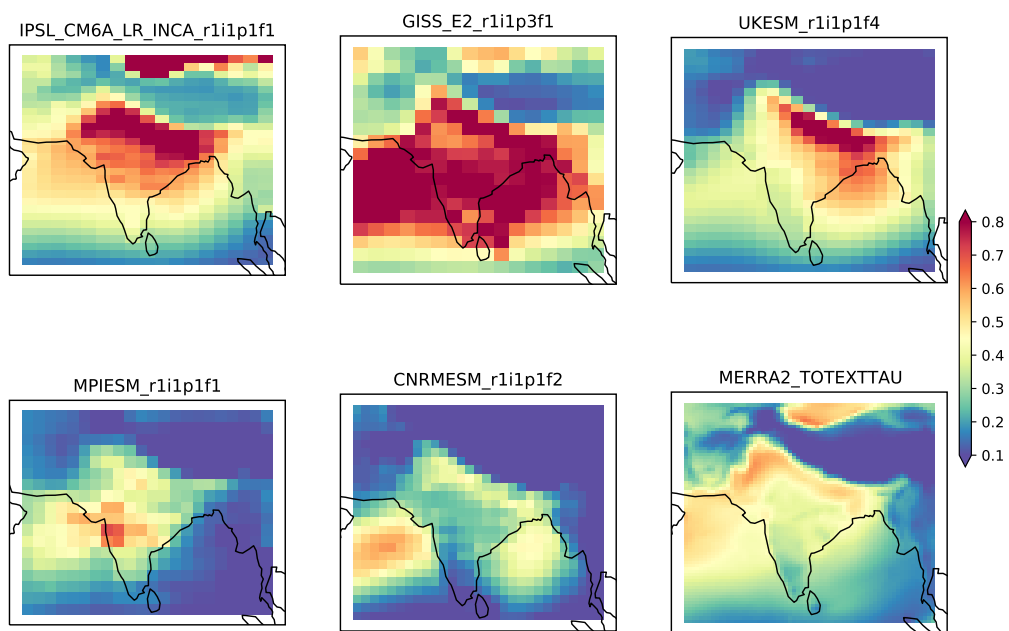


Figure 5.8: Comparison of total aerosol optical depth for May–September 2014 from AerChemMIP simulations and MERRA-2 reanalysis. It can be seen that CNRMESM represents the most realistic representation of aerosols amongst all AerChemMIP models. All the AerChemMIP models have interactive aerosols.

dataset from IMD and CMIP6 historical simulations. It shows that the models with reasonable representation of monsoon precipitation are the UKESM, CNRMESM, and IPSL models. A comparison of the aerosol optical depth (AOD) for the five models and the observed aerosol optical depth (AOD) from MERRA-2 at 550 nm shows that the AOD predicted by the GISS model is significantly higher than the AOD observed by the satellite. The spatial patterns of AOD in the other four models, namely IPSL, UKESM, MPI-ESM, and CNRMESM, are comparable to the pattern seen in AOD. Despite modeling a spatial pattern that is comparable, the IPSL model and the UKESM, significantly overestimate the optical depth across the northern plains of India. MPI-ESM and CNRMESM, on the other hand, show reasonable absolute values and spatial patterns of AOD in comparison to the observations.

Precipitation response of several AerChemMIP-CMIP6 experiments in comparison to the control for CNRMESM, which provides the most accurate depiction of Indian monsoon rainfall and the simulated aerosols that are closest to the data, demonstrates broad suppression of precipitation over the Indian area for all aerosols. This is consistent with the findings of prior investigations. The reduction is characteristic of the mixed dust-anthropogenic aerosols and cannot be seen in only dust experiment relative to the preindustrial control simulation. When only dust aerosols are taken into account, the areas that had previously seen lower rainfall in comparison to the control now experience increased precipitation; nevertheless, the central Indian area continues to experience reduction. In line with earlier research, these findings from the AerChemMIP/CMIP6 simulations show that dust particles can increase rainfall over the Indian area through a variety of processes that entail altering the flow of air circulation patterns. It is important to note that the studies indicating a reduction in rainfall take into consideration all of the aerosols. A comparison of the AER and 2xdust experiments indicates that only dust particles significantly underestimate the optical depth in the model. This underscores the significance of dust-anthropogenic aerosol mixing, which results in changes in radiative forcing as a result of the mixing.

The rainfall decrease in the AER simulation is also accompanied by a decrease in soil moisture, latent heat flux at surface and surface specific humidity. To compare different experiments (AER, 2xdust) to the control, the difference in terrestrial coupling index between the two experiments is computed. When using the AER simulation for CNRMESM, it can be shown that the terrestrial coupling index decreases, which indicates a breakdown in the land-atmosphere coupling as a result of aerosols. This disturbance in the land-atmosphere relationship may be observed in the 2xdust; however, the decrease is less than half of the drop observed in the case of all aerosols. Thus, when only dust aerosols are doubled relative to control, the response is either opposite or muted relative to AER. As in IITMESM simulations, a disruption in land-atmosphere coupling can be seen from CNRMESM, which is substantially higher in AER relative to 2xdust (Figure 5.9). From the difference in land-atmosphere coupling metrics, it can be concluded that anthropogenic aerosols cause suppression in the latent heat fluxes of up to 5-7 W/m² due to their presence. The connection between the land and the atmosphere may be di-

vided into two parts: the terrestrial component and the atmospheric leg. The terrestrial coupling index and the atmospheric component of the land-atmosphere connection, reveal a breakdown of the land-atmosphere link. Still, vanilla correlations show no change in the coupling. Simple correlation can only detect linear variations, so specific coupling measures are necessary. In addition, soil moisture memory, which is an index used to assess the predictability of a system, shows a reduction of 15-20 days, showing the decrease in the influence of soil moisture on the overlying atmosphere. For the same variables that were used to measure correlations, namely, latent (sensible) heat flow and surface specific humidity (air temperature), the mutual information was also computed, and a reduction in the mutual information was observed. This indicates that aerosols have caused a breakdown or suppression in the interactions between the land and the atmosphere. When net surface radiation and soil moisture are used as sources and the multivariate mutual information is computed with the latent heat flux as the target in Figure 5.9I and the sensible heat flux as the target in Figure 5.9J, aerosol induced suppression of land-atmosphere interactions is seen.

5.11.1 Response in the atmosphere only AerChemMIP-UKESM-CMIP6 simulations

A valid question that may arise after analysing the results from coupled IITMESM and AerChemMIP-CNRMESM-CMIP6 simulations is: Whether the precipitation suppression might be coming from sea surface temperature in the Arabian Sea or the Pacific Ocean. It has been shown earlier from IITMESM atmosphere-only simulations that the response is due to aerosols and not sea surface temperature. This is particularly very important as it can be noted from Figure 5.2 that there is high loading of anthropogenic aerosols over the Arabian Sea. Hence, the available fixed SST/AMIP type simulations of UKESM are analysed. These experiments from AerChemMIP as available for Aer and piAer are analysed for JJAS 2002. Aer corresponds to all aerosols, and piAer is similar to Aer, with the only change being that the aerosols are representative of preindustrial conditions. It can be seen from Figure 5.10 that mixed aerosols lead to reduced precipitation even when the effect of SST is removed.

5.12 Discovery of causal relationships within the monsoon context of the aerosol-land-atmosphere system

The development of causal inference and discovery algorithms, which go beyond standard linear correlations to assess the link between distinct variables, has occurred in recent years. To

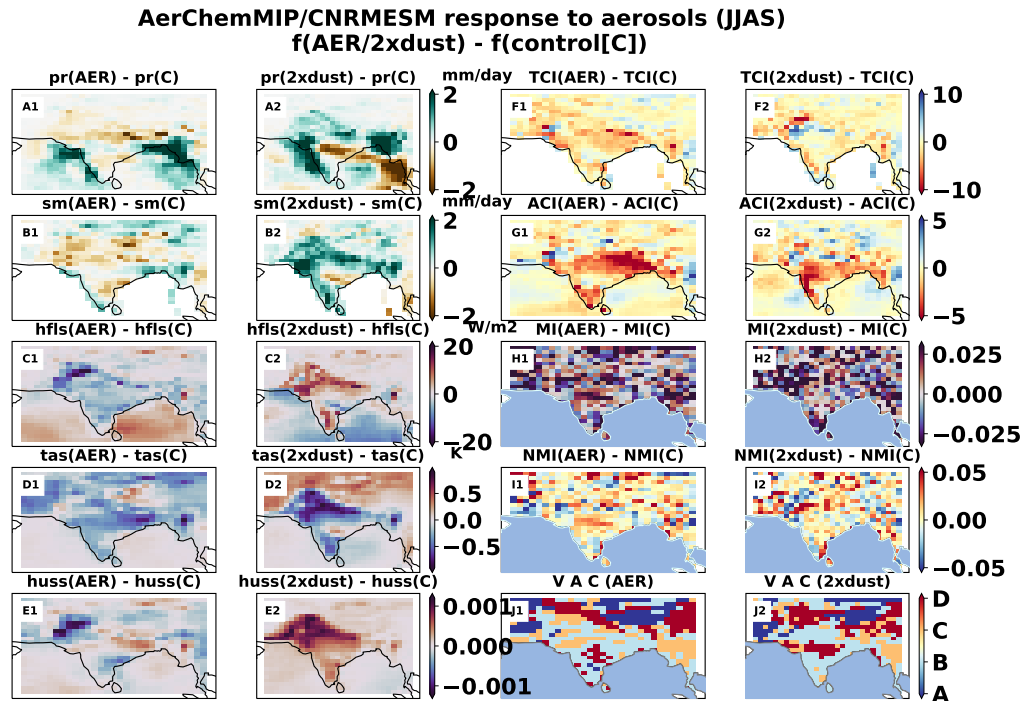


Figure 5.9: Aerosol induced changes in land-atmosphere interactions from AerChemMIP/CMIP6 outputs. The rows in the first two columns correspond to changes in precipitation, surface soil moisture, surface latent heat flux, surface air temperature and surface specific humidity. The rows in the last two columns represent terrestrial coupling index, atmospheric-leg of terrestrial coupling index, mutual information, nonlinear mutual information, and vegetative-atmosphere coupling. The first and third column show the response of all aerosol experiment relative to the preindustrial (clean). Second and fourth column represent the response of doubling dust relative to the preindustrial control.

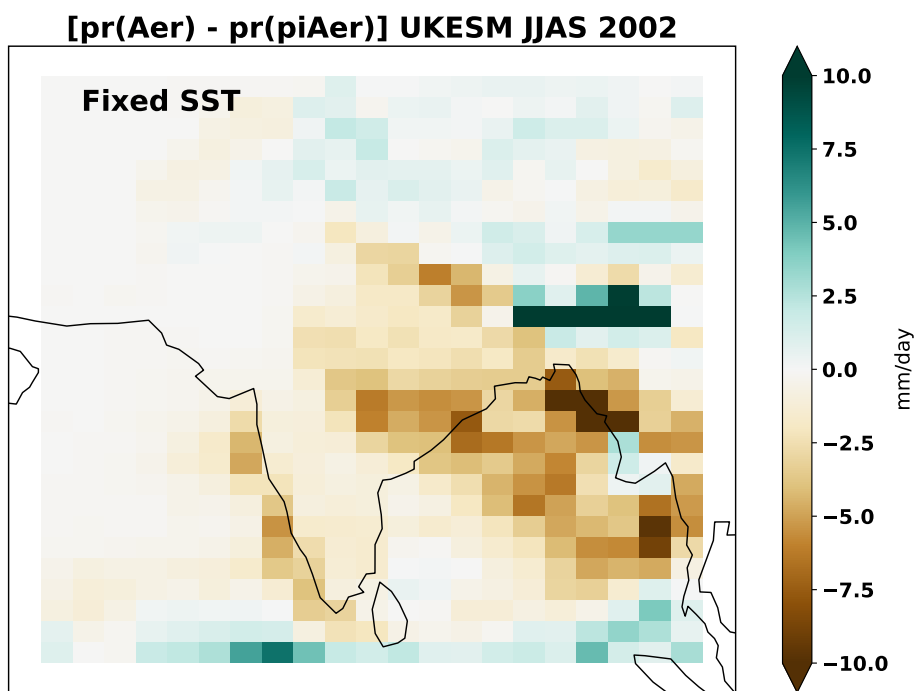


Figure 5.10: Precipitation response due to aerosols in atmosphere only simulation of UKESM/AerChemMIP/CMIP6. The control (piAer) consists of preindustrial aerosols and the sensitivity (Aer) experiment consists of aerosols corresponding to the year 2014. Sea-surface temperature is fixed in these experiments.

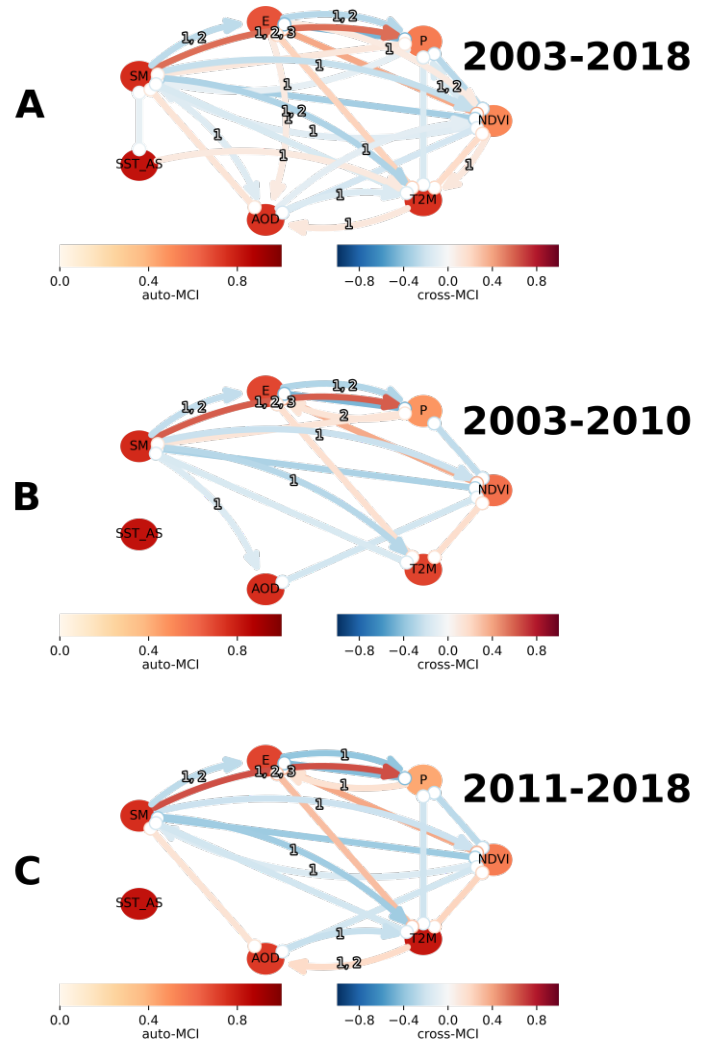


Figure 5.11: The causal discovery network was assessed using the PCMCI causal algorithm. The datasets used are daily time series of precipitation (P), evaporation (E), sea surface temperature over Arabian Sea (SST_AS), two meter air temperature (T2M), soil moisture at the surface (SM), normalized difference vegetation index (NDVI) and aerosol optical depth (AOD). The datasets used are ERA5 reanalysis, GLEAM reanalysis, IMD, NCEP/NCAR reanalysis, and MERRA-2 reanalysis. Robustness of the indirect relationship between precipitation and aerosols via land-surface is established by performing PCMCI over different epochs

analyze the causal discovery network, Peters and Clark Momentary Conditional Independence (PCMCI) test is used. PCMCI has a high level of competence in filtering out false correlations and can create connections between variables that occur at various lags from multivariate time series data. The daily time series of evaporation (E), surface temperature (T2M) from the ERA5 reanalysis, soil moisture at the surface (SM) from the GLEAM reanalysis, precipitation (P) from IMD, and aerosol optical depth (AOD) from the MERRA-2 reanalysis for the period 2003-2018 are used to construct a causal discovery network. With a maximum number of delays of 90 days, PCMCI simulations are performed. The nodes represent the variables, and the relationships between them are represented by the edges. PCMCI is also capable of determining the direction of a connection. If the arrow points from node 1 to node 2, then node one is the node that is leading node two and is the causal parent of node two. The color of the nodes indicates the strength of the link between the variable and itself. In contrast, the color of the edges indicates the strength of the interaction between the nodes and the variable. Except for precipitation and NDVI, most of the variables under consideration have a significant relationship with one another, as indicated by the color of the nodes in the graph. The strongest and most favorable inter-node connection is between soil moisture and rain. Soil moisture has relationships with all of the other factors, although these relationships are weak. A weak negative link exists between soil moisture and evaporation when the lead time is one or two days. In this relationship, soil moisture is the causal parent, and evaporation is the causal child.

Overall, this network graph shows that AOD does not directly link with P. This indirect relationship revealed by the data-driven approach underlines the importance of land-surface in the climate system. Though, it may be noted that the data-driven approaches may have their limitations and might not be able to separate the effects of different components as a physics-based model. Thus AOD has connections to P through T2M, SM, and NDVI. Even while SST-AS modulates other fields and indirectly AOD over the core monsoon zone, it does not directly relate to AOD over the core monsoon zone. Among the linked land-ocean-atmosphere systems, the soil moisture-precipitation connection is the most significant. Other activities taking place in the system, on the other hand, might alter the moisture content of the soil.

5.13 Mechanisms for aerosol-induced land-atmosphere interactions

The most likely mixed state of aerosols over the Northern Indian plains, i.e. dust-anthropogenic aerosols, necessitates the presence of both dust and anthropogenic aerosols over the Indian sub-continent. It can be seen that the summer monsoon season for dust aerosols in the year 2002 has a wider spatial extent that is positive when compared to all the previous years. The positive dust anomaly has the highest magnitude in the year 2002, and it is also the most persistent. The

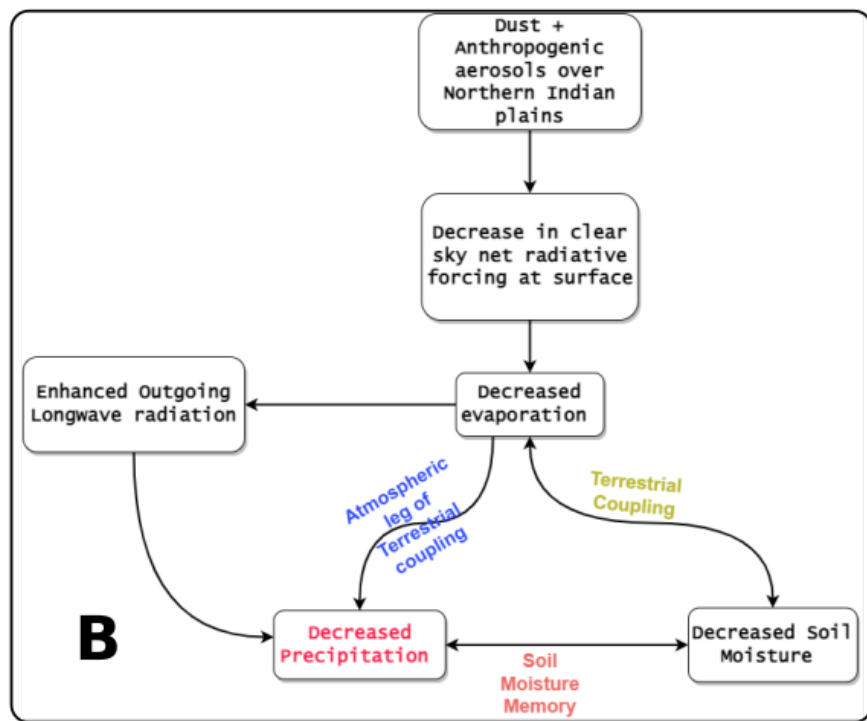
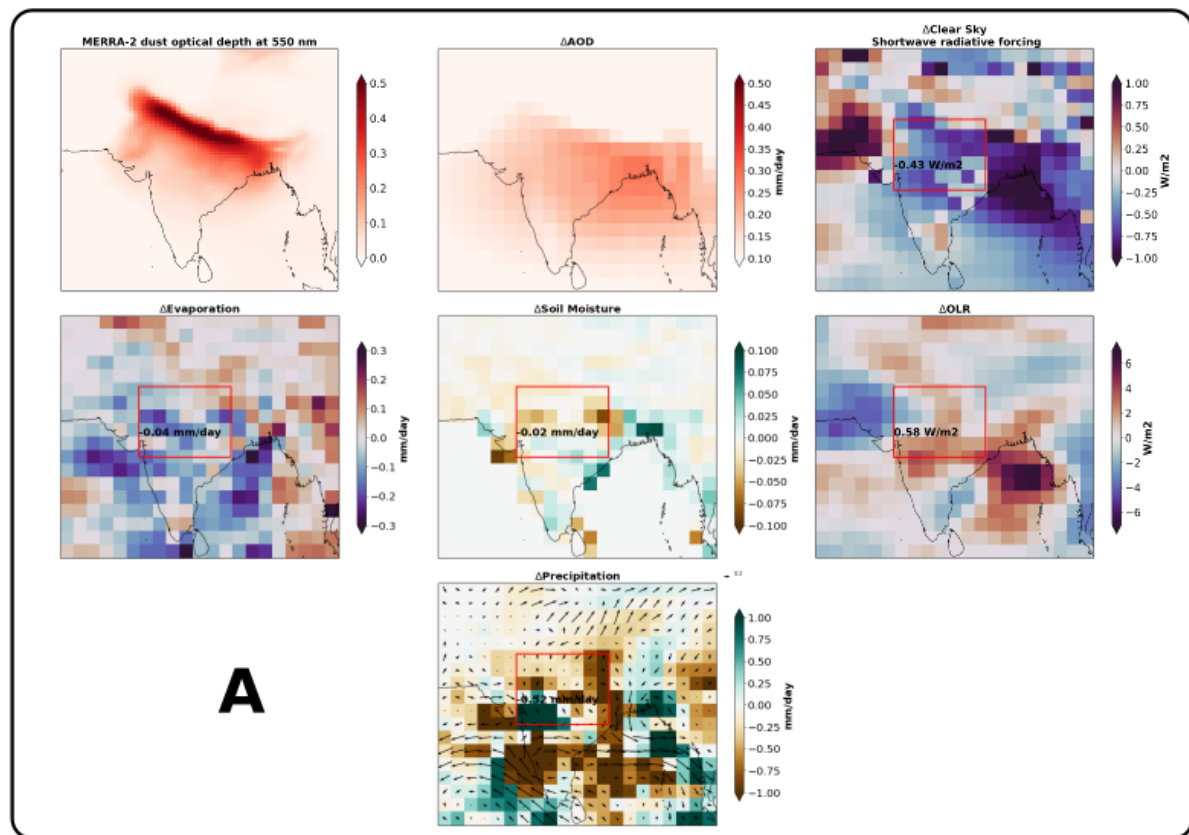


Figure 5.12: Physical mechanisms leading to precipitation suppression due to anthropogenic aerosols in IITMESM for July 2002

model simulated Anthrop minus NoAnthrop precipitation illustrates the reduction in rainfall due to anthropogenic aerosols. This is related to a decrease in soil moisture, evaporation, and latent heat flux throughout the Indian subcontinent. The presence of aerosols causes a shift in the radiative flux at the surface and absorption by the environment. Figure 5.12 shows the mechanism of suppressed precipitation due to aerosols via changes in the land-atmosphere coupling metrics.

5.14 Conclusions

This chapter examines the role of anthropogenic aerosols on the South Asian monsoon in the IITM ESM simulations and AerChemMIP outputs. It is noted that there is a suppression of precipitation, soil moisture, evaporation and surface fluxes due to anthropogenic aerosols mixed with natural aerosols. Similar inferences can be made from IITM ESM fixed SST simulations and AerChemMIP/CNRMESM outputs from coupled and atmosphere-only models. Whether the response to aerosols might be coming from sea surface temperature is tested by analysing the atmosphere-only simulations from AerChemMIP/UKESM. The physical mechanism shows that the suppression of precipitation is associated with a decrease in soil moisture, evaporation, surface radiation and fluxes. It is found that there is modulation of land-atmosphere coupling metrics associated with precipitation suppression. Causal discovery-based PCMCI approach shows that the relationship of precipitation to aerosols occurs indirectly via soil moisture.

The next and last chapter describes the work in this thesis and points to the essential highlights of this thesis. Future directions and open research questions are also discussed.

Chapter 6

Summary and Conclusions

In this thesis, insights into the role of volcanic and anthropogenic aerosols in modulating the tropical ocean-atmosphere-land coupled system is assessed. The focus is on the South Asian monsoon. Advanced statistical techniques, novel metrics, Earth system modelling, are employed on the biogeophysical big data to further the understanding on aerosols in the Earth system. This chapter concludes the results obtained through this research to achieve the thesis's objectives.

The role of natural and anthropogenic aerosols in the South Asian Monsoon system is investigated considering the proposed research objectives. Chapter 02 details the literature survey used to formulate the hypothesis and gap areas. The methodologies, datasets and results have been explained in Chapters 03-05. Finally, the key conclusions are summarized pertaining to the corresponding objectives. A summary of the results presented in the thesis is presented below:

- Volcanism induced phase coherence of ENSO and Indian monsoon:

Phase coherence analysis is a technique that is applicable to oscillators and comes from the field of nonlinear dynamics. It can be applied to a time series dataset whose phase space plot shows that the system is oscillating around a common attractor. It is shown that ENSO and Indian monsoon are oscillators in the last millennium and their coupling is robust, occurs in epochs. Large volcanic eruptions force synchronization of ENSO and Indian monsoon with the length of coupled periods extending upto 20 years in the instrumental period. State of the art statistical significance is employed by generating a large

number of surrogate time series using twin surrogates. Event synchronization analysis is employed to determine the relationship between volcanic and ENSO-IM coupling events in the last millennium.

- Volcanic fingerprint on ENSO-monsoon coupling: Climate model simulations & paleoclimate proxy records analysis:

IITMESM is used to conduct large ensemble targeted simulations forced with Krakatoa volcanic eruption. It is found that in the year after the eruption, there is a high chance of El Niño and Indian monsoon drought. Whether this would happen always is tested by using different initial conditions of tropical Pacific and changing the volcanic radiative forcing. The prevailing cold state in the Pacific leads to an earlier El Niño and more significant volcanic forcing further favors ENSO-monsoon coupling. These results are corroborated with the paleoclimate proxy records of the last millennium. Multiple combinations of ENSO, Indian monsoon, volcanic eruptions and PDO proxies are used to establish an enhanced ENSO-monsoon coincidence up to four years from the volcanic explosion. This coincidence is even stronger if the ENSO is favored by the PDO.

- Anthropogenic aerosols and land-atmosphere interactions:

Indian monsoon droughts have been challenging to simulate. Particularly notable is the monsoon drought of the year 2002. During that year, none of the models were able to predict the direction of one of the worst monsoon failures. More so because it was an El Nino year, and El Ninos have been known to have caused Indian monsoon droughts, the case of 2002 is peculiar as the models were unable to pick the precipitation suppression even after an El Nino in the Pacific. Also this was the season when the interannual dust loading was highest ever over the Northern Indian plain in the past 40 years (1980-2020). It is to be noted that the spatial pattern of anthropogenic aerosols has remained almost the same in the past 40 years with an increasing interannual trend. Observations point to the most probable mixed state, i.e. dust-anthropogenic aerosols over the Northern Indian plains as most effective in modulating the radiation balance. Moreover, the land surface is an essential component, and aerosol-land-atmosphere interactions need to be taken into account. Targeted experiments of IITMESM show that the precipitation suppression of 2002 can be partially attributed to mixed dust-anthropogenic aerosols. Similar results were noted from AerChemMIP outputs, and the reduction is associated with disruption of land-atmosphere coupling. Causality based analysis shows the aerosol pathways to precipitation via land surface, and the physical mechanism indicates the changes in the land-atmosphere coupling metrics associated with precipitation suppression.

6.1 Future directions

The recommendations and scope for future research are as follows:

- The evolution of ENSO dynamics following large volcanic eruptions is an important precursor for monsoon and needs to be evaluated.
- The role of the location of large volcanic eruptions on ENSO-Indian monsoon coupling needs to be examined.
- Use of interactive tropospheric and stratospheric aerosols modules will add value to the analysis.
- Causality based analysis of ENSO-Indian monsoon coupling.
- Testing the role of mixed dust-anthropogenic aerosols in a realistic seasonal monsoon prediction system.
- Using more number of monsoon years to test the fidelity of the aerosol-land-atmosphere interactions.
- Advanced components in IITMESM such as sophisticated land model, sea ice model are expected to improve the monsoon simulations.
- The use of artificial intelligence and deep learning to reduce aerosols' uncertainties and further improve the state of the art dynamical models.

This page was intentionally left blank.

Appendix A

Codes and tools

A.1 Volcanic imprint on ENSO-monsoon coupling

The codes for reproducing the work on fingerprinting the role of volcanic aerosols on ENSO-monsoon coupling can be found at

<https://github.com/manmeet3591/fingerprint-volcano-enso-im>

A.2 Initial conditions for IITM-ESM simulations

The codes for generating the initial conditions for IITM-ESM can be developed from

Atmospheric initial conditions: <https://github.com/tmiyachi/data2gfs>

Ocean initial conditions: <https://github.com/COSIMA/ocean-ic>

Land surface initial conditions: <http://nomads.ncdc.noaa.gov/data.php?name=accesscfs-reanal-data>

Generation of reduced Gaussian gridded dataset:

https://confluence.ecmwf.int/download/attachments/73008494/intro_interpolation_2017.pdf?api=v2

https://github.com/manmeet3591/iitmesm_initial_conditions

A.3 PCMCI based causal algorithm

The codes to perform PCMCI causal discovery algorithm have been adapted from
<https://github.com/jakobrunge/tigramite>

A.4 Event Coincidence Analysis

The codes to perform event coincidence analysis have been adapted from the CoinCalc R library and can be found at

<https://github.com/JonatanSiegmund/CoinCalc> The modified codes are maintained as a private GitHub repository and can be accessed on reasonable request. Repository link:
https://github.com/manmeet3591/event_coincidence_analysis

A.5 Event Synchronization Analysis

The codes for event synchronization have been adapted from the Pyunicorn library and can be found at

https://github.com/pik-copan/pyunicorn/blob/master/pyunicorn/funcnet/event_synchronization.py

A.6 Climate Network Analysis

The codes to perform climate network analysis have been adapted from the Pyunicorn library and can be accessed from

http://www.pik-potsdam.de/~donges/pyunicorn/tutorials/climate_network_1.html

A.7 Generation of Twin surrogates and Recurrence plots

The codes to perform the statistical significance testing using twin surrogates and recurrence plots can be found at <https://github.com/bedartha/nltsavibration/blob/master/codes/recurrence.py>

References

- Aadhar, S., Mishra, V., 2021. On the occurrence of the worst drought in south asia in the observed and future climate. *Environmental Research Letters* 16 (2), 024050.
- Achuthavarier, D., Krishnamurthy, V., Kirtman, B. P., Huang, B., 2012. Role of the indian ocean in the enso–indian summer monsoon teleconnection in the ncep climate forecast system. *Journal of Climate* 25 (7), 2490–2508.
- Adams, J. B., Mann, M. E., Ammann, C. M., 2003. Proxy evidence for an el nino-like response to volcanic forcing. *Nature* 426 (6964), 274–278.
- Alfaro-Sánchez, R., Nguyen, H., Klesse, S., Hudson, A., Belmecheri, S., Köse, N., Diaz, H., Monson, R., Villalba, R., Trouet, V., 2018. Climatic and volcanic forcing of tropical belt northern boundary over the past 800 years. *Nature Geoscience* 11 (12), 933.
- Anchukaitis, K., Buckley, B., Cook, E., Cook, B., D’Arrigo, R., Ammann, C., 2010. Influence of volcanic eruptions on the climate of the asian monsoon region. *Geophysical Research Letters* 37 (22).
- Angert, A., Biraud, S., Bonfils, C., Buermann, W., Fung, I., 2004. Co2 seasonality indicates origins of post-pinatubo sink. *Geophysical Research Letters* 31 (11).
- Annamalai, H., Hamilton, K., Sperber, K. R., 2007. The south asian summer monsoon and its relationship with enso in the ipcc ar4 simulations. *Journal of Climate* 20 (6), 1071–1092.
- Ashok, K., Guan, Z., Saji, N., Yamagata, T., 2004. Individual and combined influences of enso and the indian ocean dipole on the indian summer monsoon. *Journal of Climate* 17 (16), 3141–3155.
- Ashok, K., Guan, Z., Yamagata, T., 2001. Impact of the indian ocean dipole on the relationship between the indian monsoon rainfall and enso. *Geophysical Research Letters* 28 (23), 4499–4502.
- Ashrit, R., Kumar, K. R., Kumar, K. K., 2001. Enso-monsoon relationships in a greenhouse warming scenario. *Geophysical research letters* 28 (9), 1727–1730.
- Ayantika, D., Krishnan, R., Singh, M., Swapna, P., Sandeep, N., Prajeesh, A., Vellore, R., 2021. Understanding the combined effects of global warming and anthropogenic aerosol forcing on the south asian monsoon. *Climate Dynamics* 56 (5), 1643–1662.

- Azad, S., Rajeevan, M., 2016. Possible shift in the enso-indian monsoon rainfall relationship under future global warming. *Scientific reports* 6, 20145.
- Babu, S. S., Manoj, M., Moorthy, K. K., Gogoi, M. M., Nair, V. S., Kompalli, S. K., Satheesh, S., Niranjan, K., Ramagopal, K., Bhuyan, P., et al., 2013. Trends in aerosol optical depth over indian region: Potential causes and impact indicators. *Journal of Geophysical Research: Atmospheres* 118 (20), 11–794.
- Biondi, F., Gershunov, A., Cayan, D. R., 2001. North pacific decadal climate variability since 1661. *Journal of climate* 14 (1), 5–10.
- Blake, S. A., Lewis, S. C., LeGrande, A. N., Miller, R. L., 2018. Assessing the impact of large volcanic eruptions of the last millennium (850–1850 ce) on australian rainfall regimes. *Climate of the Past* 14 (6), 811–824.
- Bollasina, M. A., Ming, Y., 2013. The role of land-surface processes in modulating the indian monsoon annual cycle. *Climate dynamics* 41 (9-10), 2497–2509.
- Bollasina, M. A., Ming, Y., Ramaswamy, V., 2011. Anthropogenic aerosols and the weakening of the south asian summer monsoon. *science* 334 (6055), 502–505.
- Bollasina, M. A., Ming, Y., Ramaswamy, V., Schwarzkopf, M. D., Naik, V., 2014. Contribution of local and remote anthropogenic aerosols to the twentieth century weakening of the south asian monsoon. *Geophysical Research Letters* 41 (2), 680–687.
- Borgaonkar, H. P., Sikder, A., Ram, S., Pant, G. B., 2010. El niño and related monsoon drought signals in 523-year-long ring width records of teak (*tectona grandis* lf) trees from south india. *Palaeogeography, Palaeoclimatology, Palaeoecology* 285 (1-2), 74–84.
- Bourassa, A. E., Robock, A., Randel, W. J., Deshler, T., Rieger, L. A., Lloyd, N. D., Llewellyn, E., Degenstein, D. A., 2013. Large volcanic aerosol load in the stratosphere linked to asian monsoon transport. *science* 339 (6120), 647–647.
- Braganza, K., Gergis, J. L., Power, S. B., Risbey, J. S., Fowler, A. M., 2009. A multiproxy index of the el niño–southern oscillation, ad 1525–1982. *Journal of Geophysical Research: Atmospheres* 114 (D5).
- Brasseur, G. u. S. S., 2005. *Aeronomy of the Middle Atmosphere*. Kluwer Academic Publishers.
- Broccoli, A. J., Dahl, K. A., Stouffer, R. J., 2006. Response of the itcz to northern hemisphere cooling. *Geophysical Research Letters* 33 (1).
- Broccoli, A. J., Dixon, K. W., Delworth, T. L., Knutson, T. R., Stouffer, R. J., Zeng, F., 2003. Twentieth-century temperature and precipitation trends in ensemble climate simulations including natural and anthropogenic forcing. *Journal of Geophysical Research: Atmospheres* 108 (D24).

- Brönnimann, S., Franke, J., Nussbaumer, S. U., Zumbühl, H. J., Steiner, D., Trachsel, M., Hegerl, G. C., Schurer, A., Worni, M., Malik, A., et al., 2019. Last phase of the little ice age forced by volcanic eruptions. *Nature geoscience* 12 (8), 650–656.
- Brönnimann, S., Grosjean, M., Joos, F., Tinner, W., Rohr, C., 2015. Lessons from tambora. *PAGES Newsletter* 23, 69.
- Brovkin, V., Lorenz, S. J., Jungclaus, J., Raddatz, T., Timmreck, C., Reick, C. H., Segschneider, J., Six, K., 2010. Sensitivity of a coupled climate-carbon cycle model to large volcanic eruptions during the last millennium. *Tellus B* 62 (5), 674–681.
- Budakoti, S., Chauhan, T., Murtugudde, R., Karmakar, S., Ghosh, S., 2021. Feedback from vegetation to interannual variations of indian summer monsoon rainfall. *Water Resources Research* 57 (5), e2020WR028750.
- Camargo, S. J., Polvani, L. M., 2019. Little evidence of reduced global tropical cyclone activity following recent volcanic eruptions. *npj Climate and Atmospheric Science* 2 (1), 14.
- Carley E. Iles, G. H., Schurer, A., 2015. Volcanic eruptions and the global hydrological cycle. *Past Global Changes Magazine* 23, 56–57.
- Chakraborty, A., Nanjundiah, R. S., Srinivasan, J., 2014. Local and remote impacts of direct aerosol forcing on asian monsoon. *International journal of climatology* 34 (6), 2108–2121.
- Chang, C., Harr, P., Ju, J., 2001. Possible roles of atlantic circulations on the weakening indian monsoon rainfall–enso relationship. *Journal of Climate* 14 (11), 2376–2380.
- Chen, W., Dong, B., Lu, R., 2010. Impact of the atlantic ocean on the multidecadal fluctuation of el niño–southern oscillation–south asian monsoon relationship in a coupled general circulation model. *Journal of Geophysical Research: Atmospheres* 115 (D17).
- Chung, C. E., Ramanathan, V., 2006. Weakening of north indian sst gradients and the monsoon rainfall in india and the sahel. *Journal of Climate* 19 (10), 2036–2045.
- Chung, S. H., Seinfeld, J. H., 2005. Climate response of direct radiative forcing of anthropogenic black carbon. *Journal of Geophysical Research: Atmospheres* 110 (D11).
- Church, J. A., White, N. J., Arblaster, J. M., 2005. Significant decadal-scale impact of volcanic eruptions on sea level and ocean heat content. *Nature* 438 (7064), 74–77.
- Cole-Dai, J., 2010. Volcanoes and climate. *Wiley Interdisciplinary Reviews: Climate Change* 1 (6), 824–839.
- Cook, E., D'Arrigo, R., Anchukaitis, K., 2008. Enso reconstructions from long tree-ring chronologies: Unifying the differences. In: Talk presented at a special workshop on Reconciling ENSO Chronologies for the Past. Vol. 500. p. 15.

- Cook, E. R., Anchukaitis, K. J., Buckley, B. M., D'Arrigo, R. D., Jacoby, G. C., Wright, W. E., 2010. Asian monsoon failure and megadrought during the last millennium. *Science* 328 (5977), 486–489.
- Cook, E. R., Krusic, P. J., Anchukaitis, K. J., Buckley, B. M., Nakatsuka, T., Sano, M., et al., 2013. Tree-ring reconstructed summer temperature anomalies for temperate east asia since 800 ce. *Climate Dynamics* 41 (11-12), 2957–2972.
- Cooper, C. L., Swindles, G. T., Savov, I. P., Schmidt, A., Bacon, K. L., 2018. Evaluating the relationship between climate change and volcanism. *Earth-Science Reviews* 177, 238–247.
- Cui, X., Gao, Y., Sun, J., 2014. The response of the east asian summer monsoon to strong tropical volcanic eruptions. *Advances in Atmospheric Sciences* 31 (6), 1245–1255.
- Cui, Y., 2018. Climate swings in extinction. *Nature Geoscience* 11 (12), 889.
- Dani, K., Ernest Raj, P., Devara, P., Pandithurai, G., Sonbawne, S., Maheskumar, R., Saha, S., Jaya Rao, Y., 2012. Long-term trends and variability in measured multi-spectral aerosol optical depth over a tropical urban station in india. *International Journal of Climatology* 32 (1), 153–160.
- D'Arrigo, R., Cook, E. R., Wilson, R. J., Allan, R., Mann, M. E., 2005. On the variability of enso over the past six centuries. *Geophysical Research Letters* 32 (3).
- D'Arrigo, R., Wilson, R., 2006. On the asian expression of the pdo. *International Journal of Climatology: A Journal of the Royal Meteorological Society* 26 (12), 1607–1617.
- Dätwyler, C., Abram, N. J., Grosjean, M., Wahl, E. R., Neukom, R., 2019. El niño–southern oscillation variability, teleconnection changes and responses to large volcanic eruptions since ad 1000. *International journal of climatology* 39 (5), 2711–2724.
- Dee, S. G., Cobb, K. M., Emile-Geay, J., Ault, T. R., Edwards, R. L., Cheng, H., Charles, C. D., 2020. No consistent enso response to volcanic forcing over the last millennium. *Science* 367 (6485), 1477–1481.
- Delworth, T., Manabe, S., 1989. The influence of soil wetness on near-surface atmospheric variability. *Journal of Climate* 2 (12), 1447–1462.
- Delworth, T. L., Ramaswamy, V., Stenchikov, G. L., 2005. The impact of aerosols on simulated ocean temperature and heat content in the 20th century. *Geophysical Research Letters* 32 (24).
- Dey, S., Di Girolamo, L., 2011. A decade of change in aerosol properties over the indian sub-continent. *Geophysical Research Letters* 38 (14).

- Dey, S., Tripathi, S., Mishra, S., 2008. Probable mixing state of aerosols in the indo-gangetic basin, northern india. *Geophysical Research Letters* 35 (3).
- Dey, S., Tripathi, S. N., Singh, R. P., Holben, B., 2004. Influence of dust storms on the aerosol optical properties over the indo-gangetic basin. *Journal of Geophysical Research: Atmospheres* 109 (D20).
- Di Capua, G., Kretschmer, M., Runge, J., Alessandri, A., Donner, R. V., van Den Hurk, B., Vellore, R., Krishnan, R., Coumou, D., 2019. Long-lead statistical forecasts of the indian summer monsoon rainfall based on causal precursors. *Weather and Forecasting* 34 (5), 1377–1394.
- Dirmeyer, P. A., 2011. The terrestrial segment of soil moisture–climate coupling. *Geophysical Research Letters* 38 (16).
- Dirmeyer, P. A., Chen, L., Wu, J., Shin, C.-S., Huang, B., Cash, B. A., Bosilovich, M. G., Mahanama, S., Koster, R. D., Santanello, J. A., et al., 2018. Verification of land–atmosphere coupling in forecast models, reanalyses, and land surface models using flux site observations. *Journal of Hydrometeorology* 19 (2), 375–392.
- Dirmeyer, P. A., Halder, S., 2016. Sensitivity of numerical weather forecasts to initial soil moisture variations in cfsv2. *Weather and Forecasting* 31 (6), 1973–1983.
- Dirmeyer, P. A., Halder, S., 2017. Application of the land–atmosphere coupling paradigm to the operational coupled forecast system, version 2 (cfsv2). *Journal of Hydrometeorology* 18 (1), 85–108.
- Dirmeyer, P. A., Jin, Y., Singh, B., Yan, X., 2013. Trends in land–atmosphere interactions from cmip5 simulations. *Journal of Hydrometeorology* 14 (3), 829–849.
- Dogar, M. M., 2018. Impact of tropical volcanic eruptions on hadley circulation using a high-resolution agcm. *Current Science*.
- Dogar, M. M., Sato, T., 2019. Regional climate response of middle eastern, african, and south asian monsoon regions to explosive volcanism and enso forcing. *Journal of Geophysical Research: Atmospheres* 124 (14), 7580–7598.
- Donges, J. F., Schleussner, C.-F., Siegmund, J. F., Donner, R. V., 2016. Event coincidence analysis for quantifying statistical interrelationships between event time series. *The European Physical Journal Special Topics* 225 (3), 471–487.
- Driscoll, S., Bozzo, A., Gray, L. J., Robock, A., Stenchikov, G., 2012. Coupled model inter-comparison project 5 (cmip5) simulations of climate following volcanic eruptions. *Journal of Geophysical Research: Atmospheres* 117 (D17).

- Duan, J., Li, L., Ma, Z., Esper, J., Büntgen, U., Xoplaki, E., Zhang, D., Wang, L., Yin, H., Luterbacher, J., 2018. Summer cooling driven by large volcanic eruptions over the tibetan plateau. *Journal of Climate* 31 (24), 9869–9879.
- Duan, L., Cao, L., Bala, G., Caldeira, K., 2019. Climate response to pulse versus sustained stratospheric aerosol forcing. *Geophysical Research Letters* 46 (15), 8976–8984.
- Duggen, S., Olgun, N., Croot, P., Hoffmann, L. J., Dietze, H., Delmelle, P., Teschner, C., 2010. The role of airborne volcanic ash for the surface ocean biogeochemical iron-cycle: a review. *Biogeosciences (BG)* 7 (3), 827–844.
- Ek, M., Mitchell, K., Lin, Y., Rogers, E., Grunmann, P., Koren, V., Gayno, G., Tarpley, J., 2003. Implementation of noah land surface model advances in the national centers for environmental prediction operational mesoscale eta model. *Journal of Geophysical Research: Atmospheres* 108 (D22).
- Emile-Geay, J., Cobb, K. M., Mann, M. E., Wittenberg, A. T., 2013. Estimating central equatorial pacific sst variability over the past millennium. part ii: Reconstructions and implications. *Journal of Climate* 26 (7), 2329–2352.
- Emile-Geay, J., Seager, R., Cane, M. A., Cook, E. R., Haug, G. H., 2008. Volcanoes and enso over the past millennium. *Journal of Climate* 21 (13), 3134–3148.
- Erlat, E., Türkeş, M., 2019. Temperature responses of turkey's climate to the tropical volcanic eruptions over second half of the twentieth century. *Theoretical and Applied Climatology* 137 (3-4), 2369–2379.
- Fadnavis, S., Mahajan, A. S., Choudhury, A. D., Roy, C., Singh, M., Biswas, M. S., Pandithurai, G., Prabhakaran, T., Lal, S., Venkatraman, C., et al., 2020. Atmospheric aerosols and trace gases. In: *Assessment of Climate Change over the Indian Region*. Springer, pp. 93–116.
- Fang, X., Zheng, X., Zhang, X., 2020. Correspondence between the large volcanic eruptions and enso events over ad 1525–2000. *Journal of Geographical Sciences* 30 (1), 103–118.
- Feng, S., Hu, Q., Wu, Q., Mann, M. E., 2013. A gridded reconstruction of warm season precipitation for asia spanning the past half millennium. *Journal of Climate* 26 (7), 2192–2204.
- Ferranti, L., Slingo, J., Palmer, T., Hoskins, B., 1999. The effect of land-surface feedbacks on the monsoon circulation. *Quarterly Journal of the Royal Meteorological Society* 125 (557), 1527–1550.
- Fischer, E., Luterbacher, J., Zorita, E., Tett, S., Casty, C., Wanner, H., 2007. European climate response to tropical volcanic eruptions over the last half millennium. *Geophysical Research Letters* 34 (5).

- Flato, G., Marotzke, J., Abiodun, B., Braconnot, P., Chou, S. C., Collins, W., Cox, P., Driouech, F., Emori, S., Eyring, V., et al., 2014. Evaluation of climate models. In: Climate change 2013: the physical science basis. Contribution of Working Group I to the Fifth Assessment Report of the Intergovernmental Panel on Climate Change. Cambridge University Press, pp. 741–866.
- Forster, P. M., Andrews, T., Good, P., Gregory, J. M., Jackson, L. S., Zelinka, M., 2013. Evaluating adjusted forcing and model spread for historical and future scenarios in the cmip5 generation of climate models. *Journal of Geophysical Research: Atmospheres* 118 (3), 1139–1150.
- Gaddis, A. L., 2013. Evaluating predictability in community earth system model in response to eruption of mount pinatubo. Ph.D. thesis.
- Gadgil, S., 2003. The indian monsoon and its variability. *Annual Review of Earth and Planetary Sciences* 31 (1), 429–467.
- Gadgil, S., Rajeevan, M., Nanjundiah, R., 2005. Monsoon prediction—why yet another failure? *Current science* 88 (9), 1389–1400.
- Ganeshi, N. G., Mujumdar, M., Krishnan, R., Goswami, M., 2020. Understanding the linkage between soil moisture variability and temperature extremes over the indian region. *Journal of Hydrology* 589, 125183.
- Ganguly, D., Rasch, P. J., Wang, H., Yoon, J.-H., 2012. Climate response of the south asian monsoon system to anthropogenic aerosols. *Journal of Geophysical Research: Atmospheres* 117 (D13).
- Gao, C., Gao, Y., 2018. Revisited asian monsoon hydroclimate response to volcanic eruptions. *Journal of Geophysical Research: Atmospheres* 123 (15), 7883–7896.
- Gao, C., Robock, A., Ammann, C., 2008. Volcanic forcing of climate over the past 1500 years: An improved ice core-based index for climate models. *Journal of Geophysical Research: Atmospheres* 113 (D23).
- Gergis, J. L., Fowler, A. M., 2009. A history of enso events since ad 1525: implications for future climate change. *Climatic Change* 92 (3-4), 343–387.
- Gershunov, A., Schneider, N., Barnett, T., 2001. Low-frequency modulation of the enso–indian monsoon rainfall relationship: Signal or noise? *Journal of Climate* 14 (11), 2486–2492.
- Gillett, N., Weaver, A., Zwiers, F., Wehner, M., 2004. Detection of volcanic influence on global precipitation. *Geophysical Research Letters* 31 (12).
- Gleckler, P., Wigley, T., Santer, B., Gregory, J., AchutaRao, K., Taylor, K., 2006. Volcanoes and climate: Krakatoa’s signature persists in the ocean. *Nature* 439 (7077), 675–675.

- Goswami, B., Madhusoodanan, M., Neema, C., Sengupta, D., 2006. A physical mechanism for north atlantic sst influence on the indian summer monsoon. *Geophysical Research Letters* 33 (2).
- Goswami, B., Xavier, P. K., 2005. Enso control on the south asian monsoon through the length of the rainy season. *Geophysical Research Letters* 32 (18).
- Graf, H.-F., Li, Q., Giorgetta, M., 2007. Volcanic effects on climate: revisiting the mechanisms. *Atmospheric Chemistry and Physics* 7 (17), 4503–4511.
- Gregory, J. M., 2010. Long-term effect of volcanic forcing on ocean heat content. *Geophysical Research Letters* 37 (22).
- Gregory, J. M., Andrews, T., Ceppi, P., Mauritsen, T., Webb, M., 2020. How accurately can the climate sensitivity to co2 be estimated from historical climate change? *Climate Dynamics* 54 (1-2), 129–157.
- Griffies, S. M., Schmidt, M., Herzfeld, M., 2009. Elements of mom4p1. GFDL Ocean Group Tech. Rep 6, 444.
- Gu, L., Baldocchi, D. D., Wofsy, S. C., Munger, J. W., Michalsky, J. J., Urbanski, S. P., Boden, T. A., 2003. Response of a deciduous forest to the mount pinatubo eruption: enhanced photosynthesis. *Science* 299 (5615), 2035–2038.
- Guillet, S., Corona, C., Ludlow, F., Oppenheimer, C., Stoffel, M., 2020. climatic and societal impacts of a “forgotten” cluster of volcanic eruptions in 1108-1110 ce. *Scientific reports* 10 (1), 1–10.
- Gupta, M., Marshall, J., Ferreira, D., 2019. Triggering global climate transitions through volcanic eruptions. *Journal of Climate* 32 (12), 3727–3742.
- Halder, S., Dirmeyer, P. A., Marx, L., Kinter III, J. L., 2018. Impact of land surface initialization and land-atmosphere coupling on the prediction of the indian summer monsoon with the cfsv2. *Frontiers in Environmental Science* 5, 92.
- Halder, S., Dirmeyer, P. A., Saha, S. K., 2015. Sensitivity of the mean and variability of indian summer monsoon to land surface schemes in regcm4: Understanding coupled land-atmosphere feedbacks. *Journal of Geophysical Research: Atmospheres* 120 (18), 9437–9458.
- Halder, S., Saha, S. K., Dirmeyer, P. A., Chase, T. N., Goswami, B. N., 2016. Investigating the impact of land-use land-cover change on indian summer monsoon daily rainfall and temperature during 1951–2005 using a regional climate model. *Hydrology and Earth System Sciences* 20 (5), 1765–1784.
- Han, J., Pan, H.-L., 2011. Revision of convection and vertical diffusion schemes in the ncep global forecast system. *Weather and Forecasting* 26 (4), 520–533.

- Hermanson, L., Bilbao, R., Dunstone, N., Ménégoz, M., Ortega, P., Pohlmann, H., Robson, J. I., Smith, D. M., Strand, G., Timmreck, C., et al., 2020. Robust multiyear climate impacts of volcanic eruptions in decadal prediction systems. *Journal of Geophysical Research: Atmospheres* 125 (9), e2019JD031739.
- Hirono, M., 1988. On the trigger of el niño southern oscillation by the forcing of early el chichón volcanic aerosols. *Journal of Geophysical Research: Atmospheres* 93 (D5), 5365–5384.
- Hopcroft, P. O., Kandlbauer, J., Valdes, P. J., Sparks, R. S. J., 2018. Reduced cooling following future volcanic eruptions. *Climate Dynamics* 51 (4), 1449–1463.
- Hsu, H., Dirmeyer, P. A., 2021. Nonlinearity and multivariate dependencies in the terrestrial leg of land-atmosphere coupling. *Water Resources Research* 57 (2), e2020WR028179.
- Hsu, N., Gautam, R., Sayer, A., Bettenhausen, C., Li, C., Jeong, M., Tsay, S.-C., Holben, B., 2012. Global and regional trends of aerosol optical depth over land and ocean using seawifs measurements from 1997 to 2010. *Atmospheric Chemistry and Physics* 12 (17), 8037–8053.
- Hu, D., Li, M., Zhang, X., Turchyn, A. V., Gong, Y., Shen, Y., 2020. Large mass-independent sulphur isotope anomalies link stratospheric volcanism to the late ordovician mass extinction. *Nature communications* 11 (1), 1–8.
- Izumo, T., Khodri, M., Lengaigne, M., Suresh, I., 2018. A subsurface indian ocean dipole response to tropical volcanic eruptions. *Geophysical Research Letters* 45 (17), 9150–9159.
- Jin, Q., Wei, J., Yang, Z.-L., 2014. Positive response of indian summer rainfall to middle east dust. *Geophysical Research Letters* 41 (11), 4068–4074.
- Jin, Q., Wei, J., Yang, Z.-L., Pu, B., Huang, J., 2015. Consistent response of indian summer monsoon to middle east dust in observations and simulations. *Atmospheric Chemistry and Physics* 15 (17), 9897–9915.
- Jin, Q., Yang, Z.-L., Wei, J., 2016. Seasonal responses of indian summer monsoon to dust aerosols in the middle east, india, and china. *Journal of Climate* 29 (17), 6329–6349.
- Jones, C. D., Cox, P. M., 2001. Modeling the volcanic signal in the atmospheric co2 record. *Global Biogeochemical Cycles* 15 (2), 453–465.
- Jones, G. S., Gregory, J. M., Stott, P. A., Tett, S. F., Thorpe, R. B., 2005. An aogcm simulation of the climate response to a volcanic super-eruption. *Climate dynamics* 25 (7-8), 725–738.
- Joseph, R., Zeng, N., 2011. Seasonally modulated tropical drought induced by volcanic aerosol. *Journal of Climate* 24 (8), 2045–2060.
- Ju, J., Slingo, J., 1995. The asian summer monsoon and enso. *Quarterly Journal of the Royal Meteorological Society* 121 (525), 1133–1168.

Kang, S. M., Held, I. M., Frierson, D. M., Zhao, M., 2008. The response of the itcz to extra-tropical thermal forcing: Idealized slab-ocean experiments with a gcm. *Journal of Climate* 21 (14), 3521–3532.

Kaskaoutis, D. G., Gautam, R., Singh, R. P., Houssos, E., Goto, D., Singh, S., Bartzokas, A., Kosmopoulos, P., Sharma, M., Hsu, N., et al., 2012a. Influence of anomalous dry conditions on aerosols over india: transport, distribution and properties. *Journal of Geophysical Research: Atmospheres* 117 (D9).

Kaskaoutis, D. G., Singh, R. P., Gautam, R., Sharma, M., Kosmopoulos, P., Tripathi, S., 2012b. Variability and trends of aerosol properties over kanpur, northern india using aeronet data (2001–10). *Environmental Research Letters* 7 (2), 024003.

Kawamura, R., 1998. A possible mechanism of the asian summer monsoon-enso coupling. *Journal of the Meteorological Society of Japan. Ser. II* 76 (6), 1009–1027.

Kedia, S., Ramachandran, S., Holben, B. N., Tripathi, S., 2014. Quantification of aerosol type, and sources of aerosols over the indo-gangetic plain. *Atmospheric Environment* 98, 607–619.

Khodri, M., Izumo, T., Vialard, J., Janicot, S., Cassou, C., Lengaigne, M., Mignot, J., Gastineau, G., Guilyardi, E., Lebas, N., et al., 2017. Tropical explosive volcanic eruptions can trigger el niño by cooling tropical africa. *Nature Communications* 8 (1), 778.

Kinter III, J., Miyakoda, K., Yang, S., 2002. Recent change in the connection from the asian monsoon to enso. *Journal of Climate* 15 (10), 1203–1215.

Kirtman, B. P., Shukla, J., 2000. Influence of the indian summer monsoon on enso. *Quarterly Journal of the Royal Meteorological Society* 126 (562), 213–239.

Kittel, T., Ciemer, C., Lotfi, N., Peron, T., Rodrigues, F., Kurths, J., Donner, R. V., 2017. Global teleconnectivity structures of the el niño-southern oscillation and large volcanic eruptions—an evolving network perspective. *arXiv preprint arXiv:1711.04670*.

Koster, R. D., Dirmeyer, P. A., Guo, Z., Bonan, G., Chan, E., Cox, P., Gordon, C., Kanae, S., Kowalczyk, E., Lawrence, D., et al., 2004. Regions of strong coupling between soil moisture and precipitation. *Science* 305 (5687), 1138–1140.

Kothawale, D., Rajeevan, M., 2017. Monthly, seasonal, annual rainfall time series for all-india, homogeneous regions, meteorological subdivisions: 1871-2016.

Kravitz, B., Robock, A., 2011. Climate effects of high-latitude volcanic eruptions: Role of the time of year. *Journal of Geophysical Research: Atmospheres* 116 (D1).

Kravitz, B., Robock, A., Bourassa, A., 2010. Negligible climatic effects from the 2008 okmok and kasatochi volcanic eruptions. *Journal of Geophysical Research: Atmospheres* 115 (D2).

- Krishna Moorthy, K., Suresh Babu, S., Manoj, M., Satheesh, S., 2013. Buildup of aerosols over the indian region. *Geophysical Research Letters* 40 (5), 1011–1014.
- Krishnamurthy, L., Krishnamurthy, V., 2014. Influence of pdo on south asian summer monsoon and monsoon–enso relation. *Climate dynamics* 42 (9-10), 2397–2410.
- Krishnamurthy, V., Goswami, B., 2000. Indian monsoon–enso relationship on interdecadal timescale. *Journal of Climate* 13 (3), 579–595.
- Krishnamurti, T., Thomas, A., Simon, A., Kumar, V., 2010. Desert air incursions, an overlooked aspect, for the dry spells of the indian summer monsoon. *Journal of Atmospheric Sciences* 67 (10), 3423–3441.
- Krishnan, R., Sabin, T., Vellore, R., Mujumdar, M., Sanjay, J., Goswami, B., Hourdin, F., Dufresne, J.-L., Terray, P., 2016. Deciphering the desiccation trend of the south asian monsoon hydroclimate in a warming world. *Climate dynamics* 47 (3), 1007–1027.
- Krishnan, R., Sugi, M., 2003. Pacific decadal oscillation and variability of the indian summer monsoon rainfall. *Climate Dynamics* 21 (3-4), 233–242.
- Kumar, K. K., Rajagopalan, B., Cane, M. A., 1999. On the weakening relationship between the indian monsoon and enso. *Science* 284 (5423), 2156–2159.
- Kumar, K. K., Rajagopalan, B., Hoerling, M., Bates, G., Cane, M., 2006. Unraveling the mystery of indian monsoon failure during el niño. *Science* 314 (5796), 115–119.
- Large, W. G., McWilliams, J. C., Doney, S. C., 1994. Oceanic vertical mixing: A review and a model with a nonlocal boundary layer parameterization. *Reviews of geophysics* 32 (4), 363–403.
- Lau, K., Kim, M., Kim, K., 2006. Asian summer monsoon anomalies induced by aerosol direct forcing: the role of the tibetan plateau. *Climate dynamics* 26 (7-8), 855–864.
- Lau, K., Tsay, S., Hsu, C., Chin, M., Ramanathan, V., Wu, G., Li, Z., Sikka, R., Holben, B., Lu, D., et al., 2008. The joint aerosol–monsoon experiment: A new challenge for monsoon climate research. *Bulletin of the American Meteorological Society* 89 (3), 369–383.
- Lau, K.-M., Kim, K.-M., 2006. Observational relationships between aerosol and asian monsoon rainfall, and circulation. *Geophysical research letters* 33 (21).
- Li, J., Xie, S.-P., Cook, E. R., Huang, G., D'arrigo, R., Liu, F., Ma, J., Zheng, X.-T., 2011. Interdecadal modulation of el niño amplitude during the past millennium. *Nature climate change* 1 (2), 114.

- Li, J., Xie, S.-P., Cook, E. R., Morales, M. S., Christie, D. A., Johnson, N. C., Chen, F., D'Arrigo, R., Fowler, A. M., Gou, X., et al., 2013. El niño modulations over the past seven centuries. *Nature Climate Change* 3 (9), 822–826.
- Liang, E., Dawadi, B., Pederson, N., Piao, S., Zhu, H., Sigdel, S. R., Chen, D., 2019. Strong link between large tropical volcanic eruptions and severe droughts prior to monsoon in the central himalayas revealed by tree-ring records. *Science Bulletin* 64 (14), 1018–1023.
- Liu, F., Xing, C., Li, J., Wang, B., Chai, J., Gao, C., Huang, G., Liu, J., Chen, D., 2020. Could the recent taal volcano eruption trigger an el niño and lead to eurasian warming? *ADVANCES IN ATMOSPHERIC SCIENCES* 37, 1–8.
- Lodh, A., 2020. Reassessment of land–atmosphere interactions over india during summer monsoon using state-of-the-art regional climate models. *Theoretical and Applied Climatology* 142 (3), 1649–1673.
- Lu, R., Dong, B., Ding, H., 2006. Impact of the atlantic multidecadal oscillation on the asian summer monsoon. *Geophysical Research Letters* 33 (24).
- Lucht, W., Prentice, I. C., Myneni, R. B., Sitch, S., Friedlingstein, P., Cramer, W., Bousquet, P., Buermann, W., Smith, B., 2002. Climatic control of the high-latitude vegetation greening trend and pinatubo effect. *Science* 296 (5573), 1687–1689.
- MacDonald, G. M., Case, R., 2006. Pacific decadal oscillation reconstruction for the past millennium. *IGBP PAGES/World Data Center for Paleoclimatology Data Contribution Series# 2006-023. NOAA/NCDC Paleoclimatology Program, Boulder CO, USA.*
- MacDonald, G. M., Case, R. A., 2005. Variations in the pacific decadal oscillation over the past millennium. *Geophysical Research Letters* 32 (8).
- Maher, N., McGregor, S., England, M. H., Gupta, A. S., 2015. Effects of volcanism on tropical variability. *Geophysical Research Letters* 42 (14), 6024–6033.
- Mann, M. E., Cane, M. A., Zebiak, S. E., Clement, A., 2005. Volcanic and solar forcing of the tropical pacific over the past 1000 years. *Journal of Climate* 18 (3), 447–456.
- Mann, M. E., Zhang, Z., Rutherford, S., Bradley, R. S., Hughes, M. K., Shindell, D., Ammann, C., Faluvegi, G., Ni, F., 2009. Global signatures and dynamical origins of the little ice age and medieval climate anomaly. *Science* 326 (5957), 1256–1260.
- Maraun, D., Kurths, J., 2005. Epochs of phase coherence between el nino/southern oscillation and indian monsoon. *Geophysical Research Letters* 32 (15).
- Marshall, A., Scaife, A., Ineson, S., 2009. Enhanced seasonal prediction of european winter warming following volcanic eruptions. *Journal of climate* 22 (23), 6168–6180.

- McConnell, J. R., Burke, A., Dunbar, N. W., Köhler, P., Thomas, J. L., Arienzo, M. M., Chellman, N. J., Maselli, O. J., Sigl, M., Adkins, J. F., et al., 2017. Synchronous volcanic eruptions and abrupt climate change 17.7 ka plausibly linked by stratospheric ozone depletion. *Proceedings of the National Academy of Sciences*, 201705595.
- McConnell, J. R., Sigl, M., Plunkett, G., Burke, A., Kim, W. M., Raible, C. C., Wilson, A. I., Manning, J. G., Ludlow, F., Chellman, N. J., et al., 2020. Extreme climate after massive eruption of alaska's okmok volcano in 43 bce and effects on the late roman republic and ptolemaic kingdom. *Proceedings of the National Academy of Sciences* 117 (27), 15443–15449.
- McGregor, S., Timmermann, A., Timm, O., 2010. A unified proxy for enso and pdo variability since 1650. *Climate of the Past* 6 (1).
- Meehl, G. A., 1994. Influence of the land surface in the asian summer monsoon: External conditions versus internal feedbacks. *Journal of climate* 7 (7), 1033–1049.
- Meehl, G. A., Arblaster, J. M., Collins, W. D., 2008. Effects of black carbon aerosols on the indian monsoon. *Journal of Climate* 21 (12), 2869–2882.
- Mehta, V. M., Lau, K.-M., 1997. Influence of solar irradiance on the indian monsoon-enso relationship at decadal-multidecadal time scales. *Geophysical Research Letters* 24 (2), 159–162.
- Ménégoz, M., Bilbao, R., Bellprat, O., Guemas, V., Doblas-Reyes, F. J., 2018a. Forecasting the climate response to volcanic eruptions: prediction skill related to stratospheric aerosol forcing. *Environmental Research Letters* 13 (6), 064022.
- Ménégoz, M., Cassou, C., Swingedouw, D., Ruprich-Robert, Y., Bretonnière, P.-A., Doblas-Reyes, F., 2017. Role of the atlantic multidecadal variability in modulating the climate response to a pinatubo-like volcanic eruption. *Climate Dynamics*, 1–21.
- Ménégoz, M., Cassou, C., Swingedouw, D., Ruprich-Robert, Y., Bretonnière, P.-A., Doblas-Reyes, F., 2018b. Role of the atlantic multidecadal variability in modulating the climate response to a pinatubo-like volcanic eruption. *Climate dynamics* 51 (5-6), 1863–1883.
- Milinski, S., Maher, N., Olonscheck, D., 2020. How large does a large ensemble need to be? *Earth System Dynamics* 11 (4), 885–901.
- Morwal, S., Narkhedkar, S., Padmakumari, B., Maheskumar, R., Deshpande, C., Kulkarni, J., 2017. Intra-seasonal and inter-annual variability of bowen ratio over rain-shadow region of north peninsular india. *Theoretical and Applied Climatology* 128 (3-4), 835–844.
- Moy, C. M., Seltzer, G. O., Rodbell, D. T., Anderson, D. M., 2002. Variability of el niño/southern oscillation activity at millennial timescales during the holocene epoch. *Nature* 420 (6912), 162–165.

Nakatsuka, T., 2015. Toward an asian hydroclimate field reconstruction. *Past Global Changes Magazine* 23, 79.

Newhall, C., Self, S., Robock, A., 2018. Anticipating future volcanic explosivity index (vei) 7 eruptions and their chilling impacts. *Geosphere* 14 (2), 572–603.

Ning, L., Liu, J., Bradley, R. S., Yan, M., Chen, K., Sun, W., Jin, C., 2020. Elevation-dependent cooling caused by volcanic eruptions during the last millennium. *International Journal of Climatology* 40 (6), 3142–3149.

Niyogi, D., 2019. Land surface processes. In: *Current trends in the representation of physical processes in weather and climate models*. Springer, pp. 349–370.

Niyogi, D., Chang, H.-I., Chen, F., Gu, L., Kumar, A., Menon, S., Pielke, R. A., 2007. Potential impacts of aerosol–land–atmosphere interactions on the indian monsoonal rainfall characteristics. *Natural Hazards* 42 (2), 345–359.

Ohba, M., Shiogama, H., Yokohata, T., Watanabe, M., 2013. Impact of strong tropical volcanic eruptions on enso simulated in a coupled gcm. *Journal of Climate* 26 (14), 5169–5182.

Otterå, O. H., 2008. Simulating the effects of the 1991 mount pinatubo volcanic eruption using the arpege atmosphere general circulation model. *Advances in Atmospheric Sciences* 25 (2), 213–226.

Paik, S., Min, S.-K., 2018. Assessing the impact of volcanic eruptions on climate extremes using cmip5 models. *Journal of Climate* (2018).

Pandey, S. K., Vinoj, V., Landu, K., Babu, S. S., 2017. Declining pre-monsoon dust loading over south asia: Signature of a changing regional climate. *Scientific reports* 7 (1), 1–10.

Pausata, F. S., Grini, A., Caballero, R., Hannachi, A., Seland, Ø., 2015. High-latitude volcanic eruptions in the norwegian earth system model: the effect of different initial conditions and of the ensemble size. *Tellus B: Chemical and Physical Meteorology* 67 (1), 26728.

Pikovsky, A., Rosenblum, M., Kurths, J., Kurths, J., 2003. *Synchronization: a universal concept in nonlinear sciences*. Vol. 12. Cambridge university press.

Plazzotta, M., Séférian, R., Douville, H., Kravitz, B., Tjiputra, J., 2018. Land surface cooling induced by sulfate geoengineering constrained by major volcanic eruptions. *Geophysical Research Letters*.

Quiroga, R. Q., Kreuz, T., Grassberger, P., 2002. Event synchronization: a simple and fast method to measure synchronicity and time delay patterns. *Physical review E* 66 (4), 041904.

Ramachandran, S., Kedia, S., Srivastava, R., 2012. Aerosol optical depth trends over different regions of india. *Atmospheric Environment* 49, 338–347.

- Ramanathan, V., Chung, C., Kim, D., Bettge, T., Buja, L., Kiehl, J. T., Washington, W. M., Fu, Q., Sikka, D. R., Wild, M., 2005. Atmospheric brown clouds: Impacts on south asian climate and hydrological cycle. *Proceedings of the National Academy of Sciences* 102 (15), 5326–5333.
- Rayner, N., Parker, D. E., Horton, E., Folland, C. K., Alexander, L. V., Rowell, D., Kent, E., Kaplan, A., 2003. Global analyses of sea surface temperature, sea ice, and night marine air temperature since the late nineteenth century. *Journal of Geophysical Research: Atmospheres* 108 (D14).
- Ridley, H. E., Asmerom, Y., Baldini, J. U., Breitenbach, S. F., Aquino, V. V., Pruffer, K. M., Culleton, B. J., Polyak, V., Lechleitner, F. A., Kennett, D. J., et al., 2015. Aerosol forcing of the position of the intertropical convergence zone since ad 1550. *Nature Geoscience* 8 (3), 195–200.
- Robock, A., 2000. Volcanic eruptions and climate. *Reviews of Geophysics* 38 (2), 191–219.
- Robock, A., 2002. The climatic aftermath. *Science* 295 (5558), 1242–1244.
- Robock, A., Free, M. P., 1996. The volcanic record in ice cores for the past 2000 years. In: *Climatic variations and Forcing Mechanisms of the Last 2000 years*. Springer, pp. 533–546.
- Robock, A., Liu, Y., 1994. The volcanic signal in goddard institute for space studies three-dimensional model simulations. *Journal of Climate* 7 (1), 44–55.
- Robock, A., Mao, J., 1992. Winter warming from large volcanic eruptions. *Geophysical Research Letters* 19 (24), 2405–2408.
- Rothenberg, D., Mahowald, N., Lindsay, K., Doney, S., Moore, J., Thornton, P., 2012. Volcano impacts on climate and biogeochemistry in a coupled carbon climate model. *Earth System Dynamics* 3 (2).
- Saha, S., Moorthi, S., Pan, H.-L., Wu, X., Wang, J., Nadiga, S., Tripp, P., Kistler, R., Woollen, J., Behringer, D., et al., 2010. The ncep climate forecast system reanalysis. *Bulletin of the American Meteorological Society* 91 (8), 1015–1058.
- Sanap, S., Pandithurai, G., Manoj, M., 2015. On the response of indian summer monsoon to aerosol forcing in cmip5 model simulations. *Climate dynamics* 45 (9), 2949–2961.
- Sano, M., Dimri, A., Ramesh, R., Xu, C., Li, Z., Nakatsuka, T., 2017. Moisture source signals preserved in a 242-year tree-ring $\delta^{18}\text{O}$ chronology in the western himalaya. *Global and Planetary Change* 157, 73–82.
- Santer, B. D., Bonfils, C., Painter, J. F., Zelinka, M. D., Mears, C., Solomon, S., Schmidt, G. A., Fyfe, J. C., Cole, J. N., Nazarenko, L., et al., 2014. Volcanic contribution to decadal changes in tropospheric temperature. *Nature Geoscience* 7 (3), 185–189.

- Satheesh, S., Babu, S. S., Padmakumari, B., Pandithurai, G., Soni, V., 2017. Variability of atmospheric aerosols over india. In: Observed Climate Variability and Change over the Indian Region. Springer, pp. 221–248.
- Sato, M., Hansen, J. E., McCormick, M. P., Pollack, J. B., 1993. Stratospheric aerosol optical depths, 1850–1990. *Journal of Geophysical Research: Atmospheres* 98 (D12), 22987–22994.
- Saturno, J., Ditas, F., Penning de Vries, M., Holanda, B. A., Pöhlker, M. L., Carbone, S., Walter, D., Bobrowski, N., Brito, J., Chi, X., et al., 2018. African volcanic emissions influencing atmospheric aerosols over the amazon rain forest. *Atmospheric Chemistry and Physics* 18 (14), 10391–10405.
- Schmidt, A., October 2012. Impact of the 1783–1784 ad laki eruption on global aerosol formation processes and cloud condensation nuclei. Ph.D. thesis, University of Leeds.
- URL <http://libgen.io/get.php?md5=1265F26927D3A22ECB6B4C00565E29F0&key=7YIJQWHHJ73SKACT>
- Schneider, D. P., Ammann, C. M., Otto-Bliesner, B. L., Kaufman, D. S., 2009. Climate response to large, high-latitude and low-latitude volcanic eruptions in the community climate system model. *Journal of Geophysical Research: Atmospheres* 114 (D15).
- Schneider, T., Bischoff, T., Haug, G. H., 2014. Migrations and dynamics of the intertropical convergence zone. *Nature* 513 (7516), 45–53.
- Sharmila, S., Joseph, S., Sahai, A., Abhilash, S., Chattopadhyay, R., 2015. Future projection of indian summer monsoon variability under climate change scenario: An assessment from cmip5 climate models. *Global and Planetary Change* 124, 62–78.
- Shen, X., Kimoto, M., Sumi, A., 1998. Role of land surface processes associated with interannual variability of broad-scale asian summer monsoon as simulated by the ccsr/nies agcm. *Journal of the Meteorological Society of Japan. Ser. II* 76 (2), 217–236.
- Shi, F., Fang, K., Xu, C., Guo, Z., Borgaonkar, H., 2017. Interannual to centennial variability of the south asian summer monsoon over the past millennium. *Climate Dynamics* 49 (7-8), 2803–2814.
- Shi, F., Li, J., Wilson, R. J., 2014. A tree-ring reconstruction of the south asian summer monsoon index over the past millennium. *Scientific reports* 4, 6739.
- Shi, H., Wang, B., Cook, E. R., Liu, J., Liu, F., 2018. Asian summer precipitation over the past 544 years reconstructed by merging tree rings and historical documentary records. *Journal of Climate* 31 (19), 7845–7861.
- Shindell, D. T., Schmidt, G. A., Mann, M. E., Faluvegi, G., 2004. Dynamic winter climate response to large tropical volcanic eruptions since 1600. *Journal of Geophysical Research: Atmospheres* 109 (D5).

- Shiogama, H., Emori, S., Mochizuki, T., Yasunaka, S., Yokohata, T., Ishii, M., Nozawa, T., Kimoto, M., 2010. Possible influence of volcanic activity on the decadal potential predictability of the natural variability in near-term climate predictions. *Advances in Meteorology* 2010.
- Sigl, M., Winstrup, M., McConnell, J., Welten, K., Plunkett, G., Ludlow, F., Büntgen, U., Caffee, M., Chellman, N., Dahl-Jensen, D., et al., 2015. Timing and climate forcing of volcanic eruptions for the past 2,500 years. *Nature* 523 (7562), 543.
- Sikka, D., 1980. Some aspects of the large scale fluctuations of summer monsoon rainfall over India in relation to fluctuations in the planetary and regional scale circulation parameters. *Proceedings of the Indian Academy of Sciences-Earth and Planetary Sciences* 89 (2), 179–195.
- Singh, D., Ghosh, S., Roxy, M. K., McDermid, S., 2019. Indian summer monsoon: Extreme events, historical changes, and role of anthropogenic forcings. *Wiley Interdisciplinary Reviews: Climate Change* 10 (2), e571.
- Singh, M., Krishnan, R., Goswami, B., Choudhury, A. D., Swapna, P., Vellore, R., Prajesh, A., Sandeep, N., Venkataraman, C., Donner, R. V., et al., 2020. Fingerprint of volcanic forcing on the ENSO–Indian monsoon coupling. *Science Advances* 6 (38), eaba8164.
- Sinha, A., Cannariato, K. G., Stott, L. D., Cheng, H., Edwards, R. L., Yadava, M. G., Ramesh, R., Singh, I. B., 2007. A 900-year (600 to 1500 AD) record of the Indian summer monsoon precipitation from the core monsoon zone of India. *Geophysical Research Letters* 34 (16).
- Sinha, A., Kathayat, G., Cheng, H., Breitenbach, S. F., Berkelhammer, M., Mudelsee, M., Biswas, J., Edwards, R., 2015. Trends and oscillations in the Indian summer monsoon rainfall over the last two millennia. *Nature Communications* 6 (1), 1–8.
- Sinha, A., Stott, L., Berkelhammer, M., Cheng, H., Edwards, R. L., Buckley, B., Aldenderfer, M., Mudelsee, M., 2011. A global context for megadroughts in monsoon Asia during the past millennium. *Quaternary Science Reviews* 30 (1), 47–62.
- Slawinska, J., Robock, A., 2018. Impact of volcanic eruptions on decadal to centennial fluctuations of Arctic sea ice extent during the last millennium and on initiation of the Little Ice Age. *Journal of Climate* 31 (6), 2145–2167.
- Solomon, S., 1999. Stratospheric ozone depletion: A review of concepts and history. *Reviews of Geophysics* 37 (3), 275–316.
- Soni, V., Pandithurai, G., Pai, D., 2012. Evaluation of long-term changes of solar radiation in India. *International Journal of Climatology* 32 (4), 540–551.
- Srivastava, R., 2017. Trends in aerosol optical properties over South Asia. *International Journal of Climatology* 37 (1), 371–380.

Srivastava, R., Ramachandran, S., 2013. The mixing state of aerosols over the indo-gangetic plain and its impact on radiative forcing. *Quarterly Journal of the Royal Meteorological Society* 139 (670), 137–151.

Stahle, D. W., D'Arrigo, R. D., Krusic, P. J., Cleaveland, M. K., Cook, E. R., Allan, R. J., Cole, J. E., Dunbar, R. B., Therrell, M. D., Gay, D. A., et al., 1998. Experimental dendroclimatic reconstruction of the southern oscillation. *Bulletin of the American Meteorological Society* 79 (10), 2137–2152.

Stenchikov, G., Hamilton, K., Stouffer, R. J., Robock, A., Ramaswamy, V., Santer, B., Graf, H.-F., 2006. Arctic oscillation response to volcanic eruptions in the ipcc ar4 climate models. *Journal of Geophysical Research: Atmospheres* 111 (D7).

Sterl, A., Severijns, C., Van Oldenborgh, G. J., Dijkstra, H., Hazeleger, W., van den Broeke, M., Burgers, G., van den Hurk, B., van Leeuwen, P. J., van Velthoven, P., 2007. The essence project-signal to noise ratio in climate projections. *Essence* 16, 17.

Stocker, M., Ladstädter, F., Wilhelmsen, H., Steiner, A. K., 2019. Quantifying stratospheric temperature signals and climate imprints from post-2000 volcanic eruptions. *Geophysical Research Letters* 46 (21), 12486–12494.

Stocker, T., 2014. Climate change 2013: the physical science basis: Working Group I contribution to the Fifth assessment report of the Intergovernmental Panel on Climate Change. Cambridge University Press.

Sun, W., Wang, B., Liu, J., Chen, D., Gao, C., Ning, L., Chen, L., 2019. How northern high-latitude volcanic eruptions in different seasons affect enso. *Journal of Climate* 32 (11), 3245–3262.

Swapna, P., Krishnan, R., Sandeep, N., Prajeesh, A., Ayantika, D., Manmeet, S., Vellore, R., 2018. Long-term climate simulations using the iitm earth system model (iitm-esmv2) with focus on the south asian monsoon. *Journal of Advances in Modeling Earth Systems* 10 (5), 1127–1149.

Swapna, P., Roxy, M., Aparna, K., Kulkarni, K., Prajeesh, A., Ashok, K., Krishnan, R., Moorthi, S., Kumar, A., Goswami, B., 2015. The iitm earth system model: transformation of a seasonal prediction model to a long-term climate model. *Bulletin of the American Meteorological Society* 96 (8), 1351–1367.

Swingedouw, D., Ortega, P., Mignot, J., Guilyardi, E., Masson-Delmotte, V., Butler, P. G., Khodri, M., Séférian, R., 2015. Bidecadal north atlantic ocean circulation variability controlled by timing of volcanic eruptions. *Nature communications* 6, 6545.

- Tabazadeh, A., Drdla, K., Schoeberl, M., Hamill, P., Toon, O., 2002. Arctic “ozone hole” in a cold volcanic stratosphere. *Proceedings of the National Academy of Sciences* 99 (5), 2609–2612.
- Tejavath, C. T., Ashok, K., Chakraborty, S., Ramesh, R., 2019. A pmip3 narrative of modulation of enso teleconnections to the indian summer monsoon by background changes in the last millennium. *Climate Dynamics*, 1–17.
- Textor, C., Graf, H.-F., Timmreck, C., Robock, A., 2004. Emissions from volcanoes. In: *Emissions of Atmospheric Trace Compounds*. Springer, pp. 269–303.
- Thiel, M., Romano, M. C., Kurths, J., Rolfs, M., Kliegl, R., 2006. Twin surrogates to test for complex synchronisation. *EPL (Europhysics Letters)* 75 (4), 535.
- Tie, X., Brasseur, G., 1995. The response of stratospheric ozone to volcanic eruptions: Sensitivity to atmospheric chlorine loading. *Geophysical research letters* 22 (22), 3035–3038.
- Timmreck, C., Graf, H.-F., Zanchettin, D., Hagemann, S., Kleinen, T., Krüger, K., 2012. Climate response to the toba super-eruption: Regional changes. *Quaternary International* 258, 30–44.
- Tjiputra, J., Otterå, O. H., 2011. Role of volcanic forcing on future global carbon cycle.
- Toohey, M., Krüger, K., Schmidt, H., Timmreck, C., Sigl, M., Stoffel, M., Wilson, R., 2019. Disproportionately strong climate forcing from extratropical explosive volcanic eruptions. *Nature Geoscience* 12 (2), 100.
- Torrence, C., Webster, P. J., 1999. Interdecadal changes in the enso–monsoon system. *Journal of Climate* 12 (8), 2679–2690.
- Trenberth, K. E., Dai, A., 2007. Effects of mount pinatubo volcanic eruption on the hydrological cycle as an analog of geoengineering. *Geophysical Research Letters* 34 (15).
- Trisos, C. H., Gabriel, C., Robock, A., Xia, L., 2018. Ecological, agricultural, and health impacts of solar geoengineering. In: *Resilience*. Elsevier, pp. 291–303.
- Tsonis, A. A., Swanson, K. L., Roebber, P. J., 2006. What do networks have to do with climate? *Bulletin of the American Meteorological Society* 87 (5), 585–596.
- Turner, A., Inness, P., Slingo, J., 2005. The role of the basic state in the enso–monsoon relationship and implications for predictability. *Quarterly Journal of the Royal Meteorological Society: A journal of the atmospheric sciences, applied meteorology and physical oceanography* 131 (607), 781–804.

- Undorf, S., Polson, D., Bollasina, M., Ming, Y., Schurer, A., Hegerl, G., 2018. Detectable impact of local and remote anthropogenic aerosols on the 20th century changes of west african and south asian monsoon precipitation. *Journal of Geophysical Research: Atmospheres* 123 (10), 4871–4889.
- Vinoj, V., Rasch, P. J., Wang, H., Yoon, J.-H., Ma, P.-L., Landu, K., Singh, B., 2014. Short-term modulation of indian summer monsoon rainfall by west asian dust. *Nature Geoscience* 7 (4), 308–313.
- Wang, B., Liu, J., Kim, H.-J., Webster, P. J., Yim, S.-Y., Xiang, B., 2013. Northern hemisphere summer monsoon intensified by mega-el niño/southern oscillation and atlantic multidecadal oscillation. *Proceedings of the National Academy of Sciences* 110 (14), 5347–5352.
- Wang, B., Yang, J., Zhou, T., Wang, B., 2008. Interdecadal changes in the major modes of asian–australian monsoon variability: Strengthening relationship with enso since the late 1970s. *Journal of Climate* 21 (8), 1771–1789.
- Wang, C., Kim, D., Ekman, A. M., Barth, M. C., Rasch, P. J., 2009. Impact of anthropogenic aerosols on indian summer monsoon. *Geophysical Research Letters* 36 (21).
- Wang, T., Guo, D., Gao, Y., Wang, H., Zheng, F., Zhu, Y., Miao, J., Hu, Y., 2017. Modulation of enso evolution by strong tropical volcanic eruptions. *Climate Dynamics*, 1–21.
- Wang, T., Guo, D., Gao, Y., Wang, H., Zheng, F., Zhu, Y., Miao, J., Hu, Y., 2018. Modulation of enso evolution by strong tropical volcanic eruptions. *Climate dynamics* 51 (7-8), 2433–2453.
- Webster, P. J., Yang, S., 1992. Monsoon and enso: Selectively interactive systems. *Quarterly Journal of the Royal Meteorological Society* 118 (507), 877–926.
- Wilson, R., Cook, E., D'Arrigo, R., Riedwyl, N., Evans, M. N., Tudhope, A., Allan, R., 2010. Reconstructing enso: the influence of method, proxy data, climate forcing and teleconnections. *Journal of Quaternary Science* 25 (1), 62–78.
- Winton, M., 2000. A reformulated three-layer sea ice model. *Journal of atmospheric and oceanic technology* 17 (4), 525–531.
- Xavier, P. K., Marzin, C., Goswami, B., 2007. An objective definition of the indian summer monsoon season and a new perspective on the enso–monsoon relationship. *Quarterly Journal of the Royal Meteorological Society* 133 (624), 749–764.
- Xie, F., Zhang, J., Sang, W., Li, Y., Qi, Y., Sun, C., Shu, J., 2017. Delayed effect of arctic stratospheric ozone on tropical rainfall. *Atmospheric Science Letters* 18 (10), 409–416.
- Xing, C., Liu, F., Wang, B., Chen, D., Liu, J., Liu, B., 2020. Boreal winter surface air temperature responses to large tropical volcanic eruptions in cmip5 models. *Journal of Climate* 33 (6), 2407–2426.

- Xu, L., Wei, K., Wu, X., Smyshlyaev, S., Chen, W., Galin, V. Y., 2019. The effect of super volcanic eruptions on ozone depletion in a chemistry-climate model. *Advances in Atmospheric Sciences* 36 (8), 823–836.
- Yadava, M., Ramesh, R., Pant, G., 2004. Past monsoon rainfall variations in peninsular india recorded in a 331-year-old speleothem. *The Holocene* 14 (4), 517–524.
- Yan, H., Sun, L., Wang, Y., Huang, W., Qiu, S., Yang, C., 2011. A record of the southern oscillation index for the past 2,000 years from precipitation proxies. *Nature Geoscience* 4 (9), 611–614.
- Yang, S., 1996. Enso–snow–monsoon associations and seasonal–interannual predictions. *International Journal of Climatology* 16 (2), 125–134.
- Yang, W., Vecchi, G. A., Fueglistaler, S., Horowitz, L. W., Luet, D. J., Muñoz, Á. G., Paynter, D., Underwood, S., 2019. Climate impacts from large volcanic eruptions in a high-resolution climate model: The importance of forcing structure. *Geophysical Research Letters* 46 (13), 7690–7699.
- Yokohata, T., Emori, S., Nozawa, T., Tsushima, Y., Ogura, T., Kimoto, M., 2005. Climate response to volcanic forcing: Validation of climate sensitivity of a coupled atmosphere-ocean general circulation model. *Geophysical Research Letters* 32 (21).
- Yost, C. L., Jackson, L. J., Stone, J. R., Cohen, A. S., 2018. Subdecadal phytolith and charcoal records from lake malawi, east africa imply minimal effects on human evolution from the 74 ka toba supereruption. *Journal of human evolution* 116, 75–94.
- Zambri, B., Robock, A., Mills, M. J., Schmidt, A., 2019. Modeling the 1783–1784 laki eruption in iceland: 2. climate impacts. *Journal of Geophysical Research: Atmospheres* 124 (13), 6770–6790.
- Zanchettin, D., Timmreck, C., Toohey, M., Jungclaus, J. H., Bittner, M., Lorenz, S. J., Rubino, A., 2019. Clarifying the relative role of forcing uncertainties and initial-condition unknowns in spreading the climate response to volcanic eruptions. *Geophysical Research Letters* 46 (3), 1602–1611.
- Zhong, Y., Miller, G., Otto-Bliesner, B., Holland, M., Bailey, D., Schneider, D., Geirsdottir, A., 2011. Centennial-scale climate change from decadally-paced explosive volcanism: a coupled sea ice-ocean mechanism. *Climate Dynamics* 37 (11-12), 2373–2387.
- Zuo, M., Man, W., Zhou, T., Guo, Z., 2018. Different impacts of northern, tropical, and southern volcanic eruptions on the tropical pacific sst in the last millennium. *Journal of Climate* 31 (17), 6729–6744.

Zuo, M., Zhou, T., Man, W., 2019a. Hydroclimate responses over global monsoon regions following volcanic eruptions at different latitudes. *Journal of Climate* (2019).

Zuo, M., Zhou, T., Man, W., 2019b. Wetter global arid regions driven by volcanic eruptions. *Journal of Geophysical Research: Atmospheres* 124 (24), 13648–13662.

List of Publications

Book Chapters

1. Fadnavis, S., Mahajan, A.S., Choudhury, A.D., Roy, C., Singh, M., Biswas, M.S., Pandithurai, G., Prabhakaran, T., Lal, S., Venkatraman, C. and Ganguly, D., 2020. "Atmospheric aerosols and trace gases. In *Assessment of Climate Change over the Indian Region* (pp. 93-116). Springer, Singapore.
2. Krishnan, R., Gnanaseelan, C., Sanjay, J., Swapna, P., Dhara, C., Sabin, T.P., Jadhav, J., Sandeep, N., Choudhury, A.D., Singh, M. and Mujumdar, M., 2020. "Introduction to climate change over the Indian region. *Assessment of Climate Change over the Indian Region* (pp. 1-20). Springer, Singapore.
3. Krishnan, R., Swapna, P., Vellore, R., Narayanasetti, S., Prajeesh, A.G., Choudhury, A.D., Singh, M., Sabin, T.P. and Sanjay, J., 2019. "The IITM earth system model (ESM): development and future roadmap. *Current Trends in the Representation of Physical Processes in Weather and Climate Models* (pp. 183-195). Springer, Singapore.

Journals

1. Singh, M., Persad, G. G., Zong-Liang Yang, R. Krishnan, Ayantika, D. C., Wen-Ying Wu, Sabiha Tabassum, Venkataraman, C., Swapna, P., Prajeesh, A.G., Sandeep, N., Ramesh, V., Mujumdar, M., Dev Niyogi, 2021. "Interactions between anthropogenic aerosols and land-atmosphere coupling in modulating Indian summer monsoon precipitation ", (under preparation)
2. DC Ayantika, R Krishnan, M Singh, P Swapna, N Sandeep, AG Prajeesh, R Vellore, 2021. "Understanding the combined effects of global warming and anthropogenic aerosol forcing on the South Asian monsoon", *Climate Dynamics*, 56(5), pp.1643-1662.
3. Singh, M., Krishnan, R., Goswami, B., Choudhury, A.D., Swapna, P., Vellore, R., Prajeesh, A.G., Sandeep, N., Venkataraman, C., Donner, R.V. and Marwan, N., 2020. "Fingerprint of volcanic forcing on the ENSO–Indian monsoon coupling." *Science advances*,

6(38), p.eaba8164. - This article was noted as amongst the top 5 publications from IIT Bombay for the year 2020 by www.natureindex.com

4. Swapna, P., Krishnan, R., Sandeep, N., Prajeesh, A.G., Ayantika, D.C., Manmeet, S. and Vellore, R., 2018. "Long-Term Climate Simulations Using the IITM Earth System Model (IITM-ESMv2) With Focus on the South Asian Monsoon." *Journal of Advances in Modeling Earth Systems*, 10(5), pp.1127-1149.

Conferences

1. Manmeet Singh, G. G. Persad, Z. L. Yang, R. Krishnan, A. D. Choudhury, W. Y. Wu, S. Tabassum, C. Venkataraman, S. Panickal, P. A.G., S. Narayanasetti, R. Vellore, M. Mujumdar, and D. Niyogi, 2021. "Modulations of Indian summer monsoon rainfall by aerosols induced land-atmosphere coupling ", *In 102th American Meteorological Society Annual Meeting. AMS*.
2. M. Singh, R. Krishnan, B. Goswami, A. D. Choudhury, S. Panickal, R. Vellore, P. A. Gopinathan, S. Narayanasetti, C. Venkataraman, R. V. Donner, N. Marwan, J. and Kurths, 2021. "Fingerprint of volcanic forcing on the ENSO–Indian monsoon coupling", *EGU General Assembly Conference Abstracts*
3. M. Singh, R. Krishnan, B. Goswami, A. D. Choudhury, S. Panickal, R. Vellore, P. A. Gopinathan, S. Narayanasetti, C. Venkataraman, R. V. Donner, N. Marwan, J. and Kurths, 2021. "Fingerprint of volcanic forcing on the ENSO–Indian monsoon coupling", *WCRP workshop on attribution of multi-annual to decadal changes in the climate system*
4. Dey Choudhury, A., Raghavan, K., Singh, M., Panickal, S., Narayansetti, S., Gopinathan, P.A. and Vellore, R., 2020, May. "Combined effects of anthropogenic aerosols and global warming on the South Asian Monsoon. *EGU General Assembly Conference Abstracts* (p. 923).
5. Raghavan, K., Dey Choudhury, A., Singh, M., Panickal, S., Vellore, R. and Prajeesh, A.G., 2018, December. "The Indian Monsoon Response to Climate Change in the IITM Earth System Model. *AGU Fall Meeting Abstracts* (Vol. 2018, pp. A51Q-2467).

Popular science articles/Technical reports

1. R Krishnan, Singh Manmeet, Vellore Ramesh, Mujumdar Milind, 2018. “Progress and Prospects in Weather and Climate Modelling ”, Physics News
2. R. Krishnan, P. Swapna, Ayantika Dey Choudhury, Sandeep Narayansetti, A.G. Prajesh, Manmeet Singh, Aditi Modi, Roxy Mathew, Ramesh Vellore, J. Jyoti, T.P. Sabin, J. Sanjay, Sandip Ingle, 2017. “The IITM Earth System Model (IITM ESM) ”, Climate Change over INDIA: An Interim Report (2017)

This page was intentionally left blank.

Fellowship Awarded

Awarded the Fulbright-Kalam Climate Fellowship for Doctoral Research 2020-2021 for a period of 9 months ([Profile on Fulbright website](#)).

The fellowship was awarded by the United States India Educational Foundation and DST, Govt of India. The period from February 2021 to October 2021 was spent at the Jackson School of Geosciences, The University of Texas at Austin, Austin, USA. The expertise of the host institution in land surface processes and modelling was instrumental in shaping the work "Study of Aerosol-induced Land–Atmosphere Interactions on the Ocean–Atmosphere–Land Coupled System using the IITM-Earth System Model" as a part of the last proposed objective.

This page was intentionally left blank.

Acknowledgments

The work carried out in this thesis is a direct product of the research executed July 2017 as a part of the doctoral degree in Climate Studies at IIT Bombay. I would like to sincerely thank all the people who have extended their support and help to me during this period. I am eternally thankful to Dr R. Krishnan, Dr Chandra Venkataraman and Dr Ayantika Dey Choudhury, my thesis advisers for their unwavering encouragement and support. I am in fact thankful to the whole IITM-ESM model development team for giving me a stimulating working environment. The collaboration with the group at Potsdam Institute for Climate Impact Research including Dr Bedartha Goswami, Prof Reik Donner, Prof Norbert Marwan and Prof. Juergen Kurths gave me generous chances to expand my intellectual capacities, and room to work independently in my research, discussion, and expression.

Lastly, I would like to thank the collaborators at The University of Texas at Austin, Prof Dev Niyogi, Prof Geeta Persad, Prof Zong-Liang Yang, Dr Wen-Ying Wu and Sabiha Tabassum for all of their feedback and advice at all stages of my study during my stay as a Fulbright scholar at Austin which has benefited me much. I extend my heartfelt gratitude to the Director, IITM, Prof Ravi Nanjundiah for allowing me to carry out my study at UT Austin.

I would like to thank the United States India Educational Foundation, Institute of International Education and the Department of Science and Technology (DST), Government of India, for giving me the opportunity to carry out a part of my research in the USA. The computational resources at IITM, Aaditya and Pratyush HPC and the IBM & Cray/HP support teams were instrumental in my work. Numerous authors who provided the datasets which I used in the research at personal requests and also the ones who provided the open-access data are duly acknowledged. Finally, I want to express my gratitude to the international scientific community for their guidance on the subject, including, but not limited to, those who assisted by sending me emails, giving guest lectures, and direct communications at various international conferences. Heartfelt thanks goes to my past teachers, friends and family.